UNIVERSITY OF THE WEST INDIES, CAVE HILL

GRADUATE THESIS

Atmospheric Dispersion Modelling in Barbados

Author:
Patrick BARRETT

Supervisors:
Dr. Peter CHAMI
Dr. Mechelle GITTENS

A thesis submitted in fulfillment of the requirements for the degree of Master of Philosophy in Mathematics

Department of Computer Science, Mathematics and Physics

January 1, 2017

THE UNIVERSITY OF THE WEST INDIES
School for Graduate Studies and Research

CERTIFICATE OF COMPLETION OF THESIS/RESEARCH PAPER/PROJECT REPORT/CASEBOOK

Section A of this form is to be completed by the Student and Section B by both Supervisor and Head of Department. It must accompany the thesis/research paper/project report/casebook when being submitted to the Campus Office of Graduate Studies and Research for examination.

Section A:

Name of student: _____

Faculty in which student is registered: _____

Degree Programme: _____

Title of Thesis/Research Paper/Project Report/Casebook (Submission): _____

_____

_____

Declaration of Word Length and Ownership of Work

1. Word length of Submission: _____

   A candidate will not normally exceed the word limit prescribed in the Regulations. Any candidate wishing to exceed this limit must apply for permission to the Board for Graduate Studies and Research through his/her supervisor, and confirmation of suspension of Regulations must be attached.

2. Style Manual used: _____

3. I confirm that the work presented in the Submission is my own and all references are cited according to accepted University of the West Indies' conventions. I have submitted my Thesis/Research Paper/Project Report/Casebook for checking by the following plagiarism detection software:

   _____

   and have made all necessary amendments.

4. Pursuant to the University of the West Indies' policies on Plagiarism, I agree that the University has the right to use plagiarism detection software to check the electronic version of the Submission.

_____ _____

Signature of Student *Date*

Section B:

I hereby certify that:

a) Mr./Mrs./Miss _____,
(Name in Full)
is a registered student of the University of the West Indies

b) he/she has completed his/her Thesis/Research Paper/Project Report/Casebook

c) five (5) identical copies of the Submission †, or (4) identical copies of the Submission† as the case may be, have been produced in accordance with the Regulations of the University of the West Indies and to my satisfaction*.

d) the work has been checked for plagiarism and proper use of citation and referencing.

e) the work is acceptable for examination.

† ***Select as appropriate. One of these copies should be electronic, submitted on a CD/DVD (in edit-enabled format/Microsoft Word format), and certified by your supervisor.***

* ***If the supervisor is not satisfied with the student's performance he/she should delete this statement and write appropriate comments below.***

Supervisor's Comments: _____

_____

_____

_____

_____	_____	_____
Name of Supervisor	*Signature of Supervisor*	*Date*
_____	_____	_____
Name of Head of Department	*Signature of Head of Department*	*Date*

Acronyms

AERMAP AERMIC Terrain Preprocessor

AERMET AERMIC Meteorological Preprocessor

AERMIC American Meteorological Society (AMS)/United States Environmental Protection Agency (EPA) Regulatory Model Improvement Committee

AERMOD American Meteorological Society/Environmental Protection Agency Regulatory Model

AQG Air Quality Guideline

AQI Air Quality Index

BLP The Barbados Light and Power Company Limited

CAA Clean Air Act

CBL Convective Boundary Layer

CML Convective Mixing Layer

CTDMPLUS Improved Complex Terrain Dispersion

EPA Environmental Planning Agency

GIS Geographic Information Systems

GLC Ground Level Concentration

HPDM Hybrid Plume Dispersion Model

IHME Institute for Health Metrics and Evaluation

ISC3 Industrial Source Complex Model

LCL Lifting Condensation Level

LNG Liquid Nitrogen Gas

MML Mechanical Mixing Layer

MOS Monin-Obukhov Similarity

MRE Mean Relative Error

NAAQS National Ambient Air Quality Standards

ODE Ordinary Differential Equation

PBL Planetary Boundary Layer

PDE Partial Differential Equation

PDF Probability Density Function

RTDM Rough Terrain Diffusion Model

SBL Stable Boundary Layer

UNEA United Nations Environment Assembly

UNEP United Nations Environment Programme

UTC Universal Constant Time

WHO World Health Organization

List of symbols

B_0 Bowen ratio

C mass concentration

d width

f plume state weighting function

F_b stack buoyant flux

F_m stack momentum flux

H effective height

h elevation above mean sea level

h_s height

h_c receptor specific height scale

H_d height of the dividing streamline

H_p plume centroid height

J mass flux of pollutant

J_b mass flux within Eulerian box

$\mathbf{K}$ vector form of Fick's constant

K component form of Fick's constant

k_C transmittance of an individual cloud layer

k_f Froude factor

L the Monin Obukhov Length

l length

M mass

N Brunt Väisälä frequency

n fractional cloud cover

n_C fractional cloud cover of an individual cloud layer

n_j Julian Day Number

n_T fractional total cloud cover

P atmospheric pressure, mean sea level pressure

p probability density function

PM_{10} particulate matter with diameter less than 10µm

Q^L emission rate from a single line source

Q^P emission rate from a single point source

q specific humidity

$\mathbf{r}$ position vector

RH relative humidity

r_s stack radius

u_{ref} mean wind speed at the reference height for wind measurements

S source/sink term

T temperature

t time

T_{ref} ambient temperature at the reference height for temperature measurements

$\mathbf{u}$ wind vector

$\bar{u}$ vertical average of the mean horizontal wind speed within the PBL

u average wind speed

u_* surface frictional velocity

u_s mean wind speed at the stack height

V volume

w_* Deardorff velocity

w_s stack exit gas velocity

x_f the distance to plume stabilization from the point of source emission

x_m the distance at which pollutants first become uniformity mixed throughout the boundary layer

H_f the height of plume stabilization corresponding to x_f

X arbitrary pollutant

z_0 roughness length

z_g height of the receptor above local ground

$z_{i_{eff}}$ mixing layer height

z_i mixing layer height

z_{ic} depth of the convective mixing layer

z_{ie} equivalent mechanical mixing layer height

z_{im} depth of the mechanical mixing layer

$z_{T_{ref}}$ reference height for temperature measurements

$z_{u_{ref}}$ reference height for wind measurements

ρ probability density function

σ standard deviation

σ_{vc} convective portion of lateral turbulence

σ_{vm} mechanical portion of lateral turbulence

σ_{vT} total lateral turbulence

σ_{wc} convective portion of vertical turbulence

σ_{wj} vertical dispersion parameter for the skewed bi-Gaussian pdf

σ_{wm} mechanical portion of vertical turbulence

σ_{wml} mechanical portion of vertical turbulence generated in the PBL

σ_{wmr} mechanical portion of vertical turbulence generated by the residual layer above the PBL

σ_{wT} total vertical turbulence

τ residence time, time scale

τ_b atmospheric transmittance

τ_d ratio of diffuse radiation to the extraterrestrial (beam) radiation on the horizontal plane

α albedo

ϕ_{crit} critical solar zenith angle

ϕ_D declination angle

ϕ_E solar elevation angle

ϕ_H hour angle

ϕ_{lat} latitude of a particular location

ϕ_u angle between the x-axis and wind direction

ϕ_Z solar zenith angle

Φ_G ground heat flux

Φ_H sensible surface heat flux

Φ_{LE} latent heat flux

Φ_N net radiation

Φ_{on} extraterrestrial radiation measured on the plane normal to the radiation on the nth day of the year

Φ_{S_c} global clear sky radiation

Φ_{S_0} global solar radiation

$\Phi_{S_{cb}}$ direct beam component of global clear sky radiation

$\Phi_{S_{cd}}$ diffused component of global clear sky radiation

ψ_H universal stability function for potential temperature

ψ_M universal stability function for momentum

φ_p portion of the plume material trapped in the convective mixed layer

Γ rate of change of mass

Δh plume rise height

ζ stability parameter

θ potential temperature

θ_* temperature scale

List of Physical Constants

The Following is a list of physical constants used throughout this work

Symbol	Description	Value	Unit
c_{pa}	Specific heat capacity of dry air at constant pressure	1.006×10^3	$\mathrm{J\,k\,g^{-1}\,K^{-1}}$
c_{pv}	Specific heat capacity of water vapour at constant pressure	1.93×10^3	$\mathrm{J\,k\,g^{-1}\,K^{-1}}$
c_{va}	Specific heat capacity of dry air at constant volume	7.17×10^2	$\mathrm{J\,k\,g^{-1}\,K^{-1}}$
c_{vl}	Specific heat capacity of water	4.2×10^3	$\mathrm{J\,k\,g^{-1}\,K^{-1}}$
c_{vv}	Specific heat capacity of water vapour at constant volume	1.46×10^3	$\mathrm{J\,k\,g^{-1}\,K^{-1}}$
g_0	Standard acceleration due to gravity	9.80665	$\mathrm{m\,s^{-1}}$
k_v	Von Kármán constant	0.4	
R_a	Specific gas constant for dry air	2.87058×10^2	$\mathrm{J\,k\,g^{-1}\,K^{-1}}$
R_v	Specific gas constant for water vapour	4.615×10^2	$\mathrm{J\,k\,g^{-1}\,K^{-1}}$
ρ_a	Standard air density	1.225	$\mathrm{k\,g\,m^{-3}}$

ϕ_{const}	Solar constant	1367 ± 7	$\mathrm{W\,m^{-2}}$
σ_{SB}	Stefan-Boltzmann constant	5.67×10^{-8}	$\mathrm{W\,m^{-2}\,K^{-4}}$
ω	Angular velocity of the earth	7.29×10^{-5}	$\mathrm{s^{-1}}$

Contents

Chapter 1

Introduction

Barbados is a small (about 432 $\mathrm{k\,m^2}$) Caribbean island country in the Lesser Antilles of the West Indies, located at about 13.1939^0 N, 59.5432^0 W. Currently, Barbados has no established air pollution monitoring programme. Moreover, a pilot study set up in 1994 to monitor air pollution across the island has since then been discontinued. Overall, besides concerns for vehicular emissions, the traditional perspective is that air quality has not been considered a major issue for the island of Barbados (Pan American Health Organization, 2012).

In this chapter, we discuss several lines of evidence that allude to a significant role played by air pollution on health, contradicting the aforementioned traditionally held view, and present an overall case for the benefits of a historical database of air pollution across Barbados. Furthermore, we discuss the benefits and applications of air pollution modelling on the sustainable development of an economy and establish the necessity for air pollution modelling in Barbados.

1.1 Purpose

1.1.1 Purpose Statement

The purpose of this research is to measure the performance of the American Meteorological Society/Environmental Protection Agency Regulatory

Model (AERMOD) Gaussian plume dispersion model formulation in estimating Ground Level Concentrations (GLCs) of sulphur dioxide (SO_2) gas from electricity generation emission stacks in Barbados, and improve model performance by implementing reasonable modifications to the original AERMOD formulation.

1.1.1.1 Research Objectives

The objectives of this research are to:

- Derive the advection-duffision equation that describes the spatial distribution of particles under the process of atmospheric dispersion
- Derive the Eulerian form of the Gaussian plume equation from the advection-diffusion equation dispersion
- Examine the formulations of the parameters in AERMOD model
- Procure a set of alternate formulations for various parameters of the AERMOD model, suited to Caribbean meteorology, to modify the overall formulation AERMOD model
- Measure the performance of the alternate formulations in predicting measured values of the model parameters and compare this performance to the performance of the original AERMOD model formulations
- Measure the performance of the original AERMOD model, as well as the modified version(s) of the AERMOD model, in predicting measured values of SO_2 at specified locations across Barbados

1.1.1.2 Rationale for the Purpose of Study

Air quality research, and policy making, is generally centred around a group of 6 ubiquitous atmospheric contaminants, known as criteria pollutants (discussed in subsection 1.2.2). This group includes carbon monoxide (CO), sulphur dioxide (SO_2), nitrogen oxides (NO_x), lead gas (Pb), ground-level ozone (O_3) and particulate matter at both 10 µm (PM_{10}) and 2.5 µm ($PM_{2.5}$).

Atmospheric contamination contains a mixture of criteria pollutants in varying proportions from myriad sources. The mass concentration of each contaminant is measured by specific instruments, tailored to the chemical or mechanical nature of that contaminant. To adjust the project to a practical scale, we identified a single criteria pollutant to which the AERMOD model can be applied. This not only avoided substantial time and expense, but also avoided complexities which are not accounted for by the AERMOD implementation of the Gaussian plume equation.

In its simplest form, the Gaussian dispersion equation models the spatial distribution of air-bourne atmospheric contaminants emitted from station point sources at known constant rates in an ideal atmosphere (discussed in section 3.1). Several adjustments can be made to modify this idealistic form of the Gaussian dispersion equation to model a more realistic atmosphere (discussed in section 3.2). Several of these adjustments are accounted for in the AERMOD model; however, the AERMOD model does not adjust for non point sources. This eliminates a majority of contaminant sources across Barbados (discussed in section 1.3), except the industrial process of electricity generation by fossil fuel combustion. 4 of the 6 criteria pollutants, excluding Pb and O_3, are bi-products of fossil fuel combustion. Moreover, CO and NO_2 are major factors of roadway emissions (line source) and wind blown Sahara dust is a major source of PM_{10} and $PM_{2.5}$, and can also be eliminated.

The majority of SO_2 within the atmosphere is anthropomorphic in origin, and is emitted from industrial activity that processes materials that contain sulphur, e.g. the generation of electricity from coal, oil or gas that contains sulphur. With the changes the sulphur content of diesel, i.e. from Industrial spec (5000ppm) to Ultra-Low Diesel (15ppm) (The United Nations Environment Programme, 2016), the contribution from roadway emissions can be seen as negligible. Furthermore, sulphur dioxide accounts for approximately 95% of the sulphur content of fossil fuels involved in electricity generation (Department of the Environment and Heritage, Australia, 2005). Additionally, the primary fuel source used in electricity generation in Barbados is heavy fuel oil, with a substantial sulphur content (a mass % of 1.8 %).

In summary, we can conclude that electricity generation emission stacks are suitable stationary point sources and SO_2 for the implementation of the AERMOD model. Additionally, as other sources of SO_2 gas emit a negligible

amount of SO_2, in comparison to the stacks, SO_2 is the most appropriate criteria pollution for the purpose of this research.

1.2 Motivation

The term air pollution modelling encompasses a variety of mathematical implementations within the field of air quality monitoring, designed to understand, simulate and/or predict the spatio-temporal distribution of atmospheric contaminants. Air quality monitoring is currently among the primary areas of concern in the sustainable development of an economy (DiSano, 2002). With proper implementations, air pollution modelling can substantially aid the health, health policy and lifestyle choices of the population of any society. In this section, we will highlight the current need for monitoring air quality in Barbados and discuss the benefits of air pollution modelling to the health, policy and livelihood of the society of Barbados.

1.2.1 Air Quality and Health in Barbados

Continual exposure to air pollution at significant levels causes a range of health effects on the human population. The short-term effects include irritation to the eyes, nose and throat, and upper respiratory infections such as bronchitis and pneumonia, headaches, nausea, and allergic reactions. However, the more serious long term effects include chronic respiratory disease, lung cancer, heart disease, and even damage to the brain, nerves, liver, or kidneys. Additionally, air pollution exposure can aggravate the medical conditions of individuals with asthma and emphysema (Lee et al., 2014; World Health Organization, 2014, 2013, 2017).

In its 2012 publications on the global assessment and burden of disease of air pollution, the World Health Organization (WHO) cites air pollution to be the world's largest single environmental health risk, being responsible for about one-eighth of global deaths (World Health Organization, 2016, 2014). Throughout the years, air pollution has maintained its deadly status; however, in its latest publication on the global assessment and burden of disease of ambient air pollution, the WHO credits air pollution as being responsible for the slightly reduced figure of about one-ninth of global deaths

(World Health Organization, 2017). In both publications, the global burden of diseases analysis revealed that ischaemic heart disease, stroke, chronic obstructive pulmonary disease (COPD), lung cancer and acute lower respiratory infections in children are the major causes of premature death due to air pollution.

Historically, the aforementioned air-pollution-related causes of premature death, have been among the top contributors to the number of premature deaths in Barbados. A study of the burden of disease in Barbados, over the period 1990 to 2010, conducted by the Institute for Health Metrics and Evaluation (IHME) of the the University of Washington, listed ischaemic heart disease, stroke, lower respiratory infection and lung cancer among the top 25 causes of premature death. Over the period of the study, the aforementioned diseases contributed 8.7 %, 7.9%, 4.7% and 0.9%, respectively, in 1990, and 8.3%, 6.4%, 4.4% and 0.9%, respectively, in 2010 (Institute for Health Metrics and Evaluation, 2010). In a subsequent study of the burden of disease in Barbados, over the period 2005 to 2016, the IHME listed ischaemic heart disease and lower respiratory infection among the top 10 contributors to premature deaths in the island. Over the period of the study, the contribution of ischaemic heart disease and lower respiratory infection increased by 13% and 8.3%, respectively (Institute for Health Metrics and Evaluation, 2016).

In a study of asthma aggravation in Barbados, over the period 1993 to 2003, the International Union Against Tuberculosis and Lung Disease (The Union for short) estimated asthma prevalence among children of ages 13 and 14 to be 19.2% (The International Union Against Tuberculosis and Lung Disease, 2011). This estimate doubles the 10.4% estimate for asthma prevalence among children of ages 13 and 14 in Barbados, over the period 2000 to 2003, resulting from a similar study conducted by the Global Initiative for Asthma (Global Initiative for Asthma, 2016).The overall trend in asthma prevalence among adolescence seems to be decreasing, with the decreasing being mainly attributed to increased awareness (Monteil et al., 2005).

Rigid conclusions of the burden of disease attributed to air pollution usually involve combining estimates of exposure to air pollution and its distribution in the population, with results from epidemiological studies that indicate the additional disease burden from different levels of exposure to air pollution (World Health Organization, 2016; Lee et al., 2014). Without data on the present and historical spatial distribution of air pollution across Bar-

bados, any conclusions on the impact of air pollution on health in Barbados is inconclusive.

1.2.2 The Use of Air Pollution Modelling in Advising Air Quality Policies

Examples of air quality management at the governmental level, i.e. through air quality policies, are common throughout the historical period from the Industrial Revolution to present day. These policies have increased in their level of detail and sophistication and, resultantly, increased in their effectiveness. One of the earliest documented air quality policy is the 1875 Public Health Act, passed in the UK. The air quality management aspect of this general health policy was in the form of a single a section promoting smoke abatement in the effort to decrease the hazardous of smog events, which was common at the time (Her Majesty?s Stationery Office , 1875).

A prime example of the detail and sophistication of contemporary air quality policies is the Clean Air Act (CAA) of 1970, under which the US Environmental Planning Agency (EPA) was established. This act features specific National Ambient Air Quality Standards (NAAQS) for a group of 6 ubiquitous atmospheric contaminants, known as criteria pollutants, and includes carbon monoxide (CO), sulphur dioxide (SO_2), nitrogen oxides (NO_x), lead gas (Pb), ground-level ozone (O_3) and particulate matter at both 10 µm (PM_{10}) and 2.5 µm ($PM_{2.5}$). Under the enforcement of the US EPA, the CAA has lead to the phaseout of lead from gasoline in the US, which lead to a decrease in levels of lead in the air by 94 percent between 1980 and 1990 (US Environmental Protection Agency, 2017).

Air pollution modelling has become instrumental in advising air pollution policies. The US EPA achieves this through (US National Park Services, 2018):

- Dispersion Modeling - These models are typically used in the permitting process to estimate the concentration of pollutants at specified ground-level receptors surrounding an emissions source.
- Photochemical Modeling - These models are typically used in regulatory or policy assessments to simulate the impacts from all sources by

estimating pollutant concentrations and deposition of both inert and chemically reactive pollutants over large spatial scales.

- Receptor Modeling - These models are observational techniques which use the chemical and physical characteristics of gases and particles measured at source and receptor to both identify the presence of and to quantify source contributions to receptor concentrations.

Currently, there are myriad deficiencies in the air quality policies of Barbados. A 2015 examination of air quality policy in Barbados conducted by the United Nations Environment Programme (UNEP), in response to Resolution 7 of the United Nations Environment Assembly (UNEA), revealed that although Barbados has policies for renewable energy investments and incentives for clean production and installation of pollution prevention technologies, there was no information on a national air quality policy, a NAAQS, as well as several other air policies for the island (The United Nations Environment Programme, 2016).

1.2.3 Air Quality Indices as an Early Warning System using Forecasted Air Pollution Data

Another beneficial application of air pollution modelling is the developing of early warning systems issuing provide public health advisories concerning the GLCs of criteria pollutants. These advisories are produced by applying of Air Quality Indexs (AQIs) to measured/modelled air pollution data, transforming the data into easily understood, color-coded maps indicating the modelled spatio-temporal air quality over the given region.

Studies into the public awareness of air quality information, and how to access it, have produced mixed results with some research concluding that messages do not get into the public domain during potentially hazardous air quality conditions (Semenza et al., 2008; Ayres et al., 2011) and others reporting both awareness and compliance (Wen et al., 2009; McDermott et al., 2006) (Kelly et al., 2012). However, once sufficient awareness is achieved, early warning systems have been found to be quite effective. A good example of this is the effectiveness of AQIs in reducing the real-world adverse effects to air pollution for asthma-sensitive individuals, as stated by the US EPA

(The US Environmental Protection Agency, 2016). The US EPA supports this conclusion with the following studies:

- Data from the 2005 Behavioral Risk Factor Surveillance System conducted in six states (Colorado, Florida, Indiana, Kansas, Massachusetts, and Wisconsin). This data revealed that 31% of the respondents with lifetime asthma and 16% of those without asthma reported changes in outdoor activities because of media alerts of air quality. This data also highlighted the role played by health professionals as among the respondents who ever received advice from a health professional to reduce outdoor activity, about 51% of those without asthma and 57% of those with lifetime asthma reported a media alert-based outdoor activity change or reduction (for Disease Control et al., 2005).

- An activity diary study conducted by Mansfield et al. (2006). This study revealed that parents who thought that their asthmatic children were sensitive to air pollution reduced the time spent outdoor by their children by about 30 minutes on a "Code Red" day relative to a non-Code Red day. On days with Good (Green) air quality, the amount time spent outdoors was similar for asthmatic children who were believed to be sensitive and non-sensitive to air pollution.

- A correlation study on asthma hospitalizations, ozone concentrations and potential avoidance behaviour in response to forecasted air quality in Southern California, over the period 1989 to 1997 (Neidell and Kinney, 2010). This study found that individuals take substantial actions to reduce exposure to ozone with the availability of AQIs.

1.3 Air Contaminants across Barbados

The US National Park Service lists the main types of air pollution sources as (US National Park Services, 2018):

- mobile sources – such as cars, buses, planes, trucks, and trains

- stationary sources – such as power plants, oil refineries, industrial facilities, and factories

- area sources – such as agricultural areas, cities, and wood burning fireplaces
- natural sources – such as wind-blown dust, wildfires, and volcanoes

Across Barbados, major contamination sources include fossil fuel emissions from electricity generation stacks and vehicles, African Sahara dust and the occasional bush/grass fires. The activity of these sources have changed over the years.

A common result of a growing population is an increase in energy consumption, which can result in an increase in electricity generation through the burning of fossil fuels. However, over the years, the The Barbados Light and Power Company Limited (BLP), the island's sole provider of electric utility, has increasingly invested in energy production via renewable sources rather than the traditional fossil fuel burning. Additionally, the BLP introduced the Renewable Energy Rider initiative in mid–2010. This initiative allows customers to connect to the grid and sell any excess electricity generated from renewable sources to BLP. Currently, Barbados is serviced by 12 operational electricity generators, at 3 power generations stations (shown in Figure 1.1), located:

- along the Spring Garden Highway
- at the Garrison
- at the Sir Grantley Adams International Airport in Seawell

Generally, the burning of fossil fuels produce atmospheric contaminants such as CO, SO_2, NO_x and PM_{10} and $PM_{2.5}$. Other bi-products include heavy metals such as mercury and the green house gas carbon dioxide (Department of the Environment and Heritage, Australia, 2005).

Traffic emissions has been noted as a considerable issues in Barbados for years now (Pan American Health Organization, 2012), especially with the growing number of road users. Data from the Barbados Licensing Authority shows that the number of registered vehicles increased from around 17 000 in 1967 to approximately 34 000 in 1980, and from just under 40 000 in 1984 to about 57 000 in 19963. Data for June 1999 gave a total of 73 723 registered motor vehicles on the island, an average of about one per 3.6 persons in the

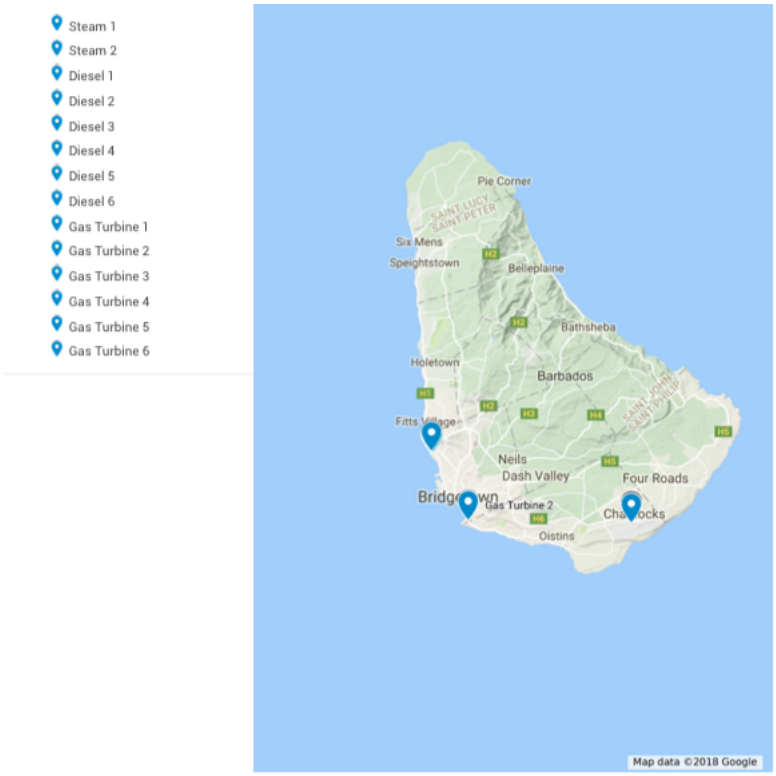

Figure 1.1: Map of Barbados: Showing the location of Electricity Generation Emission Stacks

population (The United Nations Environment Programme, 2016). Traffic emissions are generally composed of the same bi-products as those that evolve in electricity generation; however, they are present in different amounts.

Over the period 1965 to 1998, the measured concentration of dust at the easternmost point of the island (Ragged Point) showed significant climatic variability, particularly with immense dust clouds emerging from the coast of West Africa caused by dust storms. In cases of severe dust storms over the coast of West Africa, mass concentrations in Barbados often measured above 100 $\mu g\,m^{-3}$ (Prospero, 2006). This is definitely a cause for concern as this figure is well above the WHO Air Quality Guideline (AQG) 24-hour mean guideline value for particulate matter at both 10 μm (PM10) and 2.5 μm (PM2.5), being 25 $\mu g\,m^{-3}$ and 50 $\mu g\,m^{-3}$, respectively. According to WHO statistics, there is a correlated 0.2% to 0.6% increase in the all-cause mortality rate per 10 $\mu g\,m^{-3}$ of PM10 (World Health Organization, 2013).

Similarly, the occurrence of bush/grass fires show significant climatic variability, and is particularly correlated with dry weather conditions, often caused by a combination of high concentrations of Sahara dust and high temperatures. It is important to also note that the number of bush fires can be actively reduced via preventative measures, thus the number of bush fires will not necessarily correlate with drought intensity. This can easily seen in the yearly number of bush fires recorded by the Barbados Fire Station as record years of severe drought in Barbados (such as $2009 - 2010$ and 2015) experience a high number of bush fires but do no have the highest number of bush fires (shown in Table 1.1).

Major combustion by-products include carbon monoxide, carbon dioxide, nitrogen oxides, sulphur dioxide, particulate matter of various size distribution, aldehyde, polycyclic aromatic hydrocarbons and several other organic and inorganic compounds (Goh et al., 1999; Ward, 1989).

Table 1.1: Number of Bush Fires in Barbados, 2003-2017, according to the Barbados Fire Service (Barbados Fire Service, 2017)

Year	Number of Bush Fires
2003	1
2004	80
2005	1083
2006	1681
2007	1127
2008	1410
2009	910
2010	1341
2011	461
2012	964
2013	1136
2014	1397
2015	856
2016	751
2017	96

Chapter 2

Background

In this chapter, we provide a collection of theories and concepts pertaining to the structural and dynamic of the atmosphere that are involved in the spatio-temporal distribution of atmospheric contaminants under dispersion. Furthermore, we briefly discuss the dynamics of the primary types of air pollution models that lend support to the selection of the Gaussian model, and give an overview of AERMOD.

2.1 Overview of the Main Types of Air Pollution Models

The different approaches to air pollution model have their relative advantages and disadvantages. The major subdivisions of air pollution models are concerned with either the reference frame of the model (Eulerian versus Lagrangian) and the degree of predictability of the model (Deterministic versus Stochastic).

2.1.1 Deterministic versus Stochastic Air Pollution Models

Both deterministic and stochastic approaches are common in the field of air pollution modelling. Deterministic air dispersion models represent the

processes that determine the mass concentration of air pollutants within a specified area by employing dynamic equations derived using conservation laws. On the other hand, statistical models use static equations to model average (net) long-term patterns. These static equations are obtained by ignoring the local, time-varying processes that affect short-term air pollutants in true dispersion models. This simplification gives statistical models the advantage of relative ease of application and less demanding processing requirements.

The performance of statistical models are comparatively good to that of dispersion models when used to analyse relative long-term concentrations of locally-derived pollutants. However, the estimates of changes in concentration obtained are often unreliable as statistical models do not directly represent the processes determining air pollution concentrations. Deterministic models are predominantly used in air pollution simulation studies and air quality policy making while statistical models are mainly used in integrated assessments as screening tools.

2.1.2 Eulerian Models

Eulerian dispersion models define a fixed reference frame of points in a gridded system. At a particular time, t, the rate of change of mass concentration of a contaminant at a given location, referenced by the position vector $\mathbf{r} = (x, y, z)$, is seen as the summation of the processes of mass flux by advection and/or diffusion, source emission and destruction by sinks. This can be represented by the advection-diffusion equation, derived in subsection 3.1.1, given by:

$$\frac{\partial C}{\partial t} + \nabla \cdot J_A + \nabla \cdot J_D = S, \tag{2.1.1}$$

where, J_A is the mass flux due to simple linear advection, J_D is the mass flux due to diffusion and S is the source/sink term.

The advection-diffusion equation is the fundamental equation for Eulerian dispersion models. Specific Eulerian models are evolved from 2.1.1 by applying a set of physical assumptions, that describe the spread of the contaminant based on the physical and dynamic structure of the fluid medium of dispersion.

2.1.3 Lagrangian Model

Lagrangian dispersion models mathematically follow emitted contaminant plume parcels as they move in the atmosphere as a random walk process. Within the Lagrangian reference frame, the mass concentration at a particular receptor is the sum of the contribution from all emitted parcels within the system. The fundamental Lagrangian equation is given by (Nielinger et al., 2004; Zannetti, 2013):

$$< C\{\mathbf{r}, t\} >= \int_{-\infty}^{t} \int p\{\mathbf{r}, t|\mathbf{r}', t'\} S\{\mathbf{r}', t'\} d\mathbf{r}' dt', \tag{2.1.2}$$

where $p\{\mathbf{r}, t|\mathbf{r}', t'\}$ [m^{-3}] is the probability density function that an air parcel moves from position $\mathbf{r}$ at time t to position $\mathbf{r}'$ at time t' ($t > t'$) and $<>$ represents the ensemble average of a quantity.Conservation of mass requires that $p\{\mathbf{r},t|\mathbf{r}',t'\} = 1$, however, when chemical loss or deposition occurs $p\{\mathbf{r},t|\mathbf{r}',t'\} < 1$.Throughout the atmosphere, $S\{\mathbf{r}',t'\}$ can take both positive and negative values, being positive iff $\mathbf{r}'$ is a point of source emission of a primary pollutant and can be negative anywhere else. Primary pollutants is the collective name of pollutants that are added to the atmosphere by direct source emission, while secondary pollutants were formed from chemical and photochemical processes acting on primary pollutants.

By selecting an instance t_0 within the life cycle of the parcel (where $-\infty < t_0 < t$), $<C\{\mathbf{r},t\}>$ can be written as the sum of two integrals. Thus (2.1.2) becomes

$$< C\{\mathbf{r}, t\} >= \int_{-\infty}^{t_0} \int p\{\mathbf{r}, t|\mathbf{r}', t'\} S\{\mathbf{r}', t'\} d\mathbf{r}' dt' + \int_{t_0}^{t} \int p\{\mathbf{r}, t|\mathbf{r}', t'\} S\{\mathbf{r}', t'\} d\mathbf{r}' dt' \tag{2.1.3}$$

Integrating the first term in (2.1.3) with respect to t' gives

$$< C\{\mathbf{r}, t\} >= \int p\{\mathbf{r}, t|\mathbf{r}', t'\} C\{\mathbf{r}', t_0\} d\mathbf{r}' + \int_{t_0}^{t} \int p\{\mathbf{r}, t|\mathbf{r}', t'\} S\{\mathbf{r}', t'\} d\mathbf{r}' dt' \tag{2.1.4}$$

where $C\{\mathbf{r},t\}$ now becomes the sum of the indirect contribution of the source term to the background concentration of the entire computational domain, represented by the first term, and the direct contribution of the second integral. The background concentration over th entire computational domain is very difficult to calculate.

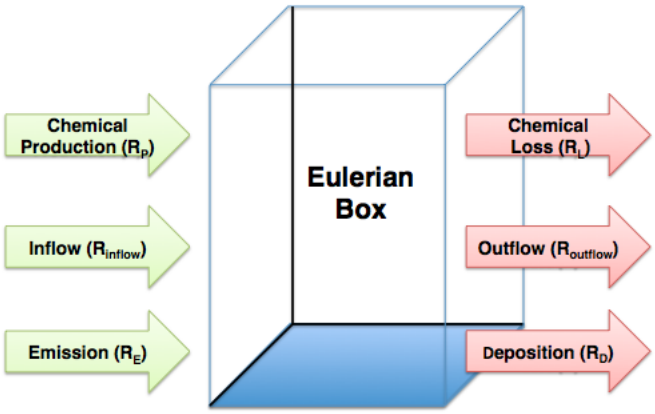

Figure 2.1: Schematic of the Eulerain Box Model with Sources and Sinks

The key parameter in (2.1.4) is the probability density function p. Different Lagrangian models are derived from (2.1.4) by making different assumptions concerning the nature of p.

2.1.4 Box Models

Box models simulate the mass concentrate within a block of air. This involves the formulation of a differential equation by controlling the number and complexity of emission sources and sinks and the dimensions of the box itself. In an Eulerian reference, the cross-sectional base of the box (Eulerian box) is set as the area of the location while the height can be either fixed or time-variant. Meanwhile, within the Lagrangian reference frame, the box models a parcel of air as it follows a trajectory and is allowed to mix with it's environment.

In its simplest form, the Eulerian box model can be used to simulate contaminant mass concentration within a fixed volume under the assumption of a steady state (i.e. $\frac{\partial C}{\partial t} = 0$), given by:

$$C = \frac{\Gamma_b \tau_b}{V_b}, \tag{2.1.5}$$

where Γ_b is the emission rate $[\mu\,\mathrm{g\,s^{-1}}]$ of the contaminant, τ_b [s] is the resi-

dence time of the contaminant particles and $V_b = ldh$ [m^3] is the volume of the Eulerian box.

(Ho et al., 2009) estimated the temporal variance of the mass concentration of PM_{10} in Thanh Xuan District, Hanoi, Vietnam, using an Eulerian box model. In this experiment, the mass concentration within the box was assumed to be in a transient state (i.e. $\frac{\partial C}{\partial t} \neq 0$), with a capacity of emission sources within the box, J_b [$\mu g\, m^2\, s^{-1}$], the linear of advection of contaminant within the box at a constant rate, C_u [$\mu g\, m^{-3}$], and removal of contaminant material from the box only by advection, and constant wind flow perpendicular to the width of the box, given by the Partial Differential Equation (PDE):

$$ldh\frac{\partial C}{\partial t} = J_b ld + dhu_b C_u - dhu_b C. \tag{2.1.6}$$

Jacob (1999) features the simulation of the mass concentration of an air parcel as it follows a trajectory and is allowed to mix with it's environment at a constant dilution or entrainment rate Γ_k, given by the Ordinary Differential Equation (ODE):

$$\frac{dm}{dt} = \Gamma_E + \Gamma_P - \Gamma_L - \Gamma_D + \Gamma_k \left(m - \frac{C_a}{V} \right) \tag{2.1.7}$$

where m [μg] is the mass of the contaminant within the parcel, C_a is the mass concentration of the surrounding air, Γ_E, Γ_P, Γ_L and Γ_D are the rate of source emission, chemical production, removal by sinks and chemical destruction, respectively.

2.1.5 Dense Gas Model

Dense gas models simulate the dispersion of negatively buoyant gas clouds which cannot be properly simulated by traditional dispersion models. They primary model the dispersion of the gas plume or cloud throughout its gravity spread phase where dispersion occurs due to the buoyancy-induced kinetic energy of the cloud and can be extended to model the stably stratified plume embedded in the mean wind flow and a probable positively buoyant phase. In this positively buoyant phase, buoyancy results in the lift-off and rise of the gas cloud; e.g. in cases of heat transfer from the ground or release of latent heat from water vapour that was mixed in the cloud.

Dense gas simulations are commonly done in both Eulerian and Lagrange reference frames, mainly using finite difference techniques to calculate direct solutions to the three dimensional conservation equations of mass, momentum and energy. Simulations are also commonly done via the modification of the box model or Gaussian model.

(Burton et al., 2017) simulated the 1986 Lake Lyos disaster in Cameroon using the Weather Research and Forecasting (WRF). The finite difference model was used to simulate the spread of the CO_2 parcel that emerged from the limnic eruption.

(Kunsch and Webber, 2000) modified a box model to describe a planar dense gas case, corresponding to a sloping channel flow, with the assumption of conservation of buoyancy (i.e. no lift-off and rise phase). The non-dimensional speed of the dense gas front is given by the equation

$$u_f = k_f \sqrt{\frac{h}{V}} = \frac{dl}{dt_x}, \tag{2.1.8}$$

where u_f is the dimensionless frontal velocity, k_f is the front Froude factor, V is the dimensionless volume of the gas cloud, l is the dimensionless distance of the front from the rear wall, h is the dimensionless height of the cloud, t is the dimensionless time. The volume of the gas cloud is given by:

$$V = lh - \frac{1}{2}\Gamma l^2, \tag{2.1.9}$$

where $\Gamma = \tan\{a\}$, a is the slope of the surface on which the cloud moves. The dilution of the initially released gas volume, due to air entrainment, which is scaled with the frontal area of the cloud is given by:

$$\frac{dv}{dt_x} = \kappa h u_f \tag{2.1.10}$$

where κ is the parameter for the entrainment scaled with the frontal area.

(Ermak et al., 1982) conducted Burro series Liquid Nitrogen Gas (LNG) spill test using a modified Gaussian Plume equation. The modified equation was in the form of a line source model in an environment where diffusion is anisotropic, further discussed in 3.2.7.

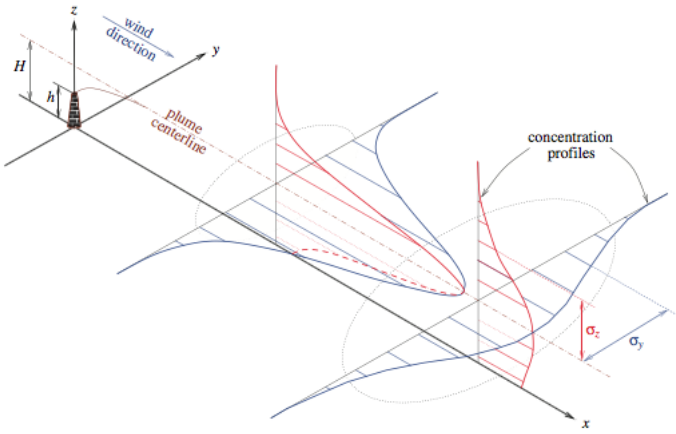

Figure 2.2: A contaminant plume emitted from a continuous point source, with wind direction aligned with the x-axis. Profiles of concentration are given at two downwind locations (vertical in red, horizontal in blue) and the Gaussian shape of the plume cross-sections are shown relative to the plume centerline

2.1.6 Gaussian Models

Gaussian models the most commonly used dispersion model and are applicable to modelling contaminant plume material as either a continuous plume or in discontinuous puffs. Gaussian models operate on the principle that the contaminant material being emitted is normally distributed about the axis synonymous with the direction of the wind.

In an Eulerian reference frame, the Gaussian plume equation, in its simplest form, is attained from 2.1.1 by assuming an ideal atmosphere. The features of this ideal atmosphere are:

- A single fixed point source emitting at a constant rate.
- Constant mean wind flow being purely horizontal (i.e. the mean wind flow has no vertical component).
- The solution is steady state.
- The eddy diffusities are functions of the downwind distance x only, and

diffusion is isotropic with the wind velocity, in the direction of the wind, being significantly large.

- Negligible variations in topology (i.e. flat terrain).
- The contaminant does not penetrate the ground.

Under these minimum assumptions, the Gaussian Plume equation is derived as:

$$C\{x,y,z\} = \frac{Q}{2\pi u\sigma^2}\exp\left\{-\frac{y^2}{2\sigma}\right\}\left[\exp\left\{-\frac{(z-H)^2}{2\sigma}\right\}+\exp\left\{-\frac{(z+H)^2}{2\sigma}\right\}\right], \tag{2.1.11}$$

where Q $[\mu\,\mathrm{g\,s^{-1}}]$ is the source emission rate, u is the speed of the mean horizontal wind, σ is the standard deviation of the emission distribution and H is the effective height. A complete derivation of the Gaussian Plume equation is provided in subsection 3.1.1.

In a Lagrangian reference frame, the Gaussian Puff model is obtained from 2.1.2 under the assumptions:

- Turbulence is stationary and homogeneous.
- p obeys a multidimensional normal distribution.
- The average displacement of a particle is due only to the mean (deterministic) wind

Under these assumptions, the Gaussian Puff equation is derived as (Yamada, 2000):

$$C\{x,y,z\} = \frac{Q\Delta t}{(2\pi)^{\frac{3}{2}}}\sum_{k=1}^{N}\frac{1}{\sigma_{xk}\sigma_{yk}\sigma_{zk}}\exp\left\{-\frac{(x_k-x)^2}{2\sigma_{xk}}\right\}\exp\left\{-\frac{(y_k-y)^2}{2\sigma_{yk}}\right\}\times \left(\exp\left\{-\frac{(z_k-z)^2}{2\sigma_{zk}}\right\}+\exp\left\{-\frac{(z_k+z-2z_g)^2}{2\sigma_{zk}}\right\}\right) \tag{2.1.12}$$

where (x,y,z) and (x_k,y_k,z_k) is the location of the receptor and the k^{th} puff, respectively, σ_{xk}, σ_{yk} and σ_{zk} are standard deviations of a Gaussian distribution and z_g is the ground elevation.

2.1.7 Overview of Aermod

AERMOD is a steady state Gaussian dispersion model developed by the American Meteorological Society (AMS)/United States Environmental Protection Agency (EPA) Regulatory Model Improvement Committee (AERMIC) to introduce state-of-the-art modelling concepts into the air quality models of the US EPA. After rigorous performance tests against leading air pollution models at that time, including Industrial Source Complex Model (ISC3) (EPA, 1995), Improved Complex Terrain Dispersion (CTDMPLUS) (Venkatram et al., 2001), Rough Terrain Diffusion Model (RTDM) (Paine and Egan, 1987) and Hybrid Plume Dispersion Model (HPDM) (Hanna and Chang, 1991), AERMOD was adopted and promulgated by the US EPA as their preferred regulatory model, effective December 9, 2005.

The AERMOD modelling system models contaminant dispersion at generated receptor grids by its dispersion model, referred to simply as AERMOD, using values of model parameters generated for each receptor grid. The required model parameters are produces by one of two preprocessors. The AERMIC Meteorological Preprocessor (AERMET) provides AERMOD with the meteorological information it needs to characterize the Planetary Boundary Layer (PBL) while AERMIC Terrain Preprocessor (AERMAP) provides information that characterizes the terrain, and generates receptor grids.

The AERMOD modelling system accounts several features of modern air pollution models (further discussed in chapter 4); including:

- Multiple point, area and volume sources
- Source dynamics of the Convective Boundary Layer (CBL), i.e. a direct, indirect and penetrated source
- Urban versus rural locations
- Continuous, buoyant plumes
- Dry or wet deposition of particles and/or gases
- Non-Gaussian (skewed) vertical distribution
- Vertical In-homogeneity of the PBL

- Simple or complex terrain
- building effects

2.2 The Planetary Bounday Layer

The PBL, also called the friction layer, is the lower most part of the earth's atmosphere, lying adjacent to and is influenced by the surface of the earth. It is a quasi-homogeneous layer, having near constant potential temperature (θ [K]) and is characterized by turbulent fluxes of heat, momentum, water and air pollutants (Panofsky and Dutton, 1984). In terms of turbulence, the PBL can be described as the layer extending from the surface of the earth to the height at which the turbulence, from the interactions between the earth's surface and its atmosphere, becomes negligible as the turbulence loses its kinetic energy to friction as well as converting the kinetic to potential energy in a density stratified flow (Nieuwstadt and Brost, 1986).

The PBL is categorized into convectively stable (referred to as the Stable Boundary Layer (SBL)) and unstable (referred to as the CBL) phases, separated by a transition phases of neutral convective stability, and are associated with the sign of the sensible surface heat flux (Φ_H). Φ_H is positive during the CBL, negative during the SBL and zero during the neutral transition phase. This categorization is important to air pollution modelling as the change in physical structure between the phases corresponds to changes in the atmospheric dynamics that describe the dispersion of air contaminants within the PBL.

2.2.1 Atmospheric Turbulence and the Physical Structure of the PBL

The physical stratification of the PBL is a direct result of the presence and magnitude of convective and mechanical turbulent kinetic energy, also known as turbulence or velocity variance, within the PBL. The result of this turbulence is a pseudo-homogeneous mixed/mixing layer having nearly constant potential temperature and specific humidity with height. Generally, the terms mixed/mixing layer and the CBL are interchangeable (**?**); however,

for the purpose of this paper, we reserve the term "mixing layer" strictly to refer to the portion of the PBL in which atmospheric properties, such as water vapour and pollutants, are mixed via turbulence.

Atmospheric turbulence can be generated by a number of convective and/or mechanical processes. Mechanical turbulence is the horizontal and/or vertical wind shear resulting from surface friction and the roughness of the underlying surface, wind strength and atmospheric stability. On the other hand, convective turbulence is wind shear caused by up-draughts and down-draughts within convective cells, outside (especially above and below) cumulonimbus clouds, in dry thermals on hot, sunny days in down-draughts associated with precipitation. (**?**). For the purpose of this paper, we define the Mechanical Mixing Layer (MML) as the portion of the PBL that hosts nearly all the mechanical turbulence within the PBL and extends to a height known as the mechanical mixing height (z_{im} [m]) and the Convective Mixing Layer (CML) as the portion of the PBL that hosts convective turbulence and extends to a height known as the convective mixing height (z_{ic} [m]). Hence, the MML is a feature of both teh CBL and SBL while the CML is only a feature of the CBL. For the purpose of this these, we reserve the term "mixing layer height" (z_i [m]) to strictly refer to the depth of the PBL, regardless of its state.

The layers of the physically stratified CBL include (Zannetti, 2013):

1. The Laminar Sub-layer (0 to z_0 m) - This is a shallow layer extending from the surface of the earth to the roughness length (z_0 [m]) (discussed in **??**). Within a thin film of the laminar sub-layer, extending from the ground (about 1 mm), motion is primarily laminar and the fluxes of heat, moisture and surface frictional effects are transferred through non-turbulent and molecular processes.

2. The Surface Layer (z_0 to about $0.1z_i$) - This layer extends from the roughness length to about a tenth of the mixing layer height (Panofsky and Dutton, 1984) (discussed in **??**). Within the surface layer, the fluxes of heat, moisture and trace gases experience their greatest vertical gradients due to the abundance of mechanical turbulence. These vertical gradients are assumed to be independent of height and the Coriolis effect is negligible.

3. The Ekman Layer or Mixed Layer ($0.1z_i$ to z_i) - The Ekman Layer

extends from the top of the surface layer to the top of the CBL. Within the Ekman layer, potential temperature (θ [K]) and specific humidity (q [dimensionless]) have become homogenized due to active turbulence.

4. The Entrainment Inter-facial Layer - The entrainment inter-facial layer is the stable layer capping of the Ekman layer. Within this layer, material from the CBL can be injected by intermittent turbulence within the CBL from overshooting convective cells.

5. Free Atmosphere - Above the CBL lies the free atmosphere, in which the effect of the earth's surface friction on the air motion is negligible, and in which the air is usually treated (dynamically) as an ideal fluid.

The layers of the physically stratified SBL include (Zannetti, 2013):

1. The Surface Layer (approximately z_0 to about $0.1z_i$)

2. The Nocturnal Inversion Layer or Stable Boundary Layer (z_0 to z_i)- The nocturnal inversion layer is a stable layer that forms at the surface of the earth in the absence of solar influx, mainly on cool, cloud free nights.

3. The Residual Layer - Above the stable boundary layer lies the collapsed Ekman layer of the previous CBL

4. Free Atmosphere

2.2.2 Monin-Obukhov Similarity Theory and Atmospheric Dynamics within the PBL

Monin and Obukhov (1954) theorized that the vertical variation of mean flow and turbulence characteristics in the surface (mxing) layer is a function of the surface momentum and buoyancy fluxes and the height, summarized a single length scale known as the stability parameter (ζ). The Monin-Obukhov Similarity (MOS) theory describes the vertical profiles of non-dimensionalized mean wind speed u [$\mathrm{m\,s^{-1}}$]and mean potential temperature θ [K], within the horizontally homogeneous and temporally stationary turbulent mixing layer,

under non-neutral conditions, by the system of equations:

$$u\{z\} = \frac{u_*}{k_v}\left[\ln\left\{\frac{z}{z_0}\right\} - \psi_M\{\zeta\} + \psi_M\{\zeta_0\}\right] \tag{2.2.1a}$$

$$\theta\{z\} = \theta\{z_0\} + \frac{\theta_*}{k_v}\left[\ln\left\{\frac{z}{z_0}\right\} - \psi_H\{\zeta\} + \psi_H\{\zeta_0\}\right] \tag{2.2.1b}$$

$$\zeta = \frac{z}{L} \tag{2.2.1c}$$

$$L = -\frac{\rho_a c_{pa} {u_*}^3 T_{ref}}{k_v g_0 \Phi_H} \tag{2.2.1d}$$

$$u_* = \frac{k_v u_{ref}}{\ln\{\frac{z_{u_{ref}}}{z_0}\} - \psi_M\{\zeta_u\} + \psi_M\{\zeta_0\}} \tag{2.2.1e}$$

$$\theta_* = \frac{k_v(\theta_2 - \theta_1)}{\ln\{\frac{z_2}{z_1}\} - \psi_H\{\zeta_2\} + \psi_M\{\zeta_1\}} \tag{2.2.1f}$$

$$\Phi_H = -\rho_a c_{pa} u_* \theta_* \tag{2.2.1g}$$

where

- u [$\mathrm{m\,s^{-1}}$] is the lateral mean wind speed within the mixing layer.
- θ [K] is the lateral mean potential temperature within the mixing layer.
- L [m] is the Obukhov length - a length scale depicting the height at which turbulence is generated more by buoyancy than by wind shear. When combined with the actual height within the PBL, L helps to form the stability parameter (ζ [dimensionless]) theorized in MOS theory (discussed in **??**).
- u_* [$\mathrm{m\,s^{-1}}$] is the Shear velocity (formerly friction velocity) - a form of shear stress between the layers of a viscous fluid. Shear stress is the force that tends to cause deformation of a material by slippage along a plane or planes parallel to the imposed stress. It is a scaling parameter for the fluctuating component of velocity in turbulent flows.
- $\zeta = \frac{z}{L}$ [dimensionless] is the stability parameter - a single non-dimensional combination of the surface momentum flux as measured by u_*, buoyancy flux and height, where $\zeta_0 = \frac{z_0}{L}$.

- θ_* [K] is the potential temperature scale - a temperature scale used to describe turbulent flow flow within the mixing layer
- Φ_H [$\mathrm{W\,s^{-1}}$] is the sensible surface heat flux - the conductive heat flux from the Earth's surface to the atmosphere(discussed in section 5.1).
- k_v [dimensionless] is the von Kármán constant
- z_0 [m] is the roughness length - the height within the turbulent mixing layer at which the wind speed theoretically becomes zero
- g_0 is the standard acceleration due to gravity
- ψ_M [dimensionless] and ψ_H [dimensionless] are universal stability functions of the momentum and heat fluxes, respectively, within the mixing layer
- ρ_a is the standard air density
- c_{pa} is the specific heat capacity of dry air at constant pressure
- u_{ref} [$\mathrm{m\,s^{-1}}$] is the wind speed measured at the reference height for wind measurements ($z_{u_{ref}}$ [m])
- T_{ref} [K] is the air temperature measured at the reference height for temperature measurements ($z_{T_{ref}}$ [m])
- θ_1 [K] and θ_2 [K] are the potential temperature corresponding to the heights z_1 and z_2, respectively.

?

Vertical-velocity spectra obey Monin-Obukhov similarity theory up to a height of about 50 m. Their shapes are reasonably uniform, the major change with stability being a change of scale of the wave number axis, i.e., any characteristic nondimensional wave number is a function of z/L only. This function appears to be the same as the relation between the normalized dissipation and z/L. These results are consistent with previously measured Kolmogorov constants and with measured ratios of standard deviation of vertical velocity to friction velocity. Up to about a height of 50 m the wavelengths of the maxima of the logarithmic spectra increase linearly with height

and more slowly thereafter, up to about 300 m. The spectra in stable air above 50 m suggest the existence of a buoyant sub-range.

(iv) Longitudinal spectra do not obey similarity theory in a number of ways. The wavelengths do not scale with height, and there may be differences between sites when the spectra are plotted in similarity coordinates.

2.2.3 Deardorff Similarity Theory

Deardorff (1970) developed an alternate for MOS theory within the CBL, commonly referred to as Deardorff similarity theory. (**?**) recognized that MOS similarity does not apply to horizontal velocity spectra, since the length scale of their peaks is independent of height. In a study of the vertical velocity spectra on data obtained from the Kansas experiment (**?**), **?** noted that the vertical velocity spectra obeys MOS theory only up to a height of about 50m. **?** argued that this could be explained by the effects of large eddies that obey mixed-layer scaling in the dominance of convective conditions within the CBL. Deardorff (1970) addressed this issue with the introduction of a convective velocity scale found to be coherent with large eddies within the CBL.

Deardorff (1970) developed a convective velocity scale, known as the Deardorff velocity (w_* [$\mathrm{m\,s^{-1}}$]), synonymous to u_* by letting $z \to z_i$, to justify the dominance of convective conditions within the CBL resulting in large eddies that obey mixed-layer scaling, given by:

$$w_* = \left(\frac{g_0 \Phi_H z_i}{\rho_a c_{pa} T_{ref}} \right)^{\frac{1}{3}}. \tag{2.2.2}$$

2.2.4 Radiative-Balance of the Earth-Atmosphere system

Generally, studies involving the Earth-Atmosphere radiative balance and energy budget are concerned with the exchange of short-wave solar and long-wave terrestrial radiation between the surface of the Earth and the top of the atmosphere. The "top of the atmosphere" represents the dividing line between the Earth's atmosphere and space where solar flux enters the Earth system and where reflected and/or refracted solar flux and terrestrial flux

exits the Earth-atmosphere system and is estimated to be about 20km above the surface of the Earth (**?**).

The net radiative flux (Φ_N [W m^{-2}]) is the radiative balance of the earth-atmosphere system, given by the equation:

$$\Phi_N = \Phi_{in} - \Phi_{out} \tag{2.2.3}$$

where:

- Φ_N [W m^{-2}] is the net radiative flux.
- Φ_{in} [W m^{-2}] represents incoming radiation. The major component of Φ_{in} is the short-wave portion of the solar influx reaching the surface of the Earth, known as the global solar radiation (Φ_{S_0} [W m^{-2}]). The minor component of Φ_{in} is long-wave radiation that is increased with increasing cloud cover due to reflected/refraction of terrestrial flux (Holtslag and Van Ulden, 1983).
- Φ_{out} [W m^{-2}] represents the outgoing radiation in the form of short-wave solar flux reflected/refracted by the Earth-Atmosphere system as well as long-wave terrestrial radiation from the surface of the Earth (Holtslag and Van Ulden, 1983).

At the top of the atmosphere, the solar influx is known as the solar constant ($\phi_{const} = 1367 \pm 7$W m^{-2} (Organization, 1982)). As the solar influx travels through the atmosphere, it undergoes attenuation from atmospheric gases and clouds and only a portion reaches the surface, with some of this portion being from the direct beam (known as the direct beam radiation ($\Phi_{S_{cb}}$ [W m^{-2}])) and the other part being diffused by atmospheric particles (known as the diffuse sky radiation ($\Phi_{S_{cd}}$ [W m^{-2}])). $\Phi_{S_{cb}}$ and $\Phi_{S_{cd}}$ are the two components of Φ_{S_0}.

Φ_N can be represented as the summation of its three component fluxes, given by:

$$\Phi_N = \Phi_H + \Phi_{LE} + \Phi_G \tag{2.2.4}$$

where:

- Φ_N [W m^{-2}] is the radiative flux

- Φ_H [$\mathrm{W\,m^{-2}}$] is surface sensible heat flux - is the vertical energy flux between the Earth's surface and its atmosphere via the dry atmosphere.
- Φ_{LE} [$\mathrm{W\,m^{-2}}$] is surface latent heat flux - the vertical energy flux between the Earth's surface and its atmosphere via evaporated water.
- Φ_G [$\mathrm{W\,m^{-2}}$] is the ground heat flux - the vertical energy flux through the soil

2.3 Synoptic and Upper Air Meteorological Reports

Chapter 3

The Gaussian PDF Dispersion Equation: Derivation and Adjustments

In this chapter, we discuss the problem of modelling the spatio-temporal distribution of air-borne contaminant particles that spread under the summed effects of linear advection and molecular diffusion, known as dispersion.

We begin with a control volume analysis and, by an application of mass conservation laws, derive the advection-diffusion equation that governs atmospheric dispersion in an Eulerian reference frame. Subsequently, by making a series of simplifying assumptions, we use the advection-diffusion equation to derive the Gaussian plume dispersion equation. Furthermore, since some of the simplifying assumptions are quite idealistic, we modify the derived Gaussian dispersion equation to account for realistic conditions within the earth-atmospheric system.

3.1 Atmospheric Dispersion and the Gaussian Equation

Let X denote an arbitrary air contaminant of mass $M\{t\}$ [µ g] within a fixed, rigid, finite control volume of length δx, width δy and height δz. We

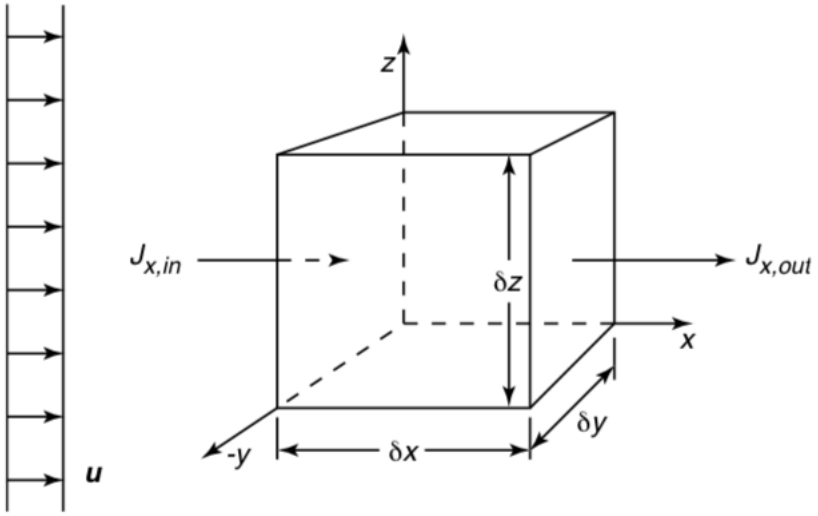

Figure 3.1: Schematic of the control volume with zonal flow

define the mass concentration of X within the control volume ($C\{t\} = \frac{M\{t\}}{\delta x \delta y \delta z}$ [µ g m^{-3}]) as the mass of X divided by the volume of the control volume.

Within the control volume, the positional change of each molecule, within a given time step (δt [s]), is determined by the strength of the wind vector ($\mathbf{u} = (u_x, u_y, u_z)$ [m s^{-1}]) and concentration gradient ($\Delta C = \left(\frac{\partial C}{\partial x}, \frac{\partial C}{\partial y}, \frac{\partial C}{\partial z}\right)$ [µ g m^{-1}]), which are both assumed to be constant throughout the time step.

The effects of advection and diffusion on molecules are clearly independent. By the principle of superposition, the effects of linearly independent processes can be summed together. Zonally, i.e. in the x-direction, each molecule of X will move a distance of $u_x \delta t$ under the influence of linear advection, and diffuse a distance of $\pm \delta x$ [m] under the influence of the concentration gradient. Thus, the total zonal distance within the time step can is given by $u_x \delta t \pm \delta x$. By generalizing, the total meridional and vertical distance, i.e. in the y-direction and z-direction respectively, within the time step can is given by $u_y \delta t \pm \delta y$ and $u_z \delta t \pm \delta z$ respectively.

Due to the rigid property of the control volume, changes in C solely depend on the resultant mass flux density ($\mathbf{J}\{t\} = (J_x\{t\}, J_y\{t\}, J_z\{t\})$ [µ g m^{-2} s^{-1}]) within the control volume. We define the mass flux density

($\mathbf{J}\{t\} = \mathbf{J}_A\{t\} + \mathbf{J}_D\{t\}$) as the rate of mass flow per unit area, where $\mathbf{J}_A\{t\} = (J_{A_x}\{t\}, J_{A_y}\{t\}, J_{A_z}\{t\})$ and $\mathbf{J}_D\{t\} = (J_{D_x}\{t\}, J_{D_y}\{t\}, J_{D_z}\{t\})$ are the contributions to the mass flux density by advection and diffusion, respectively. While $\mathbf{J}_A$ depends simply on mass concentration and flow velocity, $\mathbf{J}_D$ relates to the movement of molecules from regions of high concentration to regions of low concentration and is proportional in magnitude to the mass concentration gradient (ΔC), as described by Fick's law of diffusion.

The component forms of mass flux density by advection and diffusion are given by:

$$J_{A_x}\{t\} = u_x C\{t\} \tag{3.1.1a}$$
$$J_{A_y}\{t\} = u_y C\{t\} \tag{3.1.1b}$$
$$J_{A_z}\{t\} = u_z C\{t\} \tag{3.1.1c}$$

and

$$J_{D_x}\{t\} = -K_x \frac{\partial C\{t\}}{\partial x} \tag{3.1.2a}$$
$$J_{D_y}\{t\} = -K_y \frac{\partial C\{t\}}{\partial y} \tag{3.1.2b}$$
$$J_{D_z}\{t\} = -K_z \frac{\partial C\{t\}}{\partial z} \tag{3.1.2c}$$

where, K_x [$\mathrm{m^2\,s^{-1}}$], K_y [$\mathrm{m^2\,s^{-1}}$] and K_z) [$\mathrm{m^2\,s^{-1}}$] are the zonal, meridional and vertical constants of proportionality, respectively, defined by Fick's law of diffusion.

By applying the principle of superposition, we write the 3-D vector form of the mass flux density as:

$$\mathbf{J} = (u_x C, u_y C, u_z C) - \left(K_x \frac{\partial C}{\partial x}, K_y \frac{\partial C}{\partial y}, K_z \frac{\partial C}{\partial z} \right). \tag{3.1.3}$$

Written for convenience as:

$$\mathbf{J} = \mathbf{u}\nabla.C - \mathbf{K}\nabla^2 C, \tag{3.1.4}$$

3.1.1 The Advection-Diffusion Equation

The advection-diffusion equation is a second-order parabolic PDE obtained through conservation laws within an Eulerian reference frame. Under mass

conservation, the net mass flux through the control volume $\left(\frac{\partial M}{\partial t}\right)$ is the resultant of mass inflow and outflow. The zonal net mass flux can be calculated by:

$$\left.\frac{\partial M}{\partial t}\right|_x = \left.\frac{\delta M}{\delta t}\right|_{x_{in}} - \left.\frac{\delta M}{\delta t}\right|_{x_{out}} \tag{3.1.5}$$

where the subscripts x_{in} and x_{out} indicate mass influx and outflux.

Since our control volume is rigid, i.e., the area of the boundaries are fixed, the mass flux equates to the product of the mass flux density and boundary area. By applying this concept, we rewrite (3.1.5) as:

$$\left.\frac{\partial M}{\partial t}\right|_x = J_{x_{in}}\delta y\delta z - J_{x_{out}}\delta y\delta z. \tag{3.1.6}$$

where $J_{x_{in}}$ and $J_{x_{out}}$ are the zonal mass flux density for inflow and outflow. Moreover, by separating $J_{x_{in}}$ and $J_{x_{out}}$ into advection and diffusion contributions, expands to give:

$$\left.\frac{\partial M}{\partial t}\right|_x = \left(u_x C - K_x \left.\frac{\partial C}{\partial x}\right|_{x_{in}}\right)\delta y\delta z - \left(u_x C - K_x \left.\frac{\partial C}{\partial x}\right|_{x_{out}}\right)\delta y\delta z. \tag{3.1.7}$$

First order Taylor series approximations can be made for $u_x C|_{x_{out}}$ and $\left.\frac{\partial C}{\partial x}\right|_{x_{out}}$, given by:

$$u_x C|_{x_{out}} \approx u_x C|_{x_{in}} + \frac{\partial C}{\partial x}\delta x, \tag{3.1.8a}$$

$$\left.\frac{\partial C}{\partial x}\right|_{x_{out}} \approx \left.\frac{\partial C}{\partial x}\right|_{x_{in}} + \frac{\partial^2 C}{\partial x^2}\delta x. \tag{3.1.8b}$$

By substituting (3.1.8a) and (3.1.8b) into (3.1.1) and simplifying, we obtain:

$$\left.\frac{\partial M}{\partial t}\right|_x = \left(-\frac{\partial u_x C}{\partial x} + K_x \frac{\partial^2 C}{\partial x^2}\right)\delta x\delta y\delta z. \tag{3.1.9}$$

Dividing 3.1.9 by $\delta x\delta y\delta z$, on both sides, and generalizing for the meridional and vertical directions, the component forms of the advection-diffusion

equation is given as:

$$\left.\frac{\partial C}{\partial t}\right|_x = \left(-\frac{\partial u_x C}{\partial x} + K_x \frac{\partial^2 C}{\partial x^2}\right) \tag{3.1.10a}$$

$$\left.\frac{\partial C}{\partial t}\right|_y = \left(-\frac{\partial u_y C}{\partial y} + K_y \frac{\partial^2 C}{\partial y^2}\right) \tag{3.1.10b}$$

$$\left.\frac{\partial C}{\partial t}\right|_z = \left(-\frac{\partial u_z C}{\partial z} + K_z \frac{\partial^2 C}{\partial z^2}\right). \tag{3.1.10c}$$

The advection-diffusion equation in vector form is given by:

$$\frac{\partial C}{\partial t} + \nabla \cdot (\mathbf{u}C) - \mathbf{K}\nabla^2 C = 0, \tag{3.1.11}$$

(3.1.11) describes a scenario where mass is conserved within a system void of sources and sinks. With the addition of a source/sink term (S $[\mathrm{k\,g\,m^{-3}\,s^{-1}}]$, the advection-diffusion equation becomes:

$$\frac{\partial C}{\partial t} + \nabla \cdot (\mathbf{u}C) = \mathbf{K}\nabla^2 C + S. \tag{3.1.12}$$

Finally, by expanding the advection term,

$$\nabla.(\mathbf{u}C) = \mathbf{u}\nabla C + C\nabla \cdot \mathbf{u},$$

and the general incomprehensibly of the atmosphere under conditions of subsonic airflow,

$$\nabla \cdot \mathbf{u} = 0$$

we obtain the most common form of the advection-diffusion equation:

$$\frac{\partial C}{\partial t} + \mathbf{u}\nabla \cdot C = \mathbf{K}\nabla^2 C + S. \tag{3.1.13}$$

3.1.2 The Gaussian Plume Dispersion Equation

We Derive the Gaussian plume dispersion equation by first formulating 2 well-posed diffusion equations obtained by applying a number of simplifying assumptions to the advection-diffusion equation. Subsequently, we obtain the the Gaussian plume dispersion equation from the diffusion equations by an application of Laplace transforms.

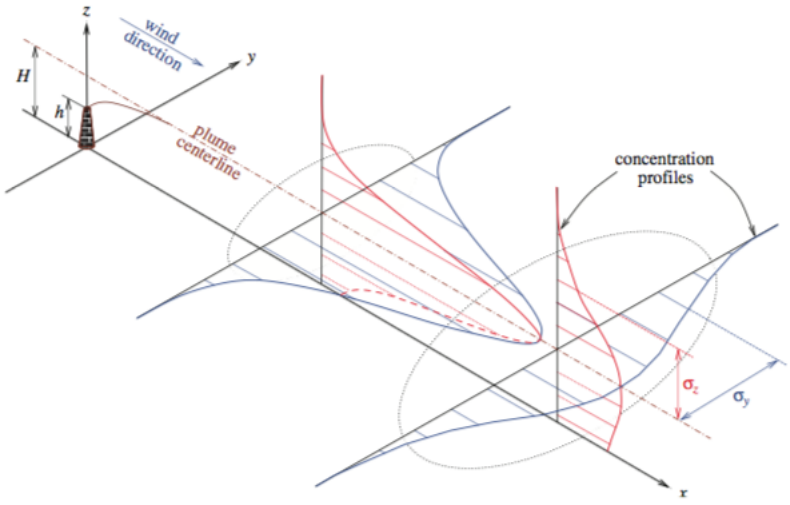

Figure 3.2: A contaminant plume emitted from a continuous point source, with wind direction aligned with the x-axis. Profiles of concentration are given at two downwind locations (vertical in red, horizontal in blue) and the Gaussian shape of the plume cross-sections are shown relative to the plume centerline.

3.1.2.1 2-Dimensional Diffusion Equations

We apply the advection-diffusion equation to vector field, with position vector $\mathbf{r} = (x, y, z)$. At a particular time (t), the mass concentration of X, within the vector field, is given by:

$$\frac{\partial C}{\partial t} + \mathbf{u}\nabla \cdot C = \mathbf{K}\nabla^2 C + S. \tag{3.1.14}$$

where:

- $C = C\{\mathbf{r}, t\}$ $[\mu\,\mathrm{g\,m^{-3}}]$ is the mass concentration of X
- $\mathbf{u} = \mathbf{u}\{\mathbf{r}, t\} = (u_x\{\mathbf{r}, t\}, u_y\{\mathbf{r}, t\}, u_z\{\mathbf{r}, t\})$ $[\mathrm{m\,s^{-2}}]$ is the wind vector
- $\mathbf{K}\{\mathbf{r}\} = (K_x, K_y, K_z)$ $[\mathrm{m^2\,s^{-1}}]$ is Fick's constant
- $S = S\{\mathbf{r}, t\}$ $[\mu\,\mathrm{g\,m^{-3}\,s^{-1}}]$ is the source/sink term

Assumption 1 (Single Point Source with Constant Rate of Emission) *Molecules of X is being emitted from a single point source located at $\mathbf{r}_s = (0, 0, H)$ [m] at a constant rate Q^P [$\mu g\, s^{-1}$], where $H = h_s + \Delta h$ is an effective height calculated from the sum of the actual stack height (h_s [m]) and the plume rise height (Δh [m]), which is determined by the buoyancy of the air.*

Assumption 2 (Negligible Variations in Topology) *Variations in topography are negligible so that the ground surface can be taken as the plane $z = 0$.*

Following Assumption 1 and 2, we rewrite S in terms of a constant emission rate (Q^P) using the Dirac delta function ($\delta\{\cdot\}$ [m^{-1}]), defined by:

$$\delta\{x\} = \begin{cases} +\infty & x = 0 \\ 0 & x \neq 0 \end{cases} \tag{3.1.15}$$

The Dirac delta function also satisfies the constrain:

$$\int_{x_1}^{x_2} \delta\{x - a\} dx = 1, \qquad\qquad a \in [x_1, x_2]$$

Applying $\delta\{\cdot\}$, we rewrite S in terms of Q^P, given by:

$$S = Q^P \delta\{x\}\delta\{y\}\delta\{z - H\}. \tag{3.1.16}$$

and hence, we rewrite 3.1.14 as:

$$\frac{\partial C}{\partial t} + \mathbf{u}\nabla \cdot C = \mathbf{K}\nabla^2 C + Q^P \delta\{x\}\delta\{y\}\delta\{z - H\}. \tag{3.1.17}$$

Assumption 3 (Purely Zonal Wind of Constant Speed) *The wind velocity is constant and aligned with the positive x-axis, i.e. $\mathbf{u} = (u, 0, 0)$, where $u \geq 0$ is the mean horizontal wind speed.*

Assumption 3 simplifies the advective term, i.e. $\mathbf{u}\nabla \cdot C = u\frac{\partial C}{\partial x}$, and hence simplifies 3.1.17 to:

$$\frac{\partial C}{\partial t} + u\frac{\partial C}{\partial x} = \mathbf{K}\nabla^2 C + Q^P \delta\{x\}\delta\{y\}\delta\{z - H\}. \tag{3.1.18}$$

Assumption 4 (Solution is Steady State) *The solution is steady state, i.e.* $\frac{\partial C}{\partial t} = 0$.

Assumption 4 demands the either wind velocity and all other parameters be independent of time or that the time scale of interest is sufficient large. This assumption simplifies 3.1.18 to:

$$u\frac{\partial C}{\partial x} = \mathbf{K}\nabla^2 C + Q^P\delta\{x\}\delta\{y\}\delta\{z-H\}. \tag{3.1.19}$$

Assumption 5 (Isotropic Diffusion) *The eddy diffusivities are functions of the downwind distance x only, and diffusion is isotropic (i.e* $K_x\{x\} = K_y\{x\} = K_z\{x\} = K\{x\}$*).*

Assumption 5 reduces the diffusive term, i.e. $\mathbf{K}\nabla^2 C = K\frac{\partial^2 C}{\partial x^2} + K\frac{\partial^2 C}{\partial y^2} + K\frac{\partial^2 C}{\partial z^2}$, and hence simplifies 3.1.19 to:

$$u\frac{\partial C}{\partial x} = K\frac{\partial^2 C}{\partial x^2} + K\frac{\partial^2 C}{\partial y^2} + K\frac{\partial^2 C}{\partial z^2} + Q^P\delta\{x\}\delta\{y\}\delta\{z-H\}. \tag{3.1.20}$$

Assumption 6 (Neglecting the Zonal Component of Diffusion) *The zonal advection is far greater than the zonal diffusion, i.e.* $\mathbf{u}\frac{\partial C}{\partial x} >> K\frac{\partial^2 C}{\partial x^2}$*, and hence the zonal diffusion can be neglected, i.e.* $K\frac{\partial^2 C}{\partial x^2} = 0$*).*

Assumption 6 simplifies 3.1.2.1 to:

$$u\frac{\partial C}{\partial x} = K\frac{\partial^2 C}{\partial y^2} + K\frac{\partial^2 C}{\partial z^2} + Q^P\delta\{x\}\delta\{y\}\delta\{z-H\}. \tag{3.1.21}$$

The formulation of a well-posed problem requires a set of natural initial conditions. Firstly, the scenario of a purely zonal wind field (Assumption 3) combined with a single, stationary, point source (Assumption 1) translates to the absence of molecules of X behind the point source, i.e. when $x < 0$, $C = 0$. Considering this, we properly define the smooth function C as: $C : I \to \mathbb{R}$, where $I = [0,\infty) \times (-\infty,\infty) \times [0,\infty)$.

For the total mass of X within the geographic field to remain finite, C must be zero at infinite boundaries. Using this concept we obtain a set of boundary conditions $C\{0, y, z\} = 0$, $C\{x, \pm\infty, z\} = 0$ and $C\{x, y, \infty\} = 0$.

Another initial condition arises from the assumption of a zero-flux condition.

Assumption 7 (Zero-Flux Condition) *The contaminant does not penetrate the ground. This suggests that the vertical flux at the ground must vanish, i.e.* $K\frac{\partial C}{\partial z}\{x, y, 0\} = 0$.

Finally, by integrating with respect to x, from $-d$ to d, then taking the limit as $d \to 0$, we eliminate the source term from the PDE and introduce it instead as a boundary condition.

$$
\begin{aligned}
u\frac{\partial C}{\partial x} &= K\frac{\partial^2 C}{\partial y^2} + K\frac{\partial^2 C}{\partial z^2} + Q^P\delta\{x\}\delta\{y\}\delta\{z-H\},\\
\int_{-d}^{d} u\frac{\partial C}{\partial x}dx &= \int_{-d}^{d}\left(K\frac{\partial^2 C}{\partial y^2} + K\frac{\partial^2 C}{\partial z^2}\right)dx + Q^P\delta\{y\}\delta\{z-H\}\int_{-d}^{d}\delta\{x\}dx,\\
uC\{d, y, z\} &= \int_{-d}^{d}\left(K\frac{\partial^2 C}{\partial y^2} + K\frac{\partial^2 C}{\partial z^2}\right)dx + Q^P\delta\{y\}\delta\{z-H\},\\
\lim_{d\to 0^+} uC\{d, y, z\} &= \lim_{d\to 0^+}\left(\int_{-d}^{d}\left(K\frac{\partial^2 C}{\partial y^2} + K\frac{\partial^2 C}{\partial z^2}\right)dx + Q^P\delta\{y\}\delta\{z-H\}\right),\\
C\{0, y, z\} &= \frac{Q^P}{u}\delta\{y\}\delta\{z-H\}.
\end{aligned}
$$

In summary, we reformulate 3.1.2.1 as a well-posed problem, given by:

$$
\begin{aligned}
u\frac{\partial C}{\partial x} &= K\frac{\partial^2 C}{\partial y^2} + K\frac{\partial^2 C}{\partial z^2}, && \text{(3.1.22a)}\\
C\{0, y, z\} &= \frac{Q^P}{u}\delta\{y\}\delta\{z-H\}, && \text{(3.1.22b)}\\
C\{x, \pm\infty, z\} &= 0, && \text{(3.1.22c)}\\
C\{x, y, \infty\} &= 0, && \text{(3.1.22d)}\\
\frac{\partial C}{\partial z}\{x, y, 0\} &= 0. && \text{(3.1.22e)}
\end{aligned}
$$

Within the PBL, K is difficult to determine in practice. This is owing to K being not only a strong function of downwind distance, but also varies with the weather and time of release (Stockie, 2011). We further simplify our well posed-problem by replacing x with a new independent variable $r\{x\} = \frac{1}{u}\int_0^x K\{\xi\}d\xi$ [m^2], and also by the substitution C with the smooth function c, defined by: $c\{r, y, z\} = C\{x, y, z\}$, $c : I \to \mathbb{R}$, where $I = [0, \infty) \times (-\infty, \infty) \times [0, \infty)$. This leads to the substitutions:

$$\frac{\partial C}{\partial x} = \frac{\partial c}{\partial r}\frac{dr}{dx} = \frac{\partial c}{\partial r}\frac{1}{u}\frac{d}{dx}\left(\int_0^x K\{\xi\}d\xi\right) = \frac{K\{x\}}{u}\frac{\partial c}{\partial r} = \frac{K}{u}\frac{\partial c}{\partial r},$$
$$\frac{\partial^2 C}{\partial y^2} = \frac{\partial^2 c}{\partial y^2},$$
$$\frac{\partial^2 C}{\partial z^2} = \frac{\partial^2 c}{\partial z^2}.$$

By applying these substitutions, we simplify to the well posed-problem:

$$\frac{\partial c}{\partial x} = \frac{\partial^2 c}{\partial y^2} + \frac{\partial^2 c}{\partial z^2} \tag{3.1.23a}$$
$$c\{0, y, z\} = \frac{Q^P}{u}\delta\{y\}\delta\{z - H\}, \tag{3.1.23b}$$
$$c\{r, \pm\infty, z\} = 0, \tag{3.1.23c}$$
$$c\{r, y, \infty\} = 0, \tag{3.1.23d}$$
$$\frac{\partial c}{\partial z}\{r, y, 0\} = 0. \tag{3.1.23e}$$

3.1.23 is in the form of a heat equation. Traditionally, solving this sort of PDE assumes the solution in the form of a product of solutions, i.e. $c\{r, y, z\} = R\{r\}Y\{y\}Z\{z\}$. However, the traditional approach in Gaussian dispersion modelling is to assume that the lateral and vertical velocity fluctuations are independent and resultantly, the horizontal and vertical Probability Density Functions (PDFs) are independent. By this assumption, the assemble mean concentration of C assumes the form (Weil et al., 1997):

$$C\{x, y, z\} = \frac{Q^P}{u}p_y p_z, \tag{3.1.24}$$

where:

- $p_y = p\{x, y, \}, 0 \leq p_y \leq 1$ is the horizontal PDF of C
- $p_z = p\{x, z\}, 0 \leq p_z \leq 1$ is the vertical PDF of C

We assume a similar form to (3.1.24), given by:

$$c\{r, y, z\} = \frac{Q^P}{u} \rho_y \rho_z, \tag{3.1.25}$$

where:

- $\rho_y = \rho\{r, y\}, 0 \leq \rho_y \leq 1$ is the horizontal PDF of c
- $\rho_z = \rho\{r, z\}, 0 \leq \rho_z \leq 1$ is the vertical PDF of c

Applying the product of solutions given in (3.1.25) to (3.1.23) gives:

$$\begin{aligned}
\frac{\partial c}{\partial x} &= \frac{\partial^2 c}{\partial y^2} + \frac{\partial^2 c}{\partial z^2}, \\
\frac{Q^P}{u}\left(\rho_z \frac{\partial \rho_y}{\partial r} + \rho_y \frac{\partial \rho_z}{\partial r}\right) &= \frac{Q^P}{u}\left(\rho_z \frac{\partial^2 \rho_y}{\partial y^2} + \rho_y \frac{\partial^2 \rho_z}{\partial z^2}\right), \\
\rho_z \frac{\partial \rho_y}{\partial r} + \rho_y \frac{\partial \rho_z}{\partial r} &= \rho_z \frac{\partial^2 \rho_y}{\partial y^2} + \rho_y \frac{\partial^2 \rho_z}{\partial z^2}.
\end{aligned}$$

and produces two separate 2-dimensional diffusion equations in the form:

$$\frac{\partial \rho_y}{\partial r} = \frac{\partial^2 \rho_y}{\partial y^2}, \tag{3.1.26}$$

and

$$\frac{\partial \rho_z}{\partial r} = \frac{\partial^2 \rho_z}{\partial z^2}. \tag{3.1.27}$$

3.1.26 and 3.1.27 can be written as two separate well-posed problems with boundary conditions given by:

$$\frac{\partial \rho_y}{\partial r} = \frac{\partial^2 \rho_y}{\partial y^2}, \tag{3.1.28a}$$

$$\rho_y\{0, y\} = \delta\{y\}, \tag{3.1.28b}$$

$$\rho_y\{\infty, y\} = 0, \tag{3.1.28c}$$

$$\rho_y\{r, \pm\infty\} = 0, \tag{3.1.28d}$$

and

$$\frac{\partial \rho_z}{\partial r} = \frac{\partial^2 \rho_z}{\partial z^2}, \tag{3.1.29a}$$

$$\rho_z\{0, z\} = \delta\{z - H\}, \tag{3.1.29b}$$

$$\rho_z\{\infty, z\} = 0, \tag{3.1.29c}$$

$$\rho_z\{r, \infty\} = 0, \tag{3.1.29d}$$

$$\frac{\partial \rho_z}{\partial z}\{r, 0\} = 0. \tag{3.1.29e}$$

3.1.2.2 Gaussian Solution to the 2-Dimensional Diffusion Equations

We derive the Gaussian nature of ρ_y and ρ_z by an application of Laplace transforms to 3.1.26 and 3.1.27, respectively. Given the 2-dimensional function $f\{a, b\}$ we define the Laplace transform of f with respect to a ($\mathcal{L}_a\{f\{a, b\}\}$), f with respect to b ($\mathcal{L}_b\{f\{a, b\}\}$) and f with respect to a followed by b ($\mathcal{L}_b\{\mathcal{L}_a\{f\{a, b\}\}\}$) by the following:

$$\mathcal{L}_a\{f\{a, b\}\} = \lim_{T\to\infty} \int_0^T \exp\{-s_a \cdot a\} f\{a, b\} da,$$

$$\mathcal{L}_b\{f\{a, b\}\} = \lim_{T\to\infty} \int_0^T \exp\{-s_b \cdot b\} f\{a, b\} db,$$

$$\mathcal{L}_b\{\mathcal{L}_a\{f\{a, b\}\}\} = \lim_{T\to\infty} \int_0^T \exp\{-s_b \cdot b\} \mathcal{L}_a\{f\{a, b\}\}\, db$$

To obtain a solution for ρ_y in 3.1.28, we must first take the Laplace transform of 3.1.28 with respect to r. Using the substitution $A\{\zeta, y\} = \mathcal{L}_r\{\rho_y\}$, where ζ is the transform variable, 3.1.28, we obtain the equation:

$$\zeta A - \rho_y\{0, y\} = \frac{\partial^2 A}{\partial y^2} \tag{3.1.30}$$

Furthermore, by applying the initial condition given by 3.1.28b, 3.1.30 simplifies to give:

$$\frac{\partial^2 A}{\partial y^2} - \zeta A = -\delta\{y\} \tag{3.1.31}$$

Next, we take the Laplace transform of 3.1.31 with respect to y. Using the substitution $\hat{A}\{\zeta,\eta\} = \mathcal{L}_y\{A\{\zeta,y\}\} = \lim_{T\to 0}\int_0^T \exp\{-\eta y\}A dy$, where η is the transform variable, we obtain the equation:

$$\eta^2\hat{A} - \eta A\{\zeta,0\} - \frac{\partial A}{\partial y}\{\zeta,0\} - \zeta\hat{A} = -1 \tag{3.1.32}$$

Using the substitutions $\beta_1 = \hat{A}\{\zeta,0\}$ and $\beta_2 = 1 - \frac{\partial A}{\partial y}\{\zeta,0\}$, 3.1.32 simplifies to give:

$$\hat{A} = \frac{\eta\beta_1 + \beta_2}{\eta^2 - \zeta} \tag{3.1.33}$$

Next, we take the inverse Laplace transform in η of 3.1.33 to obtain the equation:

$$A = \frac{\beta_1}{2}\left(\exp\{\sqrt{\zeta}y\} + \exp\{-\sqrt{\zeta}y\}\right) - \frac{\beta_2}{2\sqrt{\zeta}}\left(\exp\{\sqrt{\zeta}y\} - \exp\{-\sqrt{\zeta}y\}\right) \tag{3.1.34}$$

We obtain a substitution for β, in terms of β, by taking the limit of 3.1.34 as y tends to ∞. This gives the equation:

$$\lim_{y\to\infty} A = \lim_{y\to\infty}\frac{\beta_1}{2}\left(\exp\{\sqrt{\zeta}y\} + \exp\{-\sqrt{\zeta}y\}\right) - \frac{\beta_2}{2\sqrt{\zeta}}\left(\exp\{\sqrt{\zeta}y\} - \exp\{-\sqrt{\zeta}y\}\right) \tag{3.1.35}$$

Since $A = \lim_{T\to\infty}\int_0^T \exp\{-\zeta\cdot y\}\rho_y\{r,y\}dy$, it follows that $t\to\infty \Rightarrow A\to 0$. This substitution reduces 3.1.36 to the equation:

$$\left(\frac{\beta_1}{2} - \frac{\beta_2}{2\sqrt{\zeta}}\right)\left(\lim_{y\to\infty}\exp\{\sqrt{\zeta}y\}\right) = 0, \tag{3.1.36}$$

which is satisfied by the necessary condition $\beta_1 = \frac{\beta_2}{\sqrt{\zeta}}$.

Using the substitution $\beta_1 = \frac{\beta_2}{\sqrt{\zeta}}$, 3.1.34 simplifies to give:

$$A = \frac{\beta_2}{\sqrt{\zeta}}\exp\{-\sqrt{\zeta}y\}. \tag{3.1.37}$$

Next, we take the inverse Laplace transform in ζ of 3.1.37 to obtain the equation:

$$\rho_y = \frac{\beta_2}{\sqrt{\pi r}}\exp\left\{-\frac{y^2}{4r}\right\}. \tag{3.1.38}$$

Solving for β_2 in 3.1.38, we first take the limit of 3.1.38 as r goes to 0, given by the equation:

$$\rho_y\{0,y\} = \lim_{r\to 0}\left(\frac{\beta_2 \exp\{-\frac{y^2}{4r}\}}{\sqrt{\pi r}}\right). \tag{3.1.39}$$

Following this, we use the initial condition given by 3.1.28b, we modify 3.1.39 to give the equation:

$$\delta\{y\} = \lim_{r\to 0}\left(\frac{\beta_2 \exp\{-\frac{y^2}{4r}\}}{\sqrt{\pi r}}\right), \tag{3.1.40}$$

and apply the identity $\delta\{y\} = \lim_{r\to 0}\frac{\exp\{-\frac{v^2}{4r}\}}{\sqrt{4\pi r}}$, to obtain the equation:

$$\lim_{r\to 0}\frac{\exp\{-\frac{v^2}{4r}\}}{\sqrt{4\pi r}} = \lim_{r\to 0}\left(\frac{\beta_2 \exp\{-\frac{y^2}{4r}\}}{\sqrt{\pi r}}\right). \tag{3.1.41}$$

3.1.41 is satisfied by the solution $\beta_2 = \frac{1}{2}$, which we apply to 3.1.37 to obtain the horizontal PDF of c, given by the equation:

$$\rho_y = \frac{1}{\sqrt{4\pi r}}\exp\left\{-\frac{y^2}{4r}\right\}. \tag{3.1.42}$$

Similarly, to obtain a solution for ρ_z in 3.1.29, we must first take the Laplace transform of 3.1.29 with respect to r. Using the substitution $B\{\zeta,z\} = \mathcal{L}_r\{\rho_z\}$, where ζ is the transform variable, 3.1.29, we obtain the equation:

$$\zeta B - \rho_z\{0,z\} = \frac{\partial^2 B}{\partial z^2} \tag{3.1.43}$$

Furthermore, by applying the initial condition given by 3.1.29b, 3.1.43 simplifies to give:

$$\frac{\partial^2 B}{\partial z^2} - \zeta B = -\delta\{z-H\} \tag{3.1.44}$$

Next, we take the Laplace transform of 3.1.44 with respect to z. Using the substitution $\hat{B}\{\zeta,\eta\} = \mathcal{L}_z\{B\{\zeta,z\}\} = \lim_{T\to 0}\int_0^T \exp\{-\eta z\}B dz$, where η is the transform variable, we obtain the equation:

$$\eta^2\hat{B} - \eta B\{\zeta,0\} - \frac{\partial B}{\partial z}\{\zeta,0\} - \zeta\hat{A} = -\exp\{-\zeta H\} \tag{3.1.45}$$

By taking the Laplace transform with respect to z of the Neumann boundary condition, given by 3.1.29e, we obtain a transformed Neumann boundary condition given by:

$$\frac{\partial B}{\partial z}\{\zeta, 0\} = 0. \tag{3.1.46}$$

Substituting 3.1.46 into 3.1.45 and rearranging to make $\hat{B}$ the subject gives the equation:

$$\hat{B} = \frac{\eta B\{\zeta, 0\} - \exp\{-\zeta H\}}{\eta^2 - \zeta} \tag{3.1.47}$$

Next, we take the inverse Laplace transform in η of 3.1.47 to obtain the equation:

$$B = B\{\zeta, 0\}\cosh\{\sqrt{\zeta}z\} - \frac{1}{\sqrt{\zeta}}\sinh\{\sqrt{\zeta}(z - H)\} \tag{3.1.48}$$

We obtain a substitution for $B\{\zeta, 0\}$, in terms of ζ and H, by taking the limit of 3.1.34 as z tends to 0 and again considering the fundamental property of Laplace transform, i.e. $B \to 0 \Rightarrow z \to \infty$. This gives the equation:

$$B\{\zeta, 0\}\left(\lim_{z\to\infty}\frac{\exp\{\sqrt{\zeta}z\}}{2}\right) = \frac{\exp\{\sqrt{\zeta}H\}}{\sqrt{\zeta}}\left(\lim_{z\to\infty}\frac{\exp\{\sqrt{\zeta}z\}}{2}\right), \tag{3.1.49}$$

which is satisfied by the necessary condition $B\{\zeta, 0\} = \frac{\exp\{\sqrt{\zeta}H\}}{\sqrt{\zeta}}$.

Using the substitution $B\{\zeta, 0\} = \frac{\exp\{\sqrt{\zeta}H\}}{\sqrt{\zeta}}$, 3.1.48 simplifies to give:

$$B = \frac{1}{2\sqrt{\zeta}}\left(\exp\{-\sqrt{\zeta}(z - H)\} + \exp\{-\sqrt{\zeta}(z + H)\}\right). \tag{3.1.50}$$

Next, we take the inverse Laplace transform in ζ of 3.1.50 to obtain the vertical PDF of c, given by the equation:

$$\rho_z = \frac{1}{\sqrt{4\pi r}}\left(\exp\left\{-\frac{(z - H)^2}{4r}\right\} + \exp\left\{\left\{-\frac{(z + H)^2}{4r}\right\}\right\}\right). \tag{3.1.51}$$

Therefore, the solution for the well-posed problem in (3.1.25) is given by:

$$c\{r,y,z\} = \frac{Q^P}{u}\rho_y\rho_z \tag{3.1.52a}$$

$$\rho_y = \frac{1}{\sqrt{2\pi(2r)}}e^{-\frac{y^2}{2(2r)}} \tag{3.1.52b}$$

$$\rho_z = \frac{1}{\sqrt{2\pi(2r)}}\left(e^{-\frac{(z-H)^2}{2(2r)}} + e^{-\frac{(z+H)^2}{2(2r)}}\right) \tag{3.1.52c}$$

Finally, by making the substitution $\sigma^2\{x\} = 2r\{x\} = \frac{2}{u}\int_0^x K\{\xi\}d\xi$, and replacing c with C, we obtain the Gaussian Plume Dispersion Equation in its idealistic form, given by:

$$C\{x,y,z\} = \frac{Q^P}{u}p_y p_z \tag{3.1.53a}$$

$$p_y = \frac{1}{\sqrt{2\pi}\sigma}\exp\left(-\frac{y^2}{2\sigma^2}\right) \tag{3.1.53b}$$

$$p_z = \frac{1}{\sqrt{2\pi}\sigma}\left[\exp\left(-\frac{(z-H)^2}{2\sigma^2}\right) + \exp\left(-\frac{(z+H)^2}{2\sigma^2}\right)\right] \tag{3.1.53c}$$

3.2 Adjustments to the Gaussian PDF Model

The Gaussian plume dispersion equation, as given in (3.1.53), models mass concentrations in an idealistic situation. However, such idealistic conditions are often not observed in the PBL of the real atmosphere. Furthermore, predictions made with this idealistic form of the Gaussian equation produces mass concentration values that highly over-estimate or under-estimate true observed values (Stockie, 2011). In this section, we discuss several modifications to 3.1.53 accounting for several non-idealistic situations.

3.2.1 Rotating Coordinate System

The idealistic form of the Gaussian plume dispersion equation was derived with the assumption that the wind direction is aligned with the positive x-axis (given by Assumption 3). Fundamentally, wind is the manifestation of

moving air masses in response to differential solar heating. This differential heating is not constant, and neither is the resultant wind. To account for the changing wind direction, we define a rotating coordinate system for the Gaussian plume dispersion equation.

Let (X_r, Y_r, Z_r) be the location of a receptor in the earth's geographical coordinate system. We define the location of the receptor in the Gaussian dispersion plume equation coordinate system ($(X_r, Y_r, Z_r)_R = (x_r, y_r, z_r)$) by the rotated coordinate system:

$$\begin{bmatrix} X_r \\ Y_r \\ Z_r \end{bmatrix}_R = \begin{bmatrix} x_r \\ y_r \\ z_r \end{bmatrix} = \begin{bmatrix} \cos(\phi_u) & \sin(\phi_u) & 0 \\ -\sin(\phi_u) & \cos(\phi_u) & 0 \\ 0 & 0 & 1 \end{bmatrix} \begin{bmatrix} X_r - X_s \\ Y_r - Y_s \\ Z_r - Z_s \end{bmatrix},$$

where

- (X_r, Y_r, Z_r) is the location of the receptor in the earth's geographical coordinate system
- (X_s, Y_s, Z_s) is the location of the base of the point source in the earth's geographical coordinate system
- (x_r, y_r, z_r) is the location of the receptor with respect to the point source in the Gaussian plume equation coordinate system
- $\phi_u \in [0, 2\pi]$ is the positive angle between the wind direction and the x-axis in the earth's geographical Cartesian coordinate system

3.2.2 Anisotropic Diffusion

It is common for diffusion to be anisotropic (i.e. $K_y \neq K_z$). An anisotropic assumption leads to a substitution for Fick's constant in the form $r_{y,z}\{x\} = \frac{1}{u}\int_0^x K_{y,z}\{\xi\}d\xi$ [m^2] and consequently $\sigma_{y,z}^2 = 2r_{y,z}$. Following similar steps in subsection 3.1.2, we obtain (3.1.53) in the form (Stockie, 2011):

$$C\{x, y, z\} = \frac{Q^P}{u} p_y p_z \tag{3.2.1a}$$

$$p_y = \frac{1}{\sqrt{2\pi}\sigma_y} \exp\left(-\frac{y^2}{2\sigma_y^2}\right) \tag{3.2.1b}$$

$$p_z = \frac{1}{\sqrt{2\pi}\sigma_z} \left[\exp\left(-\frac{(z-H)^2}{2\sigma_z^2}\right) + \exp\left(-\frac{(z+H)^2}{2\sigma_z^2}\right)\right] \tag{3.2.1c}$$

3.2.3 Non-Gaussian Vertical Distribution in the CBL

In the CBL, the non-gaussian nature and positive skewness of the PDF of the vertical velocity (p_{u_z}), where u_z is the vertical velocity, is well established. It has been demonstrated both numerically Deardorff (1974) and in laboratory Willis and Deardorff (1974) and field experiments Taconet and Weill (1982); Caughey et al. (1983). In this case, an alternate derivation for p_z can be obtained from the PDF of the vertical velocity (p_{u_z}).

We derive an expression for $\frac{du_z}{dz_p}$ using particle trajectory. Since $u = \frac{dx}{dt} \Rightarrow dt = \frac{dx}{u}$ and $u_z = \frac{dz}{dt} \Rightarrow dt = \frac{dz}{u_z}$, it follows that $dz = \frac{u_z dx}{u_x}$. We assume $u_z \neq u_z\{z\}$ and form the integral:

$$\int_H^z dz = \frac{u_z}{u} \int_0^x dx, \tag{3.2.2}$$

which gives us u_z in the form:

$$u_z\{z, \frac{x}{u}\} = (z - H)\frac{u}{x}. \tag{3.2.3}$$

For a given value of x, we notice $u_z = u_z\{z\}$ becomes an increasing linear function with gradient $\frac{u}{x}$. Since u_z is increasing, we obtain an expression for p_z in terms of p_{u_z} by change of variables for PDFs, given by:

$$p_z\{z, \frac{x}{u}\} = p_{u_z}\{z, \frac{x}{u}\} \left|\frac{du_z}{dz}\right|, \tag{3.2.4}$$

where the absolute value ensures p_z is positive. We obtain an expression for $\left|\frac{du_z}{dz}\right|$ by differentiating (3.2.3), which is given by:

$$\left|\frac{du_z}{dz}\right| = \frac{u}{x} \tag{3.2.5}$$

In the CBL u_z is the summed effect of updrafts and downdraft resulting from convection, refer to. We express p_{u_z} as the superposition of the Gaussin PDFs for updrafts and downdrafts, given by (Bærentsen and Berkowicz, 1984):

$$p_{u_z} = \frac{\lambda_1}{\sqrt{2\pi}\sigma_{u_{z1}}} \exp\left(-\frac{(u_z - \overline{u_{z1}})^2}{2\sigma_{u_{z1}}^2}\right) + \frac{\lambda_2}{\sqrt{2\pi}\sigma_{u_{z2}}} \exp\left(-\frac{(u_z - \overline{u_{z2}})^2}{2\sigma_{u_{z2}}^2}\right), \tag{3.2.6}$$

where λ_1, $\overline{u_{z1}}$ and $\sigma_{u_{z1}}$ and λ_2, $\overline{u_{z2}}$ and $\sigma_{u_{z2}}$ are the weighting coefficient, mean vertical velocity and standard deviation for the updraft and downdraft distributions respectively.

By substituting (3.2.6) and (3.2.5) into (3.2.4) and making the substitution for u_z in (3.2.3), we express the vertical PDF for the direct source, p_z^d, as:

$$p_z^d = \frac{1}{\sqrt{2\pi}} \sum_{j=1}^{2} \frac{\lambda_j}{\sigma_{zj}} \exp\left(-\frac{\left(z - \psi_j^d\right)^2}{2\sigma_{zj}^2} \right), \tag{3.2.7}$$

where $\sigma_{zj} = \frac{\sigma_{u_{zj}} x}{u}$ and $\psi_j^d = H + \frac{\overline{u_{zj}} x}{u}$ and $j \in \{1, 2\}$.

3.2.4 Zero-Flux Condition and Image Sources

Within the Mixing layer, the ground acts as a rigid reflective boundary, as suggested by Assumption 7 in subsubsection 3.1.2.1. To account for this reflection, we introduce an image source at $z = -\psi_j^d$. Similarly, we assume a rigid reflective upper boundary. In the CBL, z_i is taken as the height of the reflective upper boundary, due to the natural resistance to penetration of the inversion cap.

To account for the reflection of plume material at the reflect upper boundary, we introduce an image source at $z = \psi_j^d + 2z_i$ and an image source at $z = -\psi_j^d - 2z_i$ for the associated ground reflection. The plume section reflected at the ground (i.e. emitted from the image source at $z = -\psi_j^d$) will again reflect at z_i, thus we introduce an additional image source at $z = \psi_j^d + 4z_i$ with an associated image source at $z = -\psi_j^d - 4z_i$ to account for ground reflection.

We see a cascade effect being created with sources at $z = \psi_j^d, \psi_j^d + 2z_i, \psi_j^d + 4z_i, \psi_j^d + 6z_i, \ldots$ and at $z = -\psi_j^d, -\psi_j^d - 2z_i, -\psi_j^d - 4z_i, -\psi_j^d - 6z_i, \ldots$. With the addition of image sources, we express p_z^d as:

$$p_z^d = \frac{1}{\sqrt{2\pi}} \sum_{n=0}^{N} \sum_{j=1}^{2} \frac{\lambda_j}{\sigma_{zj}} \left[\exp\left(-\frac{\left(z - 2nz_i - \psi_j^d\right)^2}{2\sigma_{zj}^2} \right) + \exp\left(-\frac{\left(z + 2nz_i + \psi_j^d\right)^2}{2\sigma_{zj}^2} \right) \right], \tag{3.2.8}$$

where N is the number of image sources.

The SBL does not have a similar cap. An effective height $z_{i_{eff}}$ is taken as the reflective upper boundary which retards but does not prevent plume

material from spreading into the region above the Mixing layer (Cimorelli et al., 2004). Given this, we express the vertical PDF in the SBL, p_z^s, as:

$$p_z^s = \frac{1}{\sqrt{2\pi}\sigma_{zs}} \sum_{n=0}^{N} \left[\exp\left(-\frac{(z - 2nz_{i_{eff}} - H)^2}{2\sigma_{zs}^2} \right) + \exp\left(-\frac{(z + 2nz_{i_{eff}} + H)^2}{2\sigma_{zs}^2} \right) \right] \tag{3.2.9}$$

3.2.5 Indirect Source in the CBL

On its first interaction with z_i, a section of the plume, which is unable to penetrate the inversion cap of the Mixing layer (Weil et al., 1997). The material in this plume section forms a second source known as the "indirect source". This material lofts at z_i and is later dispersed downward by downdrafts from am image source at $z = H + 2z_i + \Delta h_i$. Δh_i is an effective plume rise height added to reflect the lofting behaviour by delaying the downward dispersion. We can, therefore, reformulate the integral in (3.2.2) as:

$$\int_{H+2z_i+\Delta h_i}^{z} dz = \frac{u_z}{u} \int_0^x dx, \tag{3.2.10}$$

and obtain an expression for u_z in the form:

$$u_z\{z, \frac{x}{u}\} = (z - (H + 2z_i + \Delta h_i))\frac{u}{x}. \tag{3.2.11}$$

Using (3.2.11) instead of (3.2.3) and following all the steps for the non-Gaussian PDF in subsection 3.2.3 and the cascade effect caused by the zero-flux conditions in subsection 3.2.4, we express the vertical PDF for the indirect source, p_z^r, as:

$$p_z^r = \frac{1}{\sqrt{2\pi}} \sum_{n=1}^{N} \sum_{j=1}^{2} \frac{\lambda_j}{\sigma_{zj}} \left[\exp\left(-\frac{\left(z - 2nz_i + \psi_j^r\right)^2}{2\sigma_{zj}^2} \right) + \exp\left(-\frac{\left(z + 2nz_i - \psi_j^r\right)^2}{2\sigma_{zj}^2} \right) \right], \tag{3.2.12}$$

where $\psi_j^r = H + \Delta h_i + \frac{\overline{w_j}x}{u}$.

3.2.6 Penetrated Source in the CBL

In cases where the updrafts are sufficiently strong, plume material can penetrate into the inversion cap of the Mixing layer and stabilizes at a height h_{es},

about which the material is horizontally centred. This material, known as the "penetrated source", is assumed to be entrained into the growing CBL by a fumugation process (i.e. as z_i increases) (Deardorff and Willis, 1982). Penetrated source material is conceptualized to be released from an effective height $H_p = h_{es} + \Delta h_p$, where Δh_p is the equilibrium plume rise in a stratified environment. In order to maintain the zero-flux condition, a time-dependent effective height within the inversion cap $z_{i_{eff}}$, is used as the rigid reflective boundary. Therefore, we express the vertical PDF for the indirect source, p_z^p, as:

$$p_z^p = \frac{1}{\sqrt{2\pi}} \sum_{n=1}^{N} \sum_{j=1}^{2} \frac{\lambda_j}{\sigma_{zj}} \left[\exp\left(-\frac{\left(z - 2nz_{i_{eff}} + \psi_j^p\right)^2}{2\sigma_{zj}^2} \right) + \exp\left(-\frac{\left(z + 2nz_{i_{eff}} - \psi_j^p\right)^2}{2\sigma_{zj}^2} \right) \right], \tag{3.2.13}$$

where $\psi_j^p = H_p + \frac{\overline{w_j} x}{u}$.

3.2.7 Line Source

The Gaussian plume dispersion model can be tailored to model dispersion from a line source. A line source is conceptualized as the superposition of point sources along a straight line of length L, centred at a point y_c; such as a roadway. We assume that each point source has an emission rate of Q^L [$\mu\,\mathrm{g\,m^{-1}\,s^{-1}}$]. Thus, we express the total emission rate of the roadway as:

$$Q^P = \int_{-\frac{L}{2}}^{\frac{L}{2}} Q^L dy \tag{3.2.14}$$

Since vehicle exhaust is emitted close to the surface (i.e. $h \approx 0$), we reduce the effective height to the plume rise height (i.e. $H = \Delta h$)and we express the mass concentration contribution from the roadway as:

$$C^L\{x, y, z\} = \frac{Q^L}{u} p_z^L p_y^L, \tag{3.2.15}$$

where p_z^L is given by:

$$p_z^L = \frac{1}{\sqrt{2\pi}\sigma_z} \left[\exp\left(-\frac{(z - \Delta h)^2}{2\sigma_z^2} \right) + \exp\left(-\frac{(z + \Delta h)^2}{2\sigma_z^2} \right) \right], \tag{3.2.16}$$

and p_y^L is given by:

$$p_y^L = \int_{-\frac{L}{2}}^{\frac{L}{2}} \frac{1}{\sqrt{2\pi}\sigma_y} \exp\left(-\frac{(Y-y')^2}{2\sigma_y^2}\right) dy', \tag{3.2.17}$$

where $Y = y - y_c$ is the meridional distance from the receptor to the centre of the line source, and y' controls movement up and down the line. By employing the error function, $\text{erf}(\zeta) = \frac{1}{\sqrt{\pi}} \int_{-\zeta}^{\zeta} \exp(-t^2) dt$, we express (3.2.17) as:

$$p_y^L = \frac{1}{\sqrt{\pi}} \left[\text{erf}\left\{ \frac{Y + \frac{L}{2}}{\sqrt{2}\sigma_y^2} \right\} - \text{erf}\left\{ \frac{Y - \frac{L}{2}}{\sqrt{2}\sigma_y^2} \right\} \right]. \tag{3.2.18}$$

3.2.8 Influence of Terrain

Generally, in stable flows, a two-layer structure develops in which the lower layer remains horizontal while the upper layer tends to rise over the terrain. The concept of a two-layer flow, distinguished at the dividing streamline height H_d, was first suggested by theoretical arguments of Sheppard (1956) and demonstrated through laboratory experiments, particularly those of Snyder et al. (1985). As a result, in modern advanced dispersion models that handle complex terrain, terrain influence is modelled as a feature of only the SBL state.

A direct consequence of Assumption 2 is the limitation of the Gaussian plume dispersion equation in complex terrain. Terrain influence is handled by modelling plume material as being separated into a terrain-following plume state and a horizontal plume state. We model the total plume material at a given receptor located at (x_r, y_r, z_r) by (Venkatram et al., 2001):

$$C_T\{x_r, y_r, z_r\} = f \cdot C\{x_r, y_r, z_r\} + (1 - f) C\{x_r, y_r, z_g\}, \tag{3.2.19}$$

where $C_T\{x_r, y_r, z_r\}$, $C\{x_r, y_r, z_r\}$ and $C\{x_r, y_r, z_g\}$ are the total mass concentration at the receptor, the contribution from the horizontal plume state and the contribution from the terrain-following plume state, f is the plume state weighing factor, discussed in section 4.1, and z_g, discussed in **??**, is the height of the receptor above local ground.

Chapter 4

Overview of the Parameter Formulations incorporated in AERMOD

AERMOD is a steady state Gaussian Plume dispersion model designed by AERMIC and adopted by the US EPA as their preferred regulatory model since December 9, 2005. AERMOD simulates contaminant mass concentrations in a non-ideal atmosphere, making provisions for:

- Anisotropic diffusion
- Flat and/or complex terrain
- Surface and elevated emission sources
- The bi-Gaussian PDF of the vertical distribution within the CBL (Willis and Deardorff, 1981)
- Plume lofting near the top of the boundary layer
- Plume penetration into the stable layer above the PBL, which is allowed to enter the growing PBL
- Multiple Sources (including point, area and volume sources)
- Rural and urban areas

- Possible discontinuities due to small changes in input parameters.

As discussed in chapter 3, the parameters of the Gaussian dispersion depends on the adjustments accounted for by the equation. In this chapter, we give an overview of the general concentration equation employed in AERMOD and discuss the formulation of the parameters incorporated. The equations presented in this chapter are reformulated from AERMOD (Cimorelli et al., 2004).

4.1 The General Concentration Equation

We aim is to model the mass concentration at a given receptor as the summed material from a collection of point and line sources in the non-idealistic conditions representing the actual atmosphere. The non-idealistic conditions accounted for in AERMOD include anisotropic diffusion, non-homogeneous weather parameters, complex terrain as well as the inclusion of a direct, indirect and penetrated source in the CBL phase. The general concentration equation employed by AERMOD is given by:

$$C_T\{X_r, Y_r, Z_r\} = \sum_{i=0}^{N_s} C_i\{x_{ri}, y_{ri}, z_{ri}\} \tag{4.1.1}$$

where

- C_T is the total contaminant mass concentration
- C_i is the mass concentration contribution from the i^{th} point source
- (X_r, Y_r, Z_r) is the location of the receptor (in the earth's geographical co-ordinate system)
- (x_{ri}, y_{ri}, z_{ri}) is the location of the receptor with reference to the i^{th} point source (in the Gaussian plume equation coordinate system)
- N_s - the total number of point sources

The mass concentration C is given by (Venkatram et al., 2001; Cimorelli et al., 2004):

$$C\{x_r, x_r, z_r\} = f \cdot C_{c,s}\{x_r, y_r, z_r\} + (1 - f)C_{c,s}\{x_r, y_r, z_g\} \tag{4.1.2}$$

where

- f is the plume state weighting function
- $z_g = z_r - z_t$ is the height of the receptor above local ground, where z_r is the height of the receptor and z_t is the height of local ground in the Gaussian plume equation coordinate system)

The subscripts c and s represents the CBL phase and SBL phase respectively.

4.1.1 Plume State Weighting Function

As mentioned in subsection 3.2.8, the plume state weighting function f determines the portion of plume material in the plume state and terrain following state flows, and is defined by (Venkatram et al., 2001; Cimorelli et al., 2004):

$$f = 0.5(1 + \varphi_T) \tag{4.1.3a}$$

$$\varphi_T = \frac{\int_0^{H_c} C_s\{x_r, y_r, z_r\}dz}{\int_0^{\infty} C_s\{x_r, y_r, z_r\}dz} \tag{4.1.3b}$$

$$\frac{1}{2}u^2\{H_c\} = \int_{H_c}^{h_c} N\{h_c - z\}dz \tag{4.1.3c}$$

$$N\{z\} = \left(\frac{g_0}{\theta}\frac{\partial\theta}{\partial z}\{z\}\right)^{\frac{1}{2}} \tag{4.1.3d}$$

where

- H_c [m] is the critical dividing streamline
- φ_T [dimensionless] is the fraction of plume mass below (H_c)
- h_c [m] is the receptor specific terrain height scale, defined as the minimum of the highest actual terrain and the local terrain-following height which is equal to the sum of the height of the local terrain ($z_{t)}$ [m] and the plume rise height (h_e [m], given in section 4.4)
- $N\{z\}$ [s^{-1}] is the Brunt-Väisälä frequency
- g_0 is the standard acceleration due to gravity

4.2 Estimation Mass Concentration in the SBL Phase

In the SBL phase, both the horizontal and vertical PDFs are assumed to be Gaussian and $C_s\{x, y, z\}$ is given by:

$$C_s\{x_r, y_r, z_r\} = \frac{Q^P}{2\pi\tilde{u}\sigma_y\sigma_{zs}} \exp\left(-\frac{y_r^2}{2\sigma_y^2}\right) \times \sum_{m=-\infty}^{\infty} \left[\exp\left(-\frac{(z_r - 2mz_{i_{eff}} - H_s)^2}{2\sigma_{zs}^2}\right) + \exp\left(-\frac{(z_r + 2mz_{i_{eff}} + H_s)^2}{2\sigma_{zs}^2}\right)\right] \tag{4.2.1}$$

where

- Q^P [µ g s^{-1}] is the point source emission rate
- $\tilde{u}$ [m s^{-1}] is the effective mean lateral wind speed
- σ_y [m] is the lateral dispersion parameter
- σ_{zs} [m] is the vertical dispersion parameter in the SBL
- $z_{i_{eff}} = MAX\{H_s + 2.5\sigma_{zs}, z_{im}\}$ [m] is the effective mechanical mixing layer height representing the reflective upper boundary in the SBL
- $H_s = h_s + \Delta h_s$ is the effective plume rise height, where h_s is the stack height and Δh_s is the plume rise in the SBL.

4.3 Estimation Mass Concentration in the CBL Phase

In the CBL phase, the horizontal PDF is assumed to be Gaussian while the vertical PDF is assumed to be non-Gaussian, with a skewness factor S that determines the weighting coefficients (refer to subsection 4.3.2). Additionally, a portion of the plume material originating from the direct source is assumed to exhibit a lofting behaviour and results in the formation of an indirect

source (refer to subsection 3.2.5) while another portion of the plume material is assumed to penetrate the stable layer capping of the CML entering the entrainment zone and results in the formation of a penetrated source (refer to subsection 3.2.6). $C_c\{x, y, z\}$ is given by:

$$C_c\{x_r, y_r, z_r\} = \frac{Q^P}{\sqrt{2\pi}\tilde{u}\sigma_y} \exp\left(-\frac{y^2}{2\sigma_y^2}\right) \left[\varphi_p p_z^d + \varphi_p p_z^r + (1-\varphi_p) p_z^p\right] \quad (4.3.1a)$$

$$p_z^d = \frac{1}{\sqrt{2\pi}} \sum_{j=1}^{2} \sum_{n=0}^{\infty} \frac{\lambda_j}{\sigma_{zj}} \left[\exp\left(-\frac{\left(z - 2nz_i - \psi_j^d\right)^2}{2\sigma_{zj}^2}\right) + \exp\left(-\frac{\left(z + 2nz_i + \psi_j^d\right)^2}{2\sigma_{zj}^2}\right)\right] \quad (4.3.1b)$$

$$p_z^r = \frac{1}{\sqrt{2\pi}} \sum_{j=1}^{2} \sum_{n=1}^{\infty} \frac{\lambda_j}{\sigma_{zj}} \left[\exp\left(-\frac{\left(z - 2nz_i + \psi_j^r\right)^2}{2\sigma_{zj}^2}\right) + \exp\left(-\frac{\left(z + 2nz_i - \psi_j^r\right)^2}{2\sigma_{zj}^2}\right)\right] \quad (4.3.1c)$$

$$p_z^p = \frac{1}{\sqrt{2\pi}\sigma_{zp}} \sum_{n=-\infty}^{\infty} \left[\exp\left(-\frac{\left(z + 2nz_{i_{eff}} - \psi_j^p\right)^2}{2\sigma_{zp}^2}\right) + \exp\left(-\frac{\left(z + 2nz_{i_{eff}} + \psi_j^p\right)^2}{2\sigma_{zp}^2}\right)\right] \quad (4.3.1d)$$

where

- φ_p [dimensionless] is portion of plume material trapped in the CML
- p_z^d [dimensionless], p_r^d [dimensionless] and p_p^d [dimensionless] are the vertical PDF of the direct, indirect and penetrated sources, respectively
- λ_j [dimensionless] is weighting coefficient for the updraft ($j = 1$) and downdraft ($j = 2$) of the vertical PDF
- σ_{zj} [m] is the vertical dispersion parameter for the updraft ($j = 1$) and downdraft ($j = 2$) of the vertical PDF
- σ_{zp} [m] is the vertical dispersion parameter for the penetrated source
- z_i [m] is the mixing layer height
- $z_{i_{eff}}$ [m] is the height of the reflecting upper boundary in the entrainment zone above the CBL

- ψ_j^d [m], ψ_j^r [m] and ψ_j^p [m] are the effective source heights of the direct, indirect and penetrated sources for the updraft ($j = 1$) and downdraft ($j = 2$) of the vertical PDF

4.3.1 Material Trapped in the CBL

The amount of material trapped in the CBL (φ_p), is given by:

$$\varphi_p = \begin{cases} 0, & \Delta h_h < 0.5\Delta h_{eq} \\ \frac{\Delta h_h}{\Delta h_{eq}} - 0.5, & 0.5\Delta h_{eq} \leq \Delta h_h \leq 1.5\Delta h_{eq} \\ 1, & \Delta h_h > 1.5\Delta h_{eq} \end{cases} \tag{4.3.2a}$$

$$\Delta h_h = z_i - h_s \tag{4.3.2b}$$

$$\tag{4.3.2c}$$

where

- Δh_h [m] is the difference between the mixing layer height (z_i [m]) and the emission stack height (h_s [m])
- Δh_{eq} [m] is the equilibrium plume rise in a stable environment (given in 4.4.8)

4.3.2 Weighting Coefficients for the Vertical PDF in the CBL Phase

The weighting coefficients λ_1 and λ_2, discussed in subsection 3.2.3, are parameters of p_z^d and p_z^r, given by Bærentsen and Berkowicz (1984); Weil (1990);

Cimorelli et al. (2004):

$$\lambda_1 + \lambda_2 = 1 \tag{4.3.3a}$$

$$\lambda_1 = +\frac{\bar{w}_2}{\bar{w}_2 - \bar{w}_1} = \frac{a_2}{a_2 - a_1} \tag{4.3.3b}$$

$$\lambda_2 = -\frac{\bar{w}_1}{\bar{w}_2 - \bar{w}_1} = -\frac{a_1}{a_2 - a_1} \tag{4.3.3c}$$

$$a_1 = \frac{\tilde{\sigma}_{wT}}{w_*}\left(\frac{\alpha S}{2} + \frac{1}{2}\left(\alpha^2 S^2 + \frac{4}{\beta}\right)^{\frac{1}{2}}\right) \tag{4.3.3d}$$

$$a_2 = \frac{\tilde{\sigma}_{wT}}{w_*}\left(\frac{\alpha S}{2} - \frac{1}{2}\left(\alpha^2 S^2 + \frac{4}{\beta}\right)^{\frac{1}{2}}\right) \tag{4.3.3e}$$

$$\alpha = \frac{1 + R^2}{1 + 3R^2} \tag{4.3.3f}$$

$$\beta = 1 + R^2 \tag{4.3.3g}$$

$$S = \begin{cases} 0.125\left(\frac{w_*}{\tilde{\sigma}_{wT}}\right)^3, & H_p \geq 0.1 z_i \\ \frac{1.25 H_p}{z_i}\left(\frac{w_*}{\tilde{\sigma}_{wT}}\right)^3, & H_p < 0.1 z_i \end{cases} \tag{4.3.3h}$$

where

- λ_1 [dimensionless] and λ_2 [dimensionless] are the weighting coefficient for the updraft ($j = 1$) and downdraft ($j = 2$) of the vertical PDF
- $\bar{w}_1$ and $\bar{w}_2$ are the mean vertical velocity for the updraft ($j = 1$) and downdraft ($j = 2$) of the vertical PDF
- $\tilde{\sigma}_{wT}$ [$\mathrm{m\,s^{-1}}$] is the effective total vertical turbulence (discussed in section 5.7)
- w_* [$\mathrm{m\,s^{-1}}$] is the Deardorff scale (discussed in section 5.4)
- S [dimensionless] is the skewness factor, where R is assumed to be 2.0.

4.3.3 Effective Source Heights for the SBL and for the Direct, Indirect and Penetrated Sources of the CBL

Although the stack height represents the point of entry of the contaminant plume/puff into the atmosphere, it commonly does not represent the actual point from which the plume/puff begins to actually mix with the ambient environment (as depicted by Assumption 1 in subsection 3.1.2).

4.3.3.1 Effective Source Height in the SBL

The effective source height in the SBL (H_s [m]) is given by:

$$H_s = h_s + \Delta h_s \tag{4.3.4}$$

where

- H_s [m] is the effective source height in the SBL
- h_s [m] is the stack height
- Δh_s [m] is the plume rise height within the SBL

4.3.3.2 Effective Source Height for the Direct Source

The effective source height for the direct source ψ_{dj} [m] is given by:

$$\psi_{dj} = h_s + \Delta h_d + \frac{a_j w_* x}{u} \tag{4.3.5}$$

where

- ψ_{dj} [m] is the effective source height for the direct source
- h_s [m] is the stack height
- Δh_d [m] is the plume rise height for the direct source, within the CBL (given in 4.4.2)

- a_j [dimensionless] are weighting coefficients for the updraft ($j = 1$) and downdraft ($j = 2$) (given in 4.3.3d and 4.3.3e)
- w_* [$\mathrm{m\,s^{-1}}$] is the Deardorff scale (discussed in section 5.4)
- u [$\mathrm{m\,s^{-1}}$] is the mean horizontal wind speed

4.3.3.3 Effective Source Height for the Indirect Source

The effective source height for the indirect source ψ_{rj} [m] is given by:

$$\psi_{rj} = \psi_{dj} - \Delta h_i \tag{4.3.6}$$

where

- ψ_{rj} [m] is the effective source height for the indirect source
- ψ_{dj} [m] is the effective source height for the direct source
- Δh_i [m] is the the height adjustment to the plume rise (given in 4.4.3)

4.3.3.4 Effective Source Height for the Penetrated Source

The effective source height for the penetrated source ψ_{pj} [m] is given by:

$$\psi_{pj} = \begin{cases} h_s + \Delta h_{eq}, & \varphi_p = 0 \\ \frac{h_s + z_i}{2} + 0.75\Delta h_{eq}, & \varphi_p > 0 \end{cases} \tag{4.3.7}$$

where

- ψ_{pj} [m] is the effective source height for the penetrated source
- h_s [m] is the stack height
- z_i [m] is the mixing layer height
- Δh_{eq} [m] is the equivalent plume rise height (given in 4.4.8)

4.4 Plume Rise Height

Plume rise height represents a change in height from a point of emergence to a point of stabilization from which the contaminant plume/puff begins to mix with the ambient environment.

4.4.1 Calculation of Plume Rise Height in the SBL Phase

Plume rise height in the SBL phase (Δh_s [m]) is calculated iteratively by the equation:

$$F_b = g_0 w_s {r_s}^2 \frac{\Delta T}{T_s} \tag{4.4.1a}$$

$$F_m = \frac{T}{T_s} {w_s}^2 {r_s}^2 \tag{4.4.1b}$$

$$x_f = \frac{u_s}{N\{h_s\}} \arctan\left\{-\frac{0.7N\{h_s\}F_m}{F_b}\right\} \tag{4.4.1c}$$

$$\begin{aligned} N_i =& \frac{1}{2}\left[\left(N\left\{\frac{g_0}{\theta\{h_s\}}\cdot\frac{\partial\theta}{\partial z}\{h_s\}\right\}\right)^{\frac{1}{2}}\right] + \\ & \frac{1}{2}\left[\left(N\left\{\frac{g_0}{\theta\left\{\frac{h_s+\Delta h_{s_{i-1}}}{2}\right\}}\cdot\frac{\partial\theta}{\partial z}\left\{\frac{h_s+\Delta h_{s_{i-1}}}{2}\right\}\right\}\right)^{\frac{1}{2}}\right] \end{aligned} \tag{4.4.1d}$$

$$u_i = \frac{1}{2}\left(u\{h_s\} + u\left\{\frac{h_s+\Delta h_{s_{i-1}}}{2}\right\}\right) \tag{4.4.1e}$$

$$L_{n_i} = \frac{F_b}{u_i {u_*}^2} \tag{4.4.1f}$$

$$\Delta h_{s_i}\{x\} = \begin{cases} 2.66\left(\frac{F_b}{N_i^2 u_i}\right)^{\frac{1}{3}}, & x >= x_f \\ 2.66\left(\frac{F_b}{N_i^2 u_i}\right)^{\frac{1}{3}}\left[\left(\frac{0.7N_iF_m}{F_b}\right)\sin\left\{0.7\left(\frac{N_i}{u_i}\right)x\right\}\right]^{\frac{1}{3}} \times & \\ 2.66\left(\frac{F_b}{N_i^2 u_i}\right)^{\frac{1}{3}}\left[1-\cos\left\{\left(\frac{N_i}{u_i}\right)x\right\}\right]^{\frac{1}{3}}, & x < x_f \\ 1.2L_{n_i}^{\frac{3}{5}}(h_s+1.2L_{n_i})^{\frac{2}{5}}, & N_i \to 0 \\ \left(\frac{4F_b}{N_i^3}\right)^{\frac{1}{4}}, & u_i \to 0 \end{cases} \tag{4.4.1g}$$

where

- x_f [m] is the downwind distance to final plume rise
- Δh_s [m] is the stable plume rise height
- h_s [m] is the stack height
- F_b [$\mathrm{m^4\,s^{-3}}$] is the stack buoyant flux
- F_m [$\mathrm{m^4\,s^{-2}}$] is the stack momentum flux
- ΔT [K] is the difference between the ambient air temperature (T [K]) and the stack gas temperature (T_s [K])
- r_s [m] is the stack radius corrected for stack tip downwash
- w_s [$\mathrm{m\,s^{-1}}$] is the stack exit gas velocity
- g_0 is the standard acceleration due to gravity
- θ [K] is the potential temperature
- u [$\mathrm{m\,s^{-1}}$] is the mean horizontal wind speed
- $\frac{\partial \theta}{\partial z}$ [$\mathrm{K\,m^{-1}}$] is the vertical potential temperature gradient

4.4.2 Plume Rise Height for the Direct Source in the CBL

In the CBL phase, the plume rise for the direct source, Δh_d, is given by:

$$\Delta h_d = \left(\frac{3 F_m x}{\beta_1^2 {u_s}^2} + \frac{3}{2\beta 1^2} \cdot \frac{F_b x^2}{{u_s}^3} \right)^{\frac{1}{3}} \tag{4.4.2}$$

where

- Δh_d [m] is the plume rise for the direct source in the CBL
- F_b [$\mathrm{m^4\,s^{-3}}$] is the stack buoyant flux

- F_m [$\mathrm{m^4\,s^{-2}}$] is the stack momentum flux
- $\beta_1 = 0.6$ is an entrainment parameter
- u_s [$\mathrm{m\,s^{-1}}$] is the wind speed at the stack height

4.4.3 Height Adjustment to the Plume Rise Height for the Indirect Source in the CBL

In the CBL phase, the height adjustment to the plume rise for the indirect source, Δh_i, is given by:

$$\Delta h_i = \left(\frac{2 F_b z_i}{\alpha_r u_s r_y r_z} \right)^{\frac{1}{2}} \frac{x}{u_s} \tag{4.4.3}$$

$$r_y r_z = r_h^2 + \frac{a_e \lambda_y^{\frac{3}{2}}}{4} \cdot \frac{{w_*}^2 x^2}{{u_s}^2} \tag{4.4.4}$$

$$r_h = \beta_2 (z_i - h_s) \tag{4.4.5}$$

where

- Δh_i [m] is the height adjustment to the plume rise for the indirect source
- F_b [$\mathrm{m^4\,s^{-3}}$] is the stack buoyant flux
- z_i [m] is the mixing layer height
- r_y [m] and r_z [m] are the lofting plume half-widths in the lateral and vertical directions
- u_s [$\mathrm{m\,s^{-1}}$] is the wind speed at the stack height
- h_s [m] is the stack height
- w_* [$\mathrm{m\,s^{-1}}$] is the Deardorff scale
- $\alpha_r = 1.4$, $\beta_2 = 0.4$ and $\lambda_y = 2.3$ are dimensionless constants
- $a_e = 0.1$ [dimensionless] is an entrainment parameter

4.4.4 Equilibrium Plume Rise Height for the Penetrated Source in the CBL

The height that the penetrated source achieves above z_i is calculated as the equilibrium plume rise in a stratified environment Δh_{eq} [m] and is given by:

$$P_s = \frac{F_b}{u N_h^2 \Delta h_h^3} \tag{4.4.6}$$

$$N_h = \left[\frac{g_0}{\theta\{z_i\}} \frac{\partial \theta}{\partial z}\Big|_{z>z_i} \right]^{\frac{1}{2}} \tag{4.4.7}$$

$$\Delta h_{eq} = \left(2.6 P_s^3 + \left(\frac{2}{3} \right)^3 \right)^{\frac{1}{3}} \Delta h_h \tag{4.4.8}$$

where

- Δh_{eq} [m] is the equilibrium plume rise height in a stable environment
- F_b [$\mathrm{m^4\,s^{-3}}$] is the stack buoyant flux (given in subsection 4.4.1)
- u [m] is the mean horizontal wind speed
- N_h [$\mathrm{m\,s^{-1}}$] is the Brunt-V*äisälä* frequency representing the stable layer capping of the CML with potential gradient $\frac{\theta}{\partial z}\Big|_{z>z_i}$
- g_0 is the standard acceleration due to gravity
- $\theta\{z_i\}$ [K] is the potential temperature at the mixing layer height (z_i)
- Δh_h [m] is the difference between the mixing layer height (z_i [m]) and the emission stack height (h_s [m])

4.5 Effective Parameters - Vertical Inhomogeneity in the PBL

Vertical homogeneity of atmospheric parameters is quite uncommon and unrealistic. One simple example of this is the general decrease of mean horizontal wind speed in the mixing layer towards the surface of the earth. This

creates a problem as the Gaussian plume dispersion equation is derived on the assumption of vertical homogeneity of atmospheric parameters. This problem is addressed by the introduction of effective parameters. The effective parameter value at a specific point assumes the parameter has a constant value from the plume's center of mass (known as the plume centroid height H_p [m]) to that point.

Following the approach by AERMOD (Cimorelli et al., 2004), we formulate effective parameters at a receptor by averaging the value of the parameter within a representative layer. This averaging layer is determined by the vertical half-depth of the plume, defined as $2.15\sigma_z$, but is bounded by H_p and the height of the receptor.

Let ϑ represent an arbitrary parameter. We define the effective parameter ($\tilde{\vartheta}$) by:

$$\tilde{\vartheta} = \frac{1}{z_t - z_b} \int_{z_b}^{z_t} \vartheta\{z\} dz \tag{4.5.1a}$$

$$z_t = \begin{cases} H_p\{x_r, y_r\}, & H_p\{x_r, y_r\} \leq z_r \\ MAX\{H_p\{x_r, y_r\} - 2.15\sigma_z\{x_r\}, z_r\}, & H_p\{x_r, y_r\} > z_r \end{cases} \tag{4.5.1b}$$

$$z_b = \begin{cases} MIN\{H_p\{x_r, y_r\} + 2.15\sigma_z\{x_r\}, z_r\}, & H_p\{x_r, y_r\} \leq z_r \\ H_p\{x_r, y_r\}, & H_p\{x_r, y_r\} > z_r \end{cases} \tag{4.5.1c}$$

where

- H_p [m] is the plume centroid height
- σ_z [m] is the average of the vertical dispersion parameter for the updraft ($j = 1$) and downdraft ($j = 2$) of the vertical PDF

4.5.1 Plume Centroid Height

The plume centroid height H_p [m], used to calculate effective parameters, represents the plume's center of mass. For dispersion in the SBL, the plume centroid height is equivalent to the effective height (i.e. $H_p = H_s$). Similarly, for the penetrated source within the CBL, the plume centroid height is equivalent to the effective height (i.e. $H_p = \psi_{pj}$).

However, unlike in the SBL and the penetrated source contribution in the CBL, H_p is not constant for the direct source contribution in the CBL. AERMOD models H_p for the direct source as being constant to a point at which the plume stabilizes (x_f, H_f), then linearly increases to the vertical midpoint of the CBL $(x_m, \frac{z_i}{2})$, at which point the CBL would be sufficiently mixed. By this logic, we formulate H_p for the direct source, given by:

$$x_f = \begin{cases} \frac{8 r_s (w_s + 3u_s)^2}{w_s u_s}, & F_b = 0 \\ 49 F_b^{\frac{5}{8}}, & F_b < 55 \\ 119 F_b^{\frac{2}{5}}, & F_b \geq 55 \end{cases} \tag{4.5.2a}$$

$$x_m = \bar{u} \frac{z_i}{\overline{\sigma_{wT}}} \tag{4.5.2b}$$

$$H_f = h_s + \Delta h_{d,p} \tag{4.5.2c}$$

$$H_p\{x_r\} = \begin{cases} H_f, & x_r \leq x_f \\ H_f + \left(\frac{\frac{z_i}{2} - H_f}{x_m - x_f} \right) (x_r - x_f), & x_f < x_r \leq x_m \\ \frac{z_i}{2}, & x_r > x_m \end{cases} \tag{4.5.2d}$$

where

- H_p [m] is the plume centroid height
- x_f [m] is the downwind distance at which the plume stabilizes
- $H_f = H_p\{x_f\}$ [m] is the height at which the plume stabilizes
- x_m [m] is the downwind distance at the CBL becomes the sufficiently vertically mixed
- z_i [m] is the mixing layer height
- F_b [$\mathrm{m^4\,s^{-3}}$] is the stack buoyant flux
- r_s [m] is the stack radius
- w_s [$\mathrm{m\,s^{-1}}$] is the stack exit gas velocity
- u_s [$\mathrm{m\,s^{-1}}$] is the mean horizontal wind speed at the stack height

- $\bar{u}$ [$\mathrm{m\,s^{-1}}$] and $\overline{\sigma_{wT}}$ [$\mathrm{m\,s^{-1}}$] are the mean horizontal wind speed and total vertical turbulence averaged over the entire mixing layer.

The values for effective parameters for the direct source also serve for the indirect source.

4.6 Dispersion Parameters

The lateral dispersion parameter of p_y (σ_y) and the vertical dispersion parameters of p_z^s (σ_{zs}) and p_z^d and p_z^r (σ_{zj} where $j \in \{1, 2\}$) are given by:

$$\sigma_{y,z}^2 = \sigma_{ya,za}^2 + \sigma_b^2 \tag{4.6.1a}$$

$$\sigma_{ya} = \frac{\widetilde{\sigma_{vT}} x_r}{\widetilde{u}(1 + \tau\chi)^p} \tag{4.6.1b}$$

$$\sigma_{zas} = \left(1 - \frac{\Delta h_s}{z_i}\right) \sigma_{zgs} + \left(\frac{\Delta h_s}{z_i}\right) \sigma_{zes} \tag{4.6.1c}$$

$$\sigma_{zes} = \frac{\widetilde{\sigma_{wT}}\,\widetilde{t}}{\left[1 + \frac{\widetilde{\sigma_{wT}}\widetilde{t}}{2}\left(\frac{1}{0.36\Delta h_s} + \frac{N_{\{z_r\}}}{0.27\widetilde{\sigma_{wT}}}\right)\right]^{\frac{1}{2}}} \tag{4.6.1d}$$

$$\sigma_{zgs} = \sqrt{\frac{2}{\pi}}(u_* \widetilde{t}) \left(1 + 0.7\frac{x_r}{L}\right)^{-\frac{1}{3}} \tag{4.6.1e}$$

$$\sigma_{zaj}^2 = \sigma_{zej}^2 + \sigma_{zg}^2 \tag{4.6.1f}$$

$$\sigma_{zej} = \alpha_b \sigma_{wj} \widetilde{t} \tag{4.6.1g}$$

$$\sigma_{zg} = \begin{cases} b_c \left(1 - 10\left(\frac{H_p}{z_i}\right)\right)\left(\frac{u_*{}^2 \widetilde{t}^2}{|L|}\right), & H_p < z_i \\ 0, & H_p \geq z_i \end{cases} \tag{4.6.1h}$$

$$\sigma_b = \frac{0.4\Delta h}{\sqrt{2}} \tag{4.6.1i}$$

$$\sigma_{zp} = \frac{1}{2}(\sigma_{z1} + \sigma_{z2}) \tag{4.6.1j}$$

$$\chi = \frac{\widetilde{\sigma_{vT}} x_r}{\widetilde{u} z_i} \tag{4.6.1k}$$

$$\tau = \frac{z_i}{l} \tag{4.6.1l}$$

$$\alpha_b = MIN\{0.6 + \frac{4H_p}{z_i}, 1.0\} \tag{4.6.1m}$$

where

- σ [m] is the dispersion parameter, with subscripts:

  - y - lateral
  - z - vertical
  - a - ambient
  - b - buoyant
  - e - elevated
  - g - near-surface
  - s - stable
  - j - updraft $j = 1$ and downdraft $j = 2$
  - p - penetrated
- $\widetilde{\sigma_{vT}}$ [$\mathrm{m\,s^{-1}}$] is the effective total lateral turbulence
- $\widetilde{\sigma_{wT}}$ [$\mathrm{m\,s^{-1}}$] is the effective total vertical turbulence
- $\widetilde{u}$ [m] is the effective horizontal mean wind speed
- $\widetilde{t} = \frac{x_r}{\widetilde{u}}$ [s] is the effective time
- Δh_s [m] is the stable plume rise height
- z_i [m] is the mixing layer height
- $N\{z\}$ [$\mathrm{s^{-1}}$] is the Brunt-V*äisälä* frequency
- L [m] is the Obukhov length
- u_* [$\mathrm{m\,s^{-1}}$] is the shear velocity scale
- H_p [m] is the plume centroid height
- $p = 0.78$, $l = 0.3$ and $b_c = 0.5$ are empirical constants

Chapter 5

Weather Parameters

As discussed in chapter 4, GLC estimates predicted by the Gaussian plume equation depend on a number of model parameters which themselves are dependent on a number of weather and terrain parameters. Resultantly, the error in the GLCs, as estimated by the Gaussian plume dispersion equation, is an accumulated error. This emphasizes the importance of using the most accurate estimations of the parameters. In this chapter, we provide a general description of the physical structure of the PBL and examine the formulations used by AERMOD that describe the atmospheric dynamics of the aforementioned weather parameters. These weather parameters include: (1) Φ_H, (2) z_i, (3) L, (4) u_*, (5) w_* and (6) the vertical profiles of (a) $u\{z\}$, (b) $\theta\{z\}$, (c) $\frac{\partial\theta}{\partial z}\{z\}$, (d) $\sigma_{vT}\{z\}$ and (e) $\sigma_{wT}\{z\}$.

AERMOD is a collection of both theoretical formulations applicable to the general PBL and empirical formulations. These empirical formulations were established on data representing the meteorology of mid-latitude regions. A reasonable expectation of applying AERMOD to the tropical island of Barbados, instead of a typical mid-latitude country, is that the error incurred on estimating weather parameters will be larger. In this chapter, we examine the formulations for the aforementioned weather parameters, as employed by AERMOD, and introduce alternate formulations for the weather parameters that can be obtained from the input weather data (discussed in chapter 6), that are more reflective of Tropical meteorology. These parameters include: (1) Φ_H and (2) z_i.

5.1 Sensible Surface Heat Flux within the CBL

The solar flux that enters the earth-atmospheric system measures roughly 1367 ± 7 W m^{-2} (Organization, 1982). This value, known as the solar constant (ϕ_{const}) is measured on a surface perpendicular to the incoming solar flux, at the top of the atmosphere (a distance of one astronomical unit from the sun). As the solar influx travels through the atmosphere, it undergoes attenuation from atmospheric gases and clouds and only a portion reaches the surface, with some of this portion being from the direct beam (known as the direct beam radiation ($\Phi_{S_{cb}}$ [W m^{-2}])) and the other part being diffused by atmospheric particles (known as the diffuse sky radiation ($\Phi_{S_{cd}}$ [W m^{-2}])). The sum of $\Phi_{S_{cb}}$ and $\Phi_{S_{cd}}$ is known as the global solar radiation (Φ_{S_0} [W m^{-2}]).

The addition of energy into the earth-atmospheric system through solar influx is balanced by removal of energy from the system by terrestrial flux (the energy flux radiated from the earth's surface) as well as the reflecting of a portion of the solar influx by the surface of the earth and atmospheric particles (known as the earth's albedo effect). The resultant flux between the solar flux and the terrestrial flux is known as the radiative flux or the net radiation (Φ_N [W m^{-2}]). Φ_N can be represented as the summation of its three component fluxes, given by:

$$\Phi_N = \Phi_H + \Phi_{LE} + \Phi_G \tag{5.1.1}$$

where

- Φ_N [W m^{-2}] is the radiative flux
- Φ_H [W m^{-2}] is surface sensible heat flux
- Φ_{LE} [W m^{-2}] is surface latent heat flux - the vertical energy flux between the earth's surface and its atmosphere via evaporated water.
- Φ_G [W m^{-2}] is the ground heat flux - the vertical energy flux through the soil

By employing empirical formulations for Φ_{LE}, using the bowen ratio (B_0 [dimensionless]), given by (Bowen, 1926)

$$\Phi_{LE} = \frac{\Phi_H}{B_0} \tag{5.1.2}$$

and for Φ_G, given by (De Bruin and Holtslag, 1982):

$$\Phi_G = \gamma \Phi_N \tag{5.1.3}$$

where $\gamma = 0.1$ (supported by (Barad, 1958; Burridge and Gadd, 1977; Clothier et al., 1986)) for day-time calculations.

By substituting 5.1.2 and 5.1.3 into 5.1.1, we obtain an expression for Φ_H as function of Φ_N and B_0, given by:

$$\Phi_H = \frac{0.9\Phi_N}{1 + \frac{1}{B_0}} \tag{5.1.4}$$

Theoretically, Φ_N is given as the difference between the incoming solar flux (short-wave) and radiative flux from the atmosphere (long-wave) and the outgoing terrestrial flux (long-wave). However, in the absence of direct measurements of these fluxes, estimations of Φ_N can be generated from variables in routine weather observation reports, given by (Holtslag and Van Ulden, 1983):

$$\Phi_N = \frac{(1 - \overline{\alpha})\Phi_{S_0} + \beta_1 {T_{ref}}^6 - \sigma_{SB} {T_{ref}}^4 + \beta_2 n_T}{1 + \beta_3} \tag{5.1.5}$$

where

- Φ_N [$\mathrm{W\,m^{-2}}$] is the net radiative flux
- Φ_{S_0} [$\mathrm{W\,m^{-2}}$] is the global solar radiation
- T_{ref} [K] is the ambient air temperature measured at the reference height for temperature measurements ($z_{T_{ref}}$ [m])
- n_T [dimensionless] is the fractional total cloud cover
- $\overline{\alpha}$ [dimensionless] is the mean albedo over a one hour period
- $\beta_1 = 5.31 \times 10^{-13}$ $\mathrm{W\,m^{-2}\,K^{-6}}$, $\beta_2 = 60$ $\mathrm{W\,m^{-2}}$ and $\beta_3 = 0.12$ [dimensionless] are empirically determined constants
- σ_{SB} is the Stefan Boltzman constant

Since T_{ref} and n_T are both provided in routine weather observation reports, the accuracy of the estimation of Φ_H, as calculated by the method under discussion, is highly dependent on the accuracy of the measurements of Φ_{S_0}, $\overline{\alpha}_{24}$ and B_0, of which Φ_{S_0} and $\overline{\alpha}_{24}$ are functions of the angle of incidence (i.e. the angle at which the solar influx approaches the surface of the earth, known as the zenith angle (ϕ_Z [rad])).

5.1.1 Zenith Angle

The zenith is an imaginary point on an observer's celestial sphere, that lies directly above the observer. The solar zenith angle (ϕ_Z [rad]) is the angle at the surface of the earth between the solar zenith and the sun, given by (Shivalingaswamy and Kagali, 2012):

$$\phi_Z = \arccos\left\{\sin\left\{\phi_{lat}\right\}\sin\left\{\phi_D\right\} - \cos\left\{\phi_{lat}\right\}\cos\left\{\phi_D\right\}\cos\left\{\phi_H\right\}\right\} \tag{5.1.6a}$$

$$\phi_D = -\frac{23.45\pi}{180}\cos\left\{2\pi\left(\frac{n_j + 10}{365.25}\right)\right\} \tag{5.1.6b}$$

$$\phi_H = \pi\left(\frac{t_{actual} - t_{sunrise}}{t_{sunset} - t_{sunrise}}\right) - \frac{\pi}{2} \tag{5.1.6c}$$

where

- ϕ_Z [rad] is the solar zenith angle at a particular location and time.
- ϕ_{lat} [rad] is the latitude angle at the particular location.
- ϕ_D [rad] is the solar declination angle on the ${n_j}^{th}$ Julian day of the year.
- ϕ_H [rad] is the hour angle at the actual time (t_{actual} [hr]) between the time of sunrise ($t_{sunrise}$ [hr]) and sunset (t_{sunset} [hr]).

5.1.2 Average Albedo

The mean albedo ($\overline{\alpha}$ [dimensionless]), referred to in 5.1.5, is the average value of the albedo over a one hour period (i.e. between the zenith angle of the

present hour (ϕ_{Z_2}) and the past hour (ϕ_{Z_1})), given by:

$$\overline{\alpha} = \frac{1}{\phi_{Z_2} - \phi_{Z_1}} \int_{\phi_{Z_1}}^{\phi_{Z_2}} \alpha\{\phi_Z\} d\phi_Z \tag{5.1.7}$$

The albedo (α [dimensionless]) is the fractional amount of solar influx reflected at the surface of the earth at a particular location, given by (Cimorelli et al., 2004):

$$\alpha\{\phi_Z\} = \alpha_0 + (1 - \alpha_0) \exp\left\{-\frac{18}{\pi}\left(\frac{\pi}{2} - \phi_Z\right) - 0.5\,(1 - \alpha_0)^2\right\} \tag{5.1.8}$$

where:

- $\alpha_0 = \alpha\{\phi_Z = 0\}$

5.1.3 Global Solar Radiation - AERMOD vs Alternate Formulation

At the top of the atmosphere, the incoming solar radiation is a relatively constant value known as the solar constant (Φ_{const}). As this solar radiation travels through the atmosphere, a portion of it is attenuated by the atmosphere as well as by clouds. The total amount of solar radiation that reaches the ground in known as the global solar radiation (Φ_{S_0} [$\mathrm{W\,m^{-2}}$]). In the absence of clouds, Φ_{S_0} is known as the sky clear global solar radiation (Φ_{S_c} [$\mathrm{W\,m^{-2}}$]). Φ_{S_0} is commonly formulated as Φ_{S_c} multiplied by an transmittance factor (A [dimensionless]), i.e. $\Phi_{S_0} = A \times \Phi_{S_c}$.

5.1.3.1 Sky Clear Global Solar Radiation

AERMOD estimates Φ_{S_c} as a function of ϕ_Z, given by the regression formula (Van Ulden and Holtslag, 1985; Lumb, 1964; Collier and Lockwood, 1975; Kasten and Czeplak, 1980):

$$\Phi_{S_c} = 990 \cos\{\phi_Z\} - 30 \tag{5.1.9}$$

Khan and Ahmad (2012) developed an alternate formulation to estimate Φ_{S_c} as the summation of its direct ($\Phi_{S_{cb}}$ [$\mathrm{W\,m^{-2}}$]) and diffused ($\Phi_{S_{cd}}$ [$\mathrm{W\,m^{-2}}$])

components. This formulation models the attenuation effect on the solar radiation by the atmosphere as it travels towards the surface of the earth; as well as fluctuations in Φ_{const} that result from the elliptical orbit of the earth. This alternate formulation is given by the equation:

$$\Phi_{S_c} = \Phi_{S_{cb}} + \Phi_{S_{cd}} \tag{5.1.10a}$$
$$\Phi_{S_{cb}} = \Phi_{on} \cdot \tau_d \cdot \cos\{\phi_Z\} \tag{5.1.10b}$$
$$\Phi_{S_{cd}} = \Phi_{on} \cdot \tau_b \tag{5.1.10c}$$
$$\Phi_{on} = \Phi_{const} \cdot \left[1 + \frac{7}{1367}\cos\left\{2\pi\frac{(n_j - 3)}{365.25}\right\}\right] \tag{5.1.10d}$$
$$\tau_d = 0.271 - 0.294\tau_b \tag{5.1.10e}$$
$$\tau_b = \beta_{10} + \beta_{11}\exp\left\{-\frac{k_t}{\cos\{\phi_Z\}}\right\} \tag{5.1.10f}$$
$$\beta_{10} = a_{10}(0.4237 - 0.00821(6 - h')^2) \tag{5.1.10g}$$
$$\beta_{11} = a_{11}(0.5055 + 0.00595(6.5 - h')^2) \tag{5.1.10h}$$
$$k_t = a_k(0.2711 + 0.01858(2.5 - h')^2) \tag{5.1.10i}$$
$$\tag{5.1.10j}$$

where:

- $\Phi_{S_{cd}}$ [$\mathrm{W\,m^{-2}}$] is the direct beam radiation
- $\Phi_{S_{cb}}$ [$\mathrm{W\,m^{-2}}$] is the diffuse sky radiation
- Φ_{const} is the solar constant
- Φ_{on} [$\mathrm{W\,m^{-2}}$] is the solar flux at the top of the atmosphere on the $n_j{}^{th}$ Julian day of the year
- h' is the elevation at the particular location
- τ_b [dimensionless] is the atmospheric transmittance for the direct beam radiation (as given by (Hottel, 1976)) with the corrective factors β_{10} [dimensionless], β_{11} dimensionless] and k_t dimensionless] and dimensionless constants a_{10}, a_{11} and a_k (which are valued at 0.95, 0.98 and 1.02 for tropical regions)

- τ_d [dimensionless] is the atmospheric transmittance for diffuse sky radiation
- ϕ_Z [rad] is the zenith angle

5.1.3.2 Transmittance Factor

AERMOD employs an transmittance factor (A) as a function of n_T, given by (Kasten and Czeplak, 1980)):

$$A\{n_T\} = 1 - 0.75{n_T}^{3.4}. \tag{5.1.11}$$

In addition to cloud cover, cloud type has been shown to significantly affect the transmittance factor of clouds. Kasten and Czeplak (1980) and Waleed and Yussra (2006) estimated the transmittance of the different cloud types using measured data of Φ_{S_0} (refer to Appendix C and Appendix D). Davies and Uboegbulam (1979) proposed an alternate formulation that estimates A in terms of the fractional cloud cover (n_{Ci} [dimensionless]) and transmittance (k_{Ci}) of individual cloud layers, given by:

$$A = \prod_{i=1}^{n} \left(1 - \left(1 - k_{Ci}\right) n_{Ci}\right) \tag{5.1.12}$$

where:

- n is the number of cloud layers
- k_{Ci} [dimensionless] is the transmittance of the i^{th} cloud layer (summarized in Table D.1)
- n_{Ci} is the fractional cloud cover of the i^{th} cloud layer

By applying the above transmittance factor only to the portion of the sky covered by clouds and allowing the solar radiation passing through the cloudless portion of the sky to be unaffected attenuation, we propose an alternate formulation for estimating A that applies a weight to 5.1.12, given by the equation:

$$A = \left(1 - n_T\right) + n_T \prod_{i=1}^{n} \left(1 - \left(1 - k_{Ci}\right) n_{Ci}\right) \tag{5.1.13}$$

5.1.4 Bowen Ratio - AERMOD vs Alternate Formulation

AERMOD uses B_0 as its mean value during a given season and for a specific vegetative ground cover (refer to Appendix F).

Lin et al. (2016) developed an alternate formulation for estimating B_0 using the relative humidity, in its fractional form, (RH [dimensionless]) and T_{ref}, given by the equation:

$$B_0 = 1.46 \left(\frac{1}{RH}\right) \left(\frac{T_{ref}}{273}\right)^2 \exp\left\{-19.83 \left(1 - \frac{273}{T_{ref}}\right)\right\} \tag{5.1.14}$$

5.2 Obukhov Length, Shear Velocity and Potential Temperature Scale in the CBL

As shown in 2.2.1, L, u_* and θ_* are inter-dependent and, resultantly, cannot be solved analytically. In the absence of analytic solutions, numeric approaches, specifically iterative approaches, have been employed to provide accurate solutions (Wyngaard, 1988).

The aforementioned iterative method requires a re-estimate of Φ_H. The iterative process begins by substituting L_0 into 2.2.1e, obtaining an a preliminary estimate for u_*, denoted as u_{*0}. u_{*0} is then substituted into 2.2.1d to obtain the estimate L_1. This continues until the convergence is achieved, with the criteria for convergence being $\left|\frac{L_i - L_{i-1}}{L_{i-1}}\right| \leq 0.01$.

We represent this iterative approach by the equation:

$$L_{i+1} = \frac{\rho_a c_{pa} T_{ref} {k_v}^2 {u_{ref}}^3}{g_0 \Phi_H \left(\ln\left\{\frac{z_{u_{ref}}}{z_0}\right\} - \psi_M\left\{\zeta\left\{z_{u_{ref}}, L_i\right\}\right\} + \psi_M\left\{\zeta\left\{z_0, L_i\right\}\right\}\right)^3} \tag{5.2.1}$$

where:

- $\psi_M\left\{\zeta\left\{z, L\right\}\right\} = 2\ln\left\{\frac{1+\mu_M\left\{\zeta\left\{z,L\right\}\right\}}{2}\right\} + \ln\left\{\frac{1+\left(\mu_M\left\{\zeta\left\{z,L\right\}\right\}\right)^2}{2}\right\}$
- $\mu_M\left\{\zeta\left\{z, L\right\}\right\} = \left(1 - 16\zeta\left\{z, L\right\}\right)^{\frac{1}{4}}$

- $\zeta\{z, L\} = \frac{z}{L}$

and

- L [m] is the Obukhov length
- ζ [dimensionless] is the stability parameter, where $\zeta_u = \frac{z_{u_{ref}}}{L}$ and $\zeta_0 = \frac{z_0}{L}$
- ψ_M [dimensionless] is the universal stability function in the CBL, as defined by Dyer and Hicks (1970); Panofsky and Dutton (1984); Holtslag (1984)
- ρ_a is the standard air density
- c_{pa} is the specific heat capacity of dry air at constant pressure
- u_{ref} [$\mathrm{m\,s^{-1}}$] is the wind speed measured at the reference height for wind measurements ($z_{u_{ref}}$ [m])
- T_{ref} [K] is the air temperature measured at the reference height for temperature measurements ($z_{T_{ref}}$ [m])
- Φ_H [$\mathrm{W\,s^{-1}}$] is the sensible surface heat flux
- k_v is the Von Kármán constant
- g_0 is the standard acceleration due to gravity

After the final estimate for L is obtained, it is substituted into 2.2.1e and 2.2.1f to obtain estimates for u_* and θ_*.

5.3 Obukhov Length, Shear Velocity and Potential Temperature Scale in the SBL

The iterative formulation employed to find section 5.2 L in the CBL, uses a pre-estimate of Φ_H, whose typical estimation involves B_0. However, the use

of B_0 is limited to day-time applications (refer to Appendix A), and is not applicable to the SBL.

Consequently, AERMOD employs an analytic solution for u_*, using a pre-estimate of θ_*, given by (Venkatram, 1980):

$$u_* = \frac{C_D u_{ref}}{2} \pm \sqrt{\left(\frac{C_D u_{ref}}{2}\right)^2 - C_D u_0}. \tag{5.3.1}$$

5.3.1 is the solution to a quadratic equation obtained by substituting 2.2.1g and 2.2.1d into 2.2.1a, given by:

$${u_*}^2 - C_D u_{ref} u_* + C_D u_0^2 = 0 \tag{5.3.2a}$$

$$C_D = \frac{k_v}{\left(\ln\{\frac{z_{u_{ref}}}{z_0}\}\right)} \tag{5.3.2b}$$

$$u_0^2 = \frac{5 z_{u_{ref}} g_0 \widehat{\theta_*}}{T_{ref}} \tag{5.3.2c}$$

where:

- u_* [m s^{-1}] is the shear velocity
- $\widehat{\theta_*}$ [K] is the pre-estimate of the potential temperature scale
- C_D is the drag coefficient (as defined by (Garratt et al., 1992))
- u_{ref} [m s^{-1}] is the wind speed measured at the reference height for wind measurements ($z_{u_{ref}}$ [m])
- T_{ref} [K] is the air temperature measured at the reference height for temperature measurements ($z_{T_{ref}}$ [m])
- k_v is the Von Kármán constant
- z_0 [m] is the roughness length
- g_0 is the standard acceleration due to gravity

The universal stability function (ψ_M [dimensonless]) used in 2.2.1d is given by (Dyer, 1974):

$$\psi_M = 1 + 5\zeta, \tag{5.3.3}$$

Since $\zeta_u >> \zeta_0$, Dyer (1974) approximates $-\psi_M\{\zeta_u\} + \psi_M\{\zeta_0\} \approx -\psi_M\zeta_u$, as used in 5.3.2c.

$\widehat{\theta_*}$, as employed by AERMOD, is calculated as a function of n_T, given by (Van Ulden and Holtslag, 1985):

$$\theta_* = 0.09\left(1 - 0.5n_T^2\right) \tag{5.3.4}$$

where:

- n_T [dimensionless] is the fractional total cloud cover.

5.3.1 produces real-valued solutions for u_* on the interval $u_{ref} \in [u_{crit}, \infty)$, where $u_{crit} = \sqrt{\frac{4u_0}{C_D}}$. In cases where u_{ref} is below u_{crit}, AERMOD gives u_* and θ_* by applying a scaling factor of $\frac{u_{ref}}{u_{crit}}$ to both u_* and θ_*, given by:

$$u_* = u_*\{u_{crit}\}\left(\frac{u_{ref}}{u_{crit}}\right)$$
$$\theta_* = 0.09\left(1 - 0.5n_T^2\right)\left(\frac{u_{ref}}{u_{crit}}\right).$$

Having obtained estimates for u_* and θ_*, L can be estimated by substituting 2.2.1g into 2.2.1d, yielding the equation:

$$L = \frac{T_{ref}{u_*}^2}{k_v g_0 \theta_*} \tag{5.3.5}$$

5.4 Deardorff Velocity

AERMOD estimates w_* by the equation (Deardorff, 1970; Wyngaard, 1988):

$$w_* = \left(\frac{g_0 \Phi_H z_i}{\rho_a c_{pa} T_{ref}}\right)^{\frac{1}{3}}. \tag{5.1.10 revisited}$$

5.5 Vertical Profile of the Mean Lateral Wind Speed

The vertical profile of mean lateral wind speed, as theorized by the MOS theory is applicable only within the interval $z_0 \leq z \leq z_i$. Hence, 2.2.1a produces unrealistic values of u close to the surface (i.e. below z_0).

AERMOD accounted for these unrealistic values of u obtained approaching z_0 by allowing u to decrease linearly towards the surface, given by (Cenedese et al., 1998):

$$u\{z\} = \begin{cases} u\{z_i\} & z_i < z \\ \frac{u_*}{k_v}\left(\ln\{\frac{z}{z_0}\} - \psi_M\{\zeta\} + \psi_M\{\zeta_0\}\right) & 7z_0 \leq z \leq z_i \\ u\{7z_0\}\left(\frac{z}{7z_0}\right) & z < 7z_0 \end{cases} \tag{5.5.1}$$

where

- u [$\mathrm{m\,s^{-2}}$] is the mean lateral wind speed
- u_* [$\mathrm{m\,s^{-2}}$] is the shear velocity
- k_v is the Von Kármán constant
- z_0 [m] is the roughness length
- ψ_M [dimensionless] is the universal stability function

5.6 Vertical Profile of the Potential Temperature

Theoretically, the vertical profile of the potential temperature, within the mixing layer is described by the log mean potential temperature profile of the MOS theory (given in 2.2.1b). However, AERMOD estimates the potential temperature at a height z by linear interpolation, given by:

$$\theta\{z\} = \theta\{z_{base}\} + \overline{\frac{\partial\theta}{\partial z}}\Delta z, \tag{5.6.1}$$

where

- θ [K] is the potential temperature
- z_{base} [m] is the height of the base of the current layer
- Δz is the depth of the current layer
- $\overline{\frac{\partial \theta}{\partial z}}$ [$\mathrm{K\,m^{-1}}$] is average the potential temperature gradient within the each layer of the PBL.

5.6.1 Estimation of the Vertical Profile of the Vertical Potential Temperature Gradient in the SBL - AERMOD

In the SBL, AERMOD estimates the vertical profile of the potential temperature gradient ($\frac{\partial \theta}{\partial z}\{z\}$ $\mathrm{K\,m^{-1}}$), with minimum value of $\frac{\partial \theta}{\partial z}\{z\}$ bounded by 0.002 $\mathrm{K\,m^{-1}}$ (as given in (Paine and Kendall, 1993)). This is given by the equation (Dyer, 1974; Panofsky and Dutton, 1984; Stull, 1983; Van Ulden and Holtslag, 1985):

$$z_{mx} = 100m \tag{5.6.2a}$$

$$z_{i\theta} = MAX\{z_i, z_{mx}\} \tag{5.6.2b}$$

$$\frac{\partial \theta}{\partial z}\{z\} = \begin{cases} MAX\left\{\frac{\theta_*}{k_v(2)}\left[1+5\frac{2}{L}\right], 0.002\right\}, & z \leq 2m \\ MAX\left\{\frac{\theta_*}{k_v z}\left[1+5\frac{z}{L}\right], 0.002\right\}, & 2m < z \leq 100m \\ MAX\left\{\frac{\partial \theta}{\partial z}\{z=100m\}\exp\left\{-\frac{z-100m}{0.44 z_{i\theta}}\right\}, 0.002\right\}, & z > 100m \end{cases} \tag{5.6.2c}$$

where

- $\frac{\partial \theta}{\partial z}$ [$\mathrm{K\,m^{-1}}$] is the vertical potential temperature gradient
- θ_* [K] is the potential temperature scale
- k_v is the Von Kármán constant
- L [m] is the Obukhov Length

5.6.2 Estimation of the Vertical Profile of the Vertical Potential Temperature Gradient in the CBL - AERMOD

AERMOD bases the vertical potential temperature gradient ($\frac{\partial\theta}{\partial z}$ [K m^{-1}]) on the characteristic of potential temperature in the well-mixed CBL, as opposed to the MOS theory definition. In the CBL, above the super-adiabatic surface layer, $\frac{\partial\theta}{\partial z} = 0$.

In the stable entrainment interfacial layer, that caps the CBL, $\frac{\partial\theta}{\partial z}$ is taken from the 1200 Universal Constant Time (UTC) atmospheric sounding and is persisted through the day under the assumption that $\frac{\partial\theta}{\partial z}$ in the entrainment interfacial layer remains constant throughout the day (as supported by field measurements from the Wangara Experiment (Clarke et al., 1971)). The value for $\frac{\partial\theta}{\partial z}$ in the entrainment interfacial layer is obtained by linear interpolation $\frac{\partial\theta}{\partial z}$ over a 500 m layer above the mixing layer height. The selected thickness of the entrainment interfacial layer was selected to avoid the strong gradients (unrealistic kinks) that are common to atmospheric sounding data, as shown in (Deardorff, 1979).

Above the interfacial layer, θ is assumed to be constant, hence $\frac{\partial\theta}{\partial z} = 0$.

We give the entire vertical profile of $\frac{\partial\theta}{\partial z}$, given by AERMOD as:

$$\frac{\partial\theta}{\partial z}\{z\} = \begin{cases} 0, & 0 \leq z \leq z_i \\ \left(\overline{\frac{\partial\theta}{\partial z}}\right)_{interfacial}, & z_i < z < z_i + 500 \\ 0, & z \geq z_i + 500 \end{cases} \tag{5.6.3a}$$

where

- $\left(\overline{\frac{\partial\theta}{\partial z}}\right)_{interfacial}$ [K m^{-1}] is the gradient in the entrainment interfacial layer

5.7 Vertical Profile of Vertical and Lateral Turbulence - AERMOD

AERMOD estimates the vertical profile of the total vertical turbulence σ_{wT} [m s^{-1}] using the system of equations outlined in AERMOD (Cimorelli et al., 2004), given by:

$$\sigma_{wT}{}^2\{z\} = \sigma_{wc}{}^2\{z\} + \sigma_{wm}{}^2\{z\} \tag{5.7.1a}$$

$$\sigma_{wc}{}^2\{z\} = \begin{cases} 1.6\left(\frac{z}{z_i}\right)^{\frac{2}{3}} w_*{}^2, & z \leq 0.1 z_{ic} \\ 0.35 w_*{}^2, & 0.1 z_{ic} < z \leq z_{ic} \\ 0.35 w_*{}^2 \exp\{-\frac{6(z-z_{ic})}{z_{ic}}\}, & z_{ic} < z \end{cases} \tag{5.7.1b}$$

$$\sigma_{wm}{}^2\{z\} = \sigma_{wml}{}^2 + \sigma_{wmr}{}^2 \tag{5.7.1c}$$

$$\sigma_{wml}\{z\} = \begin{cases} 1.3 u_* \left(1 - \frac{z}{z_i}\right)^{\frac{1}{2}}, & z < z_i \\ 0, & z_i \leq z \end{cases} \tag{5.7.1d}$$

$$\sigma_{wmr}\{z\} = \begin{cases} 0.02\left(\frac{z}{z_i}\right), & z < z_i \\ 0.02, & z_i \leq z \end{cases}, \tag{5.7.1e}$$

where

- σ_{wT} [m s^{-1}] is the total vertical turbulence
- σ_{wc} [m s^{-1}] is the convective portion of the vertical turbulence
- σ_{wm} [m s^{-1}] is the mechanical portion of the vertical turbulence
- σ_{wml} [m s^{-1}] is the mechanical portion of the vertical turbulence generated in the PBL
- σ_{wmr} [m s^{-1}] is the mechanical portion of the vertical turbulence generated by the residual layer above the PBL
- z_{ic} [m] is the depth of the CML
- u_* [m s^{-1}] is the shear velocity

- w_* [m s^{-1}] is the Deardorff velocity

AERMOD estimates the vertical profile of the total lateral turbulence σ_{vT} using the system of equations outlined in AERMOD (Cimorelli et al., 2004), given by:

$$\sigma_{vT}{}^2\{z\} = \sigma_{vc}{}^2\{z\} + \sigma_{vm}{}^2\{z\} \tag{5.7.2a}$$

$$\sigma_{v0}^2 = 3.6{u_*}^2 \tag{5.7.2b}$$

$$\sigma_{vm}{}^2\{z_{im}\} = MIN\{\sigma_{v0}^2, 0.25m^2s^{-2}\} \tag{5.7.2c}$$

$$\sigma_{vm}{}^2\{z\} = \begin{cases} \left[\frac{\sigma_{vm}{}^2\{z_{im}\}-\sigma_{v0}^2}{z_{im}}\right] z + \sigma_{v0}^2, & z \le z_{im} \\ \sigma_{vm}{}^2\{z_{im}\}, & z_{im} < z \end{cases} \tag{5.7.2d}$$

$$\sigma_{vc}{}^2\{z\} = \begin{cases} 0.35{w_*}^2, & z \le z_{ic} \\ MIN\{0.25 + \left(\frac{0.25-\sigma_{vc}{}^2\{z_{ic}\}}{0.2}\right)(z - 1.2z_{ic}), \sigma_{vc}{}^2\{z_{ic}\}\}, & z_{ic} \le z \le 1.2z_{ic} \\ MIN\{0.25m^2s^{-1}, \sigma_{vc}{}^2\{z_{ic}\}\}, & 1.2z_{ic} < z \end{cases} \tag{5.7.2e}$$

where

- σ_{vT} [m s^{-1}] is the total vertical turbulence
- σ_{vc} [m s^{-1}] is the convective portion of the vertical turbulence
- σ_{vm} [m s^{-1}] is the mechanical portion of the vertical turbulence

Both 5.7.1 and 5.7.2 are applicable to the CBL and SBL. However, it is important to note that while both the MML and the CML are features of the CBL, the SBL features only the MML. Resultantly σ_{wc} and σ_{vc} assume a value of zero in the SBL.

5.8 Mixing Layer Height

As mentioned in chapter 2, $z_i = MAX\{z_{ic}, z_{im}\}$. Historically, z_i has been identified by different optimal or critical value criteria in different variables. These include:

- A significant change in vertical temperature gradient $\frac{\partial T}{\partial z}$ in the SBL (Beyrich, 1997)
- The first important variation in the virtual potential temperature gradient ($\frac{\partial \theta_v}{\partial z}$) in the SBL (Dupont et al., 1999)
- An inversion base of the virtual potential temperature (θ_v) vertical profile in the CBL (Dupont et al., 1999)
- $\frac{\partial \theta_v}{\partial z} \geq 8.3\ \mathrm{K\,k\,m^{-1}}$ in the CBL (Bianco and Wilczak, 2002)
- $\frac{\partial \theta_v}{\partial z} \geq 3.0\ \mathrm{K\,k\,m^{-1}}$ in the CBL (Zeng et al., 2004)
- A maximum in temperature gradient in the CBL (Hennemuth and Lammert, 2006)
- A maximum in $\frac{\partial \theta}{\partial z}$ in both the SBL and CBL (Martucci et al., 2007)
- The height from the surface to which the mixing ratio remains constant in both the SBL and CBL (Nielsen-Gammon et al., 2008; Feng et al., 2015)
- A maximum in the humidity gradient (Hennemuth and Lammert, 2006)
- The wind shear, calculated by $\sqrt{\left(\frac{\partial u_x}{\partial z}\right)^2 + \left(\frac{\partial u_y}{\partial z}\right)^2}$, is less than $0.04\mathrm{s}^{-1}$ (Hyun et al., 2005)
- A minimum in wind shear (Zilitinkevich, 1972; Balsley et al., 2006)
- A maximum in the Brunt Väisälä frequency $N = \sqrt{\frac{g}{\theta}\frac{\partial \theta}{\partial z}}$ (Balsley et al., 2006).
- The Richardson number $R_i = \frac{g\frac{\partial \theta}{\partial z}}{\left(\frac{\partial u}{\partial z}\right)^2}$, Gradient Richardson number $R_g = \frac{\frac{g}{T_v}\frac{\partial \theta_v}{\partial z}}{\left(\frac{\partial u_x}{\partial z}\right)^2 + \left(\frac{\partial u_y}{\partial z}\right)^2}$ or Bulk Richardson number $R_B = \frac{\frac{g}{T_v}\frac{\Delta \theta_v}{\Delta z}}{(\Delta u_x)^2 + (\Delta u_y)^2}$ equals that of a critical value $R_{ic} = 0.25$ (Taylor, 1931).

5.8.1 Estimation of the Mixing Layer Height as the Lifting Condensation Level within the CBL

The Lifting Condensation Level (LCL) (h_{LCL} [m]) is the level at which a parcel of moist air lifted dry-adiabatically would become saturated. (i.e. when the relative humidity reaches 100%). This concurs with the criteria used by Hennemuth and Lammert (2006), i.e. a theoretical local maximum in relative humidity.

5.8.1.1 Temporal Evolution of the Lifting Condensation Level within the CBL - AERMOD

AERMOD obtains an initial estimate for the convective mixing height (z_{ic} [m]), as the LCL, from the 1200 UTC atmospheric sounding. The 1200 UTC upper-air report for each participating weather observation station gives the temperature and pressure at the LCL (denoted by T_{LCL} [K] and P_{LCL} [h Pa] respectively). Firstly, T_{LCL} is estimated by the equation Bolton (1980):

$$T_{LCL} = \left[(T_{D500} - 56)^{-1} + 0.00125 \ln \left\{ \frac{T_{500}}{T_{D500}} \right\} \right]^{-1} + 56 \tag{5.8.1}$$

where:

- T_{LCL} [K] is the temperature at the LCL
- T_{500} and T_{D500} are the average temperature and dew point temperature within the 500m layer extending from the surface of the earth

T_{LCL}, is then used to estimate P_{LCL} by Poison's equation, given by:

$$P_{LCL} = P_0 \left(\frac{T_{LCL}}{T_0} \right)^{\frac{cpa}{Ra}} \tag{5.8.2}$$

where:

- P_{LCL} [h Pa] is the pressure at the LCL
- T_{LCL} [K] is the temperature at the LCL

- P_0 [K] and T_0 are the atmospheric pressure and temperate at the surface (base of the layer)
- c_{pa} is the specific heat capacity of air under constant pressure
- $R_a = 287.04$ is the specific gas constant of dry air

We estimate h_{LCL} by interpolating between the 2 consecutive pressure levels in the 1200 UTC upper-air report, within which P_{LCL} falls, using the Hypsometric equation, given by:

$$h_{LCL} = z_0 + \frac{R_a \overline{T_v}}{g_0} \ln\left\{\frac{P_0}{P_{LCL}}\right\} \tag{5.8.3}$$

where:

- h_{LCL} [m] is the height at the LCL
- P_{LCL} [h Pa] is the pressure at the LCL
- z_0 [m] and P_0 [K] are the corresponding height and pressure at the base of the layer (i.e. the lower of the two levels)
- $\overline{T_v}$ is the mean virtual potential temperature within the layer
- R_a is the specific gas constant of dry air
- g_0 is the standard acceleration due to gravity

Using this initial estimate for z_{ic} at 1200 UTC, subsequent values of z_{ic} are obtained from modelling the temporal evolution of z_{ic}, given by Carson (1973); Weil and Brower (1983):

$$z_{ic} \cdot \theta\{z_{ic}\} - \int_0^{z_{ic}} \theta\{z\} dz = (1 - 2A) \int_0^{t'} \frac{\Phi_H\{t\}}{\rho_a c_{pa}} dt \tag{5.8.4}$$

where

- z_{ic} [m] is the convective mixing layer height
- θ [K] is the potential temperature

- Φ_H [$\mathrm{W\,m^{-2}}$] is the sensible surface heat flux
- t' [hr] is the hour after sunrise
- ρ_a is the standard air density
- c_{pa} is the specific heat capacity of air at constant pressure
- $A = 0.2$ (Deardorff, 1980).

5.8.1.2 Exact Expression for the Height of the LCL - Alternate

Alternately, we estimate z_i and T_{LCL} using an exact expression, given by (Romps, 2017):

$$R_m = (1-q)R_a + qR_v \tag{5.8.5a}$$
$$c_{pm} = (1-q)c_{pa} + qc_{pv} \tag{5.8.5b}$$
$$a = \frac{c_{pm}}{R_m} + \frac{c_{vl} - c_{pv}}{R_v} \tag{5.8.5c}$$
$$b = -\frac{E_{0v} - (c_{vv} - c_{vl})T_{trip}}{R_v T_{ref}} \tag{5.8.5d}$$
$$c = a/b \tag{5.8.5e}$$
$$T_{LCL} = c\left[W^{-1}\{(RH)^{\frac{1}{a}} c\exp\{c\}\}\right]^{-1} T_{ref} \tag{5.8.5f}$$
$$h_{LCL} = z_{T_{ref}} + \frac{c_{pm}}{g_0}(T_{ref} - T_{LCL}) \tag{5.8.5g}$$

where

- W_{-1} is the -1 branch of the Lambert W function
- q [dimensionless] is the specific humidity
- T_{ref} [K], q [dimensionless] and RH [dimensionless] are the air temperature, specific humidity and fractional form of the relative humidity at the reference height for temperature measurements ($z_{T_{ref}}$ [m])
- c_{pa} is the specific heat capacity of air at constant pressure
- c_{va} is the specific heat capacity of dry air at constant volume

- c_{pv} is the specific heat capacity of water vapour at constant pressure
- c_{vv} is the specific heat capacity of water vapour at constant volume
- R_a is the specific gas constant of dry air
- R_v is the specific gas constant of water vapour
- g_0 is the standard acceleration due to gravity
- c_{vl} is the specific heat capacity of liquid water
- $T_{trip} = 273.16$ K
- $E_{0v} = 2.3740 \times 10^6$ J k g^{-1}

5.8.2 Estimation of the Mixing Layer Height within the SBL - AERMOD

AERMOD estimates z_{im} by modelling the time evolution of z_{im}, given by Venkatram (1982):

$$z_{im}\{t + \Delta t\} = z_{im}\{t\} \exp\{-\frac{\Delta t}{\tau}\} + z_{ie}\{t + \Delta t\} \left[1 - \exp\{-\frac{\Delta t}{\tau}\}\right] \quad (5.8.6a)$$

$$z_{ie} = 0.4 \left(\frac{u_* L}{f}\right) \quad (5.8.6b)$$

$$\tau = \frac{z_{im}}{\beta_T u_*} \quad (5.8.6c)$$

$$f = 2\omega \sin\{\phi_{lat} = 0.35\} \quad (5.8.6d)$$

where

- z_{im} [m] is the depth of the mechanical mixing layer
- z_{ie} [m] is the equivalent mechanical mixing layer height
- u_* [m s^{-1}] is the shear velocity
- *tau* [s] is a time scale that governs the rate of change of height within the MML

- f [s^{-1}] is the Coriolis parameter with latitude sets to 0.35 rad to avoid unrealistic values of z_{ie} (Sugiyama and Nasstrom, 1999)
- ω is the angular velocity of the earth
- $\beta_T = 2$ is an empirical constant
- ϕ_{lat} [rad] is the latitudinal angle

5.9 Transition between CBL and SBL

As mentioned in section 5.1, the sign of the sensible surface heat flux Φ_H [$W\,m^{-2}$] is associated directly associated with the current stage of the PBL. The neutral convective transition phase occurs when $\Phi_H \to 0$, which translates to $\Phi_N \to 0$. By this concept, an average solar zenith critical angle ($\phi_Z = \phi_{crit}$ [rad]) can be defined which relates to the transition between phases of the PBL.

5.9.1 Estimation of the Critical Angle - AERMOD

AERMOD estimates the average solar zenith critical angle (ϕ_{crit} [rad]) at which this transition occurs, ϕ_{crit}, using **??** and setting Φ_N to zero to obtain an iterative equation, given by:

$$\cos\{\phi_{crit}\} = \frac{1}{990}\left[\frac{-\beta_1 {T_{ref}}^6 + \sigma_{SB} {T_{ref}}^4 - \beta_2 n_T}{(1-\alpha\{\phi_Z\})\,(1-0.75{n_T}^{3.4})} + 30\right] \tag{5.9.1}$$

Using the daytime average values, Holtslag and Van Ulden (1983) found that the average critical solar zenith angle ($\overline{\phi_{crit}}$ [rad]) varied from a minimum of about 77 degrees, on clear days, to about 67 degrees on overcast days. This translates to an average elevation angle ($\overline{\phi_E}$) of 13 to 23 degrees. These critical values are adopted by AERMOD to demarcate the transition between the CBL and SBL phases.

5.9.2 Estimation Method of the Critical Angle - ALTERNATE

We develop an alternate estimation method for the average critical solar zenith angle (ϕ_{crit} [rad]) using the alternate estimation method for the global solar radiation (given in 5.1.12), which incorporates the alternate estimation method for the clear sky global solar radiation (given in 5.1.10). By substituting 5.1.12 and 5.1.10 into **??**, we develop and iterative solution for ϕ_{crit}, given by:

$$\alpha\{\phi_{crit}\} = 1 + \frac{\beta_1 {T_{ref}}^6 - \sigma_{SB} {T_{ref}}^4 + \beta_2 n_T}{\Phi_{S_c}\{\phi_{crit}\} \left(\prod_{i=1}^{4} \left(1 - \left(1 - k_{t_i}\right) n_{C_i}\right) \right)} \tag{5.9.2}$$

Chapter 6

Model Evaluation

In this chapter, we mix and match the different formulations of the Bowen ratio ($B_{0i}, i \in \{1, 2\}$ [dimensionless]), sky clear global radiation ($\Phi_{S_c j}, j \in \{1, 2\}$ [W m^{-2}]), cloud transmittance factor ($A_k, k \in \{1, 2, 3\}$ [dimensionless]) to obtain 12 different estimators for the sensible surface heat flux ($\Phi_{H\,i,j,k}$ [W m^{-2}])) in the CBL, where $\Phi_{H\,1,1,1}$ represents the formulation for Φ_H used in AERMOD.

We use each $\Phi_{H\,i,j,k}$ formulation to develop corresponding formulations estimating the vertical profiles of the mean lateral wind speed ($u_{i,j,k}\{z\}$ [m s^{-1}]), the potential temperature ($\theta_{i,j,k}\{z\}$ [K]) and the overall mass concentration of SO_2 ($C_{i,j,k}$ [µ g m^{-3}]). Finally, we calculate the Mean Squared Error (MSE) of each formulation on a similar data set, using both formulations of z_{ic} given in subsection 5.8.1, as a measure of the performance of each estimator.

6.1 Description of Datasets and Conversion Methods

Generating each $\Phi_{H\,i,j,k}$ estimation (as described in 6.3.1), and subsequently $L_{i,j,k}$ and $u_{*i,j,k}$ and $u_{i,j,k}$ estimation, requires various primary parameters. This includes:

- Hours of sunrise ($H_{sunrise} \in [0, 24]$ [hr]) and sunset ($H_s unset \in [0, 24]$ [hr])

- Latitudinal angle of Barbados (ϕ_{lat} [rad])
- Fractional total cloud cover ($n_T \in [0, 1]$ [dimensionless])
- Fraction cloud cover ($n_{Ci} \in [0, 1]$ [dimensionless]) and transmittance ($k_{Cn} \in [0, 1]$ [dimensionless]) of the i^{th} cloud layer
- Mean albedo at solar noon ($\alpha_0 = \alpha\{\phi_Z = 0\}$ [dimensionless])
- Height of the ground above mean sea level ($h = h\{X, Y\}$ [m]), where X and Y represent the longitude and latitude at the particular location.
- Air temperature (T_{ref} [K]) and fractional relative humidity (RH [dimensionless]) measured at the reference height for temperature measurements ($z_{T_{ref}}$ [m])
- Mean lateral wind speed (u_{ref} [$\mathrm{m\,s^{-1}}$]) measured at the reference height for wind measurements ($z_{u_{ref}} = 10$ [m])
- Temperature at the mixing layer height (T_{LCL} [K])

We obtain values for the aforementioned primary parameters, over the period extending from January 1, 2008 to September 8, 2015 at 1200 UTC, using the following datasets:

1. Dataset 1 - 75624 entries of hourly synoptic weather observation data (The Barbados Meteorological Services, 2017) covering 3151 days and 24 hours. Important variables within this dataset include:
    - Total cloud cover (measured in oktas) - converted to its fraction form (n_T) by applying a multiplicative factor of 0.125.
    - Cloud cover of the i^{th} cloud layer (measured in oktas), $i \in \{1, 2, 3, 4\}$ - converted to its fractional form (n_{Ci}) by applying a multiplicative factor of 0.125.
    - Cloud number of the i^{th} cloud layer - converted to the transmittance of the i^{th} cloud layer (k_{Ci}) using the conversion summarized in Table D.1.

- Reference temperature (measured in degrees Celsius) measured at the reference height for temperature measurements ($z_{T_{ref}} = 2$ m) - converted to its thermodynamic temperature form (T_{ref}) by applying an additive factor of 273.15.
- Relative humidity (as a percentage) measured at the reference height for temperature measurements ($z_{T_{ref}} = 2$ m) - converted to its fractional form (RH) by applying a multiplicative factor of 0.01.
- Mean lateral wind speed (measured in knots) at the reference height for wind measurements ($z_{u_{ref}} = 10$ m) - converted to its SI-units value (u_{ref}) by applying a multiplicative factor of $\frac{49}{90}$.

2. Dataset 2 - 2545 days of available atmospheric sounding data. Important variables within this dataset include:
   - Mean lateral wind speed (measured in knots) at a number of n levels of height - converted to its SI-units value ($u = u\{z\}$) by applying a multiplicative factor of $\frac{49}{90}$.
   - Atmospheric Pressure at the height of the LCL (P_{LCL} [h Pa]).
   - Potential temperature (θ [K]) at a number of n levels of height.
3. Dataset 3 - A Geographic Information Systems (GIS) data set of the height of ground above mean sea level across Barbados at 100 m resolution (The Caribbean Institute for Meteorological and Hydrology, 2017). Important variables within this dataset include:
   - The height (h [m]) of ground given from the reference of mean sea level (0 m).
4. Dataset 4 - Sunrise and sunset time database for Barbados (Timeanddate.com, 2018). Important variables within this database include:
   - Sunrise and sunset times (in hours and minutes) - converted to $H_{sunrise}$ and H_{sunset}, respectively, by changing the time from hours and minutes (hh:mm) to hours

6.2 Average Value of Atmospheric Transmittance Corrective Factors

We calculate the average value of each atmospheric transmittance corrective factor ($\beta_{10}\{h'\}$, $\beta_{11}\{h'\}$ and $k_t\{h'\}$, discussed in subsection 5.1.3) by estimating the value of each corrective value function over the terrain of Barbados using the height data in Dataset 3, given by:

$$\overline{\beta_{10}} = \frac{1}{N \cdot M} \sum_{n=1}^{N} \sum_{m=1}^{M} a_{10}(0.4237 - 0.00821(6 - h'_{n,m})^2) = 0.1310428$$

$$\overline{\beta_{11}} = \frac{1}{N \cdot M} \sum_{n=1}^{N} \sum_{m=1}^{M} a_{11}(0.5055 + 0.00595(6.5 - h'_{n,m})^2) = 0.7342016$$

$$\overline{k_t} = \frac{1}{N \cdot M} \sum_{n=1}^{N} \sum_{m=1}^{M} a_{k}(0.2711 + 0.01858(2.5 - h'_{n,m})^2) = 0.1368551$$

(5.1.10 revisited)

where:

- $\overline{\beta_{10}}$, $\overline{\beta_{11}}$ and $\overline{k_t}$ are the average value of β_{10}, β_{11} and k_t respectively
- n indexes the N longitude points and m indexes the M latitude points across Barbados, within the dataset

6.3 Sensible Surface Heat Flux Formulations

As detailed in chapter 4, the sensible surface heat flux (Φ_H [$\mathrm{W\,m^{-2}}$]) has a cascading effect on the resulting estimation of mass concentration. Φ_H is a key parameter used in estimating the Obukhov length (L [m]), Deardorff velocity (w_* [$\mathrm{m\,s^{-1}}$]) and the temporal evolution of the convective mixing layer height (z_{ic} [m]), in the CBL phase. Successively, L, w_*, w_* and z_{ic} are used in the estimation of several model parameters.

We obtain 12 different formulations to estimate Φ_H (denoted by $\Phi_{H\,i,j,k}$, as displayed in Table 6.1) in the CBL using the different formulations of

the Bowen ratio ($B_{0i}, i \in \{1, 2\}$, discussed in subsection 5.1.4), the clear sky global solar radiation ($\Phi_{S_c j}, j \in \{1, 2\}$, discussed in subsection 5.1.3) and the transmittance factor ($A_k, k \in \{1, 2, 3\}$, discussed in subsection 5.1.3). The formulation of $\Phi_{H i,j,k}$ can be represented by a system of equations, given by:

$$\Phi_{H i,j,k} = \frac{0.9\Phi_{N j,k}}{1 + \frac{1}{B_{0i}}} \tag{6.3.1a}$$

$$\Phi_{N j,k} = \frac{(1 - \overline{\alpha}\{\phi_Z\})\Phi_{S_0 j,k} + \beta_1 {T_{ref}}^6 - \sigma_{SB} {T_{ref}}^4 + \beta_2 n_T}{1 + \beta_3} \tag{6.3.1b}$$

$$\Phi_{S_0 j,k} = A_k \cdot \Phi_{S_c j} \tag{6.3.1c}$$

$$\overline{\alpha}\{\phi_Z\} = \int_{\phi_{Z_2}}^{\phi_{Z_1}} \left(\alpha_{B_0} + (1 - \alpha_{B_0}) \exp\left\{ \frac{180\beta_4}{\pi} \left(\frac{\pi}{2} - \phi_Z \right) + \beta_5 \right\} \right) d\phi_Z \tag{6.3.1d}$$

$$\phi_Z = \arccos\left\{ \sin\left\{\phi_{lat_B}\right\} \sin\left\{\phi_D\right\} - \cos\left\{\phi_{lat_B}\right\} \cos\left\{\phi_D\right\} \cos\left\{\phi_H\right\} \right\} \tag{6.3.1e}$$

$$\phi_D = -\frac{23.45\pi}{180} \cos\left\{ 2\pi \left(\frac{n_j + 10}{365.25} \right) \right\} \tag{6.3.1f}$$

$$\phi_H = \pi \left(\frac{H_{actual} - H_{sunrise}}{H_{sunset} - H_{sunrise}} \right) - \frac{\pi}{2} \tag{6.3.1g}$$

where:

- B_{01} is summarized in Appendix F and B_{02} is given by 5.1.14
- $\Phi_{S_c 1}$ is given by 5.1.9 and $\Phi_{S_c 2}$ is given by 5.1.10
- A_1 is given by 5.1.11, $A_2, 3$ is given by 5.1.13.
- $\Phi_{S_0 j,k}$ [$\mathrm{W\,m^{-2}}$] is the global solar radiation estimate, calculated using $\Phi_{S_c j}$ and A_k
- $\Phi_{N j,k}$ [$\mathrm{W\,m^{-2}}$] is the net radiation estimate, calculated using $\Phi_{S_0 j,k}$
- T_{ref} [K] is the ambient air at the reference level for temperature ($z_{T_{ref}}$)
- n_T [dimensionless] is the fractional total cloud cover

Table 6.1: Formulations for $\Phi_{H_{i,j,k}}$

	Parameter Formulations						
	B_0		Φ_{S_c}		A_i		
Φ_H	B_{01}	B_{02}	Φ_{S_c1}	Φ_{S_c2}	A_1	A_2	A_3
$\Phi_{H\,\text{AERMOD}}$	●		●		●		
$\Phi_{H\,1,1,2}$	●		●			●	
$\Phi_{H\,1,1,3}$	●		●				●
$\Phi_{H\,1,2,1}$	●			●	●		
$\Phi_{H\,1,2,2}$	●			●		●	
$\Phi_{H\,1,2,3}$	●			●			●
$\Phi_{H\,2,1,1}$		●	●		●		
$\Phi_{H\,2,1,2}$		●	●			●	
$\Phi_{H\,2,1,3}$		●	●				●
$\Phi_{H\,2,2,1}$		●		●	●		
$\Phi_{H\,2,2,2}$		●		●		●	
$\Phi_{H\,2,2,3}$		●		●			●

- α [dimensionless] is the albedo with $\alpha_{B_0} = 0.1865$ being the mean albedo at solar noon across Barbados (refer to Appendix E)
- ϕ_Z [rad] is the solar zenith angle
- ϕ_H [rad] is the solar hour angle
- ϕ_D [rad] is the solar declination angle
- $\phi_{lat_B} = 13.19^0$ N is the latitudinal angle of Barbados
- $H_{sunrise}$, H_{sunset}, H_{actual} are the times for sunrise, sunset and the current time converted to decimal values
- n_j is the n^{th} Julian day of the year
- $\beta_1 = 5.31 \times 10^{-13}$ W m^{-2} K^{-6}, $\beta_2 = 60$ W m^{-2} and $\beta_3 = 0.12$ [dimensionless], $\beta_4 = -0.1$ [dimensionless] and $\beta_5 = -0.5(1 - \alpha_{B_0})^2$ [dimensionless] are empirical constants
- σ_{SB} is the Stefan Boltzmann constant

6.3.1 Evaluation of the Formulations of the Bowen Ratio

According to the land cover class definitions developed by the United States Geological Survey (usgs), Barbados classifies as a low intensity residential area (refer to Appendix G). The table of average B_0 values employed by AERMOD (refer to Appendix F), shows five different estimates of the mean value of B_0 for each usgs class over the entire year; as well as during the dry and wet seasons. The specific estimate used by AERMOD depends information entered by the user when setting up the model that describes the land surface and ice cover of the site (EPA, 2018). Due to the tropical location of Barbados, AERMOD select seasonal value of B_0 from column one.

Resultantly, we use define B_{01} by the equation:

$$B_{01} = \begin{cases} 0.6 & \text{, during the wet season,} \\ 2.0 & \text{, during the dry season,} \\ 0.8 & \text{, overall mean} \end{cases} \tag{6.3.2}$$

Alternately, we estimate B_0 as a function of T_{ref} and RH. Let $B_{02} : D_1 \times D_2 \to C)$ be the function defined by the equation:

$$B_{02}\{T_{ref}, RH\} = 1.46 \left(\frac{1}{RH}\right) \left(\frac{T_{ref}}{273}\right)^2 \exp\left\{-19.83\left(1 - \frac{273}{T_{ref}}\right)\right\} \tag{5.1.14 revisited}$$

where:

- $T_{ref} \in D_1 = (0, \infty)$ is the reference temperature
- $RH \in D_2 = (0, 1]$ is the relative humidity in fraction form
- $B_{02} \in C = (0, \infty)$

We obtain a 2 dataset of B_0 values by applying B_{01} and B_{02} to dataset 1. Furthermore, we obtain 2 datasets of Φ_H values, in terms of Φ_N, by applying 6.3.1a to dataset 1 using B_0 as the corresponding pair of estimates obtained from B_{01} and B_{02}. The obtained B_0 datasets show that on dataset 1, the B_0 estimates produced by B_{02} are approximately 20%, 59% and 47% of that

Table 6.2: Comparion of B_0 estimates

Season	B_0 Estimate	Mean B_0	Mean Φ_H
Dry	B_{01}	2.0	$0.6\Phi_N$
	B_{02}	0.4007 ± 0.0396	$0.2570\Phi_N \pm 0.0178\Phi_N$
Wet	B_{01}	0.6	$0.3375\Phi_N$
	B_{02}	0.3526 ± 0.0243	$0.234\Phi_N \pm 0.0118\Phi_N$
Overall	B_{01}	0.8	$0.4\Phi_N$
	B_{02}	0.3726 ± 0.0394	$0.2438\Phi_N \pm 0.0183\Phi_N$

produced by B_{01} during the dry season, wet season and overall respectively. Resultantly, the Φ_H values obtained by B_{02} on dataset 1 are approximately 43%, 69% and 61% of that produced by B_{01} during the dry season, wet season and overall respectively (refer to Table 6.2).

6.3.2 Evaluation of the Formulations of the Sky Clear Global Radiation

As discussed in subsection 5.1.3, AERMOD estimates Φ_{S_c} as a function of ϕ_Z. Let $\Phi_{S_c1} : D \to C$ be the function defined by the equation:

$$\Phi_{S_c1}\{\phi_Z\} = 990\cos\{\phi_Z\} - 30 \qquad \text{(5.1.9 revisited)}$$

where:

- $\phi_Z \in D = \left(0, \arccos\left\{\frac{1}{33}\right\}\right)$ is the solar zenith angle.
- $\Phi_{S_c1} \in C = (0, 960)$ is the sky clear global solar radiation.

Although ϕ_Z varies from 0[rad] at solar noon to $\frac{\pi}{2}$ at sunrise and sunset, the domain of Φ_{S_c1} is restricted to $D = \left(0, \arccos\left\{\frac{1}{33}\right\}\right)$. This ensures the theoretical boundary constraints on ϕ_Z (i.e. $0 \leq \phi_Z \leq \frac{\pi}{2}$) is met as $\Phi_{S_c1} < 0$ on the interval $\phi_Z \in \left(\arccos\frac{1}{33}, \frac{\pi}{2}\right)$.

Alternately, we estimate Φ_{S_c} as a function of ϕ_Z and n_j. Let Φ_{S_c2} :

$D_1 \times D_2 \to C$ be the function defined by the equation:

$$\begin{aligned}
\Phi_{S_c2}\{\phi_Z, n_j\} &= \Phi_{S_{cb}}\{\phi_Z, n_j\} + \Phi_{S_{cd}}\{\phi_Z, n_j\} \\
\Phi_{S_{cb}}\{\phi_Z, n_j\} &= \Phi_{on}\{n_j\} \cdot \tau_d\{\phi_Z\} \cdot \cos\{\phi_Z\} \\
\Phi_{S_{cd}}\{\phi_Z, n_j\} &= \Phi_{on} \cdot \tau_b\{\phi_Z\} \\
\Phi_{on}\{n_j\} &= \Phi_{const} \cdot \left[1 + \frac{7}{1367}\cos\left\{2\pi\frac{(n_j - 3)}{365.25}\right\}\right] \\
\tau_d\{\phi_Z\} &= 0.271 - 0.294\tau_b\{\phi_Z\} \\
\tau_b\{\phi_Z\} &= 0.1310428 + 0.7342016\exp\left\{-\frac{0.1368551}{\cos\{\phi_Z\}}\right\}
\end{aligned}$$

(5.1.10 revisited)

where:

- $\phi_Z \in D_1 = \left(0, \frac{\pi}{2}\right)$ [rad] is the solar zenith angle.
- $n_j \in D_2 = (1, 366)$ is the Julian day of the year.
- $\Phi_{S_c2} \in C = (0, 1120.5853208)$ is the sky clear global solar radiation.
- $\Phi_{S_{cd}}$ [$\mathrm{W\,m^{-2}}$] is the direct beam radiation.
- $\Phi_{S_{cb}}$ [$\mathrm{W\,m^{-2}}$] is the diffuse sky radiation.
- Φ_{const} is the solar constant.
- Φ_{on} [$\mathrm{W\,m^{-2}}$] is the solar flux at the top of the atmosphere on the ${n_j}^{th}$ Julian day of the year.
- τ_b [dimensionless] is the atmospheric transmittance for the direct beam radiation.
- τ_d [dimensionless] is the atmospheric transmittance for diffuse sky radiation.

We define upper and lower bounds of Φ_{S_c2} defining the range by the global maximum (i.e. $MAX\{\Phi_{S_c2}\} = \Phi_{S_c2}\{0, 3\} = 1120.5853208$) and the global minimum (i.e. $MIN\{\Phi_{S_c2}\} = \Phi_{S_c2}\left\{\frac{\pi}{2}, n_j\right\} = 0$)

To compare Φ_{S_c1} and Φ_{S_c2} we calculate the maximum and minimum values of the difference function (i.e. $\Phi_{S_c2} - \Phi_{S_c1}$) on the interval where both

functions are defined (i.e. $\phi_Z \in \left(0, \arccos\left\{\frac{1}{33}\right\}\right)$ and $n_j \in (1, 366)$). Let $\Phi_{S_c diff}$ be the function that defines the difference between $\Phi_{S_c 2}$ and $\Phi_{S_c 1}$, given by the equation:

$$\Phi_{S_c diff}\{\phi_Z, n_j\} = |\Phi_{S_c 2}\{\phi_Z, n_j\} - \Phi_{S_c 1}\{\phi_Z\}|$$

The largest and smallest discrepancy between $\Phi_{S_c 1}$ and $\Phi_{S_c 2}$ should occur at the global maximum and minimum points of $\Phi_{S_c diff}$ on its defined domian, denoted by $MAX\{\Phi_{S_c diff}\}$ and $MIN\{\Phi_{S_c diff}\}$ respectively. Over its defined domain, $\Phi_{S_c diff}$ achieves a global maximum value $\Phi_{S_c diff}\{1.263, 3\} \approx 591.824$ and a global minimum value $\Phi_{S_c diff}\{0, 185.625\} \approx 149.167$.

The point value of $\Phi_{S_c 1}$ and $\Phi_{S_c 2}$ at the global maximum and minimum of $\Phi_{S_c diff}$ reveals that$|\Phi_{S_c 2}\{\phi_Z, n_j\} - \Phi_{S_c 1}\{\phi_Z\}| = \Phi_{S_c 2}\{\phi_Z, n_j\} - \Phi_{S_c 1}\{\phi_Z\}$. At the point $(\phi_Z, n_j) = (1.263, 3)$, $\Phi_{S_c 2} = 861.774$ and $\Phi_{S_c 1} = 269.930$, and at the point $(\phi_Z, n_j) = (0, 185.625)$, $\Phi_{S_c 2} = 1109.167$ and $\Phi_{S_c 1} = 960.0$. Following this logic, we see that $MAX\{\Phi_{S_c diff}\} = \Phi_{S_c 2}(1.263, 3) - \Phi_{S_c 1}(1.263)$ and $MIN\{\Phi_{S_c diff}\} = \Phi_{S_c 2}(0, 185.625) - \Phi_{S_c 1}(0)$. Hence we can derive that $0 < \Phi_{S_c 2} - \Phi_{S_c 1}$ and conclude that $\Phi_{S_c 1} < \Phi_{S_c 2}$.

This result implies that values of Φ_{S_c} estimated by $\Phi_{S_c 2}$ should be greater than that estimated by $\Phi_{S_c 1}$ by a factor ranging from $\frac{\Phi_{S_c 2}\{0,186.625\}}{\Phi_{S_c 2}\{0\}} \approx \frac{1109.167}{960.0} \approx 1.155$ to $\frac{\Phi_{S_c 2}\{1.263,3\}}{\Phi_{S_c 2}\{1.263\}} \approx \frac{861.754}{269.930} \approx 3.193$. On data set 1, estimates of Φ_{S_c} using $\Phi_{S_c 2}$ was greater than estimates of Φ_{S_c} using $\Phi_{S_c 1}$ by a average factor of 3.0338.

6.3.3 Evaluation of the Formulations of the Transmittance Factor

As discussed in subsection 5.1.3, Φ_{S_0} is defined as Φ_{S_c} to which an transmittance factor has been applied to account for the attenuation effect of clouds. AERMOD uses an transmittance factor, as a function of n_T. Let $A_1 : D \to C$ be the function defined by the equation:

$$A_1\{n_T\} = 1 - 0.75{n_T}^{3.4} \qquad \text{(5.1.11 revisited)}$$

where:

- $n_{Ti} \in D_1 = (0, 1)$ is the fractional total cloud cover.
- $A_1 \in C = (0.25, 1)$ is the transmittance factor

Alternately, we formulated two functions that estimate A considering n_{Ci} and (k_{Ci} for a maximum of four cloud layers, denoted A_2 and A_3. Let $A_{2,3} : D_1 \times D_2^{k1} \times ... \times D_2^{k4} \times D_3^{n1} \times ... \times D_3^{n4} \to C$ be functions defined by the equation:

$$A_{2,3} = (1 - n_T) + n_T \prod_{i=1}^{4} \left(1 - \left(1 - k_{C2,3_i}\right) n_{Ci}\right) \qquad \text{(5.1.12 revisited)}$$

where:

- $n_{Ti} \in D_1 = (0, 1)$ is the fractional total cloud cover.
- $n_{Ci} \in D_2 = (0, 1)$ is the fractional cloud cover for the i^{th} cloud layer, where $0 \leq n_{Ci} \leq n_T$.
- $k_{C2_i} \in D_3 = (0, 1)$ is the transmittance of the i^{th} cloud layer as estimated by Waleed and Yussra (2006) (refer to Appendix D).
- $k_{C3_i} \in D_3 = (0, 1)$ is the transmittance of the i^{th} cloud layer as estimated by Kasten and Czeplak (1980) (as given Appendix C).
- $A_{2,3} \in C = (0, 1)$ is the transmittance factor estimated using the corresponding $k_{C2,3_i}$

In the absence of clouds, A_1, A_2 and A_3 all satisfy the base condition of the transmittance factor (i.e as $n_T \to 0$ $A \to 1$). In the presence of clouds, however, the value of A estimated by A_1, A_2 and A_3 vary in magnitude depending on the value of n_T as well as the values of n_{Ci} and k_{C2_i} for each individual cloud layer. The base condition as well as the variability in A, resulting from the difference in transmittance of each cloud type and number of cloud layers, is clearly reflected in estimates of A generated by A_1, A_2 and A_3 on dataset 1. Not only is there a general decrease in A as n_T increases but there is also an increase in the variability of A estimates using A_1 and A_2 as n_T. This is shown in both the increase in standard deviation of estimates using A_2 and A_3 as well as the increase in the range of the estimates (refer to Table 6.3).

Table 6.3: Cloud Transmittance Estimator Statistics on Dataset 1

n_T	A Estimate	Mean	Std.	Max.	Min.
0.0	A_1	1.0	0.0	1.0	1.0
	A_2	1.0	0.0	1.0	1.0
	A_3	1.0	0.0	1.0	1.0
0.125	A_1	0.99936	0.0	0.99936	0.99936
	A_2	0.88078	0.00018	0.88126	0.87789
	A_3	0.87561	0	0.87564	0.87513
0.25	A_1	0.99327	0.0	0.99327	0.99327
	A_2	0.76195	0.00025	0.76251	0.75578
	A_3	0.75124	0	0.75128	0.75026
0.375	A_1	0.97328	0.0	0.97328	0.97328
	A_2	0.64441	0.00329	0.66561	0.63368
	A_3	0.6272	0.00111	0.63444	0.62539
0.5	A_1	0.92895	0.0	0.92895	0.92895
	A_2	0.53026	0.00828	0.55615	0.51609
	A_3	0.5042	0.00281	0.51278	0.50112
0.625	A_1	0.84828	0.0	0.84828	0.84828
	A_2	0.42344	0.01393	0.50883	0.38946
	A_3	0.38358	0.00519	0.4355	0.37566
0.75	A_1	0.71799	0.0	0.71799	0.71799
	A_2	0.32423	0.02178	0.44408	0.28431
	A_3	0.26618	0.0118	0.34666	0.25303
0.875	A_1	0.52369	0.0	0.52369	0.52369
	A_2	0.2463	0.04814	0.68047	0.15712
	A_3	0.16164	0.03437	0.69607	0.12749
1.0	A_1	0.25	0.0	0.25	0.25
	A_2	0.19459	0.08034	0.64649	0.05376
	A_3	0.07886	0.06688	0.68881	0.00542

Table 6.4: My caption

Ratio between $\Phi_{H_{i,j,k}}$ and $\Phi_{H_{1,1,1}}$	Mean	Std	Max	Min
$\Phi_{H_{1,1,1}}/\Phi_{H_{1,1,1}}$	1.0	0.0	1.0	1.0
$\Phi_{H_{1,1,2}}/\Phi_{H_{1,1,1}}$	0.51	0.17561	8.40444	0.04893
$\Phi_{H_{1,1,3}}/\Phi_{H_{1,1,1}}$	0.40507	0.20001	8.78029	0.0001
$\Phi_{H_{1,2,1}}/\Phi_{H_{1,1,1}}$	2.21332	1.6428	37.43103	1.16496
$\Phi_{H_{1,2,2}}/\Phi_{H_{1,1,1}}$	1.21715	1.20864	76.62156	0.33215
$\Phi_{H_{1,2,3}}/\Phi_{H_{1,1,1}}$	1.00877	1.16711	79.07262	0.02516
$\Phi_{H_{2,1,1}}/\Phi_{H_{1,1,1}}$	0.40139	0.08922	1.01237	0.30572
$\Phi_{H_{2,1,2}}/\Phi_{H_{1,1,1}}$	0.20484	0.08494	2.86876	0.02022
$\Phi_{H_{2,1,3}}/\Phi_{H_{1,1,1}}$	0.16345	0.0914	2.99706	0
$\Phi_{H_{2,2,1}}/\Phi_{H_{1,1,1}}$	0.89593	0.71676	16.05647	0.362
$\Phi_{H_{2,2,2}}/\Phi_{H_{1,1,1}}$	0.49325	0.50559	26.15392	0.11435
$\Phi_{H_{2,2,3}}/\Phi_{H_{1,1,1}}$	0.49325	0.50559	26.15392	0.11435

6.3.4 Evaluation of the Formulations of Sensible Surface Heat Flux

As discussed in subsection 6.3.2, the functions to estimate Φ_{S_c} (i.e. Φ_{S_c1} and Φ_{S_c2}) are solely dependent on the position of the sun relative to the earth and generally $0 \leq \Phi_{S_c1} < \Phi_{S_c2}$. On the other hand, the functions to estimate B_0 (i.e. B_{01} and B_{02}) and A (i.e. A_1, A_2 and A_3) depend on the climate of the location and show no general precedence. However, due to the climate of Barbados (as represented by Dataset 1) we can conclude that generally $0 < B_{02} < B_{01}$ and that on average $A_{2,3} < A_1$. Resultantly, we find that on average the greatest estimates of Φ_{S_c} are obtained using $\Phi_{S_c1,2,1}$ and the least estimates using $\Phi_{S_c2,1,2}$ and $\Phi_{S_c2,1,3}$. On Dataset 1, $\Phi_{S_c1,2,1}$ produces values greater than the estimate used in AERMOD ($\Phi_{S_c1,1,1}$) by an average multiplicative factor of 2.21332 while $\Phi_{S_c2,1,2}$ and $\Phi_{S_c2,1,3}$ produces values less than $\Phi_{S_c1,1,1}$ by an average multiplicative factor of 0.20484 and 0.16345 respectively (refer to Table 6.4)

In the absence of measured values of Φ_{S_c}, we test the accuracy of each $\Phi_{S_ci,j,k}$ formulation by its accuracy in predicting the vertical profiles of the mean lateral wind speed ($u\{z\}$) and potential temperature ($\theta\{z\}$) in the CBL, as modelled by MOS theory (refer to 2.2.1). This is achieved by the following process:

1. Using Dataset 1, we obtain estimates of Φ_H using each of the $\Phi_{Hi,j,k}$ formulations (refer to 6.3.1).

2. We employ each $\Phi_{Hi,j,k}$ estimate to the iterative process discussed in section 5.2 (restated in 6.3.4a), using stoppage criteria $\left|\frac{L_{i+1}-L_i}{L_i}\right| < 0.00001$, as discussed in section 5.2. We denote the value of L obtained using each $\Phi_{Hi,j,k}$ formulation as $L_{i,j,k}$.

3. We employ each $L_{i,j,k}$ estimate to calculate corresponding estimates of u_* (refer to 6.3.4b) and θ_* (6.3.4c), denoted as $u_{*i,j,k}$ and $\theta_{*i,j,k}$ respectively.

4. - We obtain estimates of the $u\{z\}$ profile using the each corresponding pair of L and u_* estimates. We denote each $u\{z\}$ estimation as $u_{i,j,k}\{z\}$.
   - We obtain estimates of the $\theta\{z\}$ profile using the each corresponding pair of L and θ_* estimates. We denote each $\theta\{z\}$ estimation as $\theta_{i,j,k}\{z\}$. Additionally, we also estimate Additionally, we also estimate θ by the method employed in AERMOD (discussed in subsection 5.6.2).

5. We estimate the height of the CBL (z_i [m]) using the two methods mentioned in subsection 5.8.1. We denote the estimate of z_i obtained using the the exact expression for the lifting condensation (refer to 5.8.5) level by h_{LCL} and the estimate obtained via linear interpolation of the atmospheric sounding at 1200 UTC from Dataset 2 (refer to 6.3.6) by Z_{LCL}.

6. Using the measured values for the vertical profiles of u and θ in Dataset 2, we calculate the weighted mean squared error (refer to 6.3.7) for each $u_{i,j,k}\{z\}$ and $\theta_{i,j,k}\{z\}$ estimator for the days where Dataset 1 and Dataset 2 correspond (i.e. 1200 UTC in the CBL) using each z_i estimate.

Upper air reports features data measured at both mandatory and significant levels within the atmosphere as measured by radiosonde. While mandatory levels are fixed, significant levels are levels at which measured parameters change by significant amounts and hence depend on the state of

the atmosphere at the time of measurement (**?**). Resultantly, the total number of levels and their corresponding heights in each report in inconsistent and will likely influence the size of MSEs for each day. To address this, we apply a weighting factor to the MSE and average the weighted MSE for each upper air report in Dataset 2.

Our calculations of the average weighted MSE reveals that regardless of the estimate of z_i employed, the $\Phi_{S_c 1,2,1}$ estimator leads to the most accurate estimations of u, followed by $\Phi_{S_c 1,2,2}$ and $\Phi_{S_c 1,2,3}$, while the estimator $\Phi_{S_c 1,2,1}$ leads to the least accurate estimations of u, followed by $\Phi_{S_c 1,2,2}$ then $\Phi_{S_c 1,2,3}$. On the other hand, the estimator $\Phi_{S_c 2,1,3}$ leads to the least accurate estimations of u, followed by $\Phi_{S_c 2,1,2}$ then $\Phi_{S_c 2,1,1}$, while the estimator $\Phi_{S_c 2,1,1}$ leads to the least accurate estimations of θ, followed by $\Phi_{S_c 2,1,2}$ then $\Phi_{S_c 2,1,3}$ (refer to Table 6.5 and Table 6.6).

$$L_{i+1} = \frac{\rho_a c_{pa} T_{ref} {k_v}^2 {u_{ref}}^3}{g_0 \Phi_H \left(\ln\left\{\frac{z_{u_{ref}}}{z_0}\right\} - \psi_M\left\{\zeta\left\{z_{u_{ref}}, L_i\right\}\right\} + \psi_M\left\{\zeta\left\{z_0, L_i\right\}\right\}\right)^3} \tag{6.3.4a}$$

$$u_* = \frac{k_v u_{ref}}{\ln\{\frac{z_{u_{ref}}}{z_0}\} - \psi_M\{\zeta_u\} + \psi_M\{\zeta_0\}} \tag{6.3.4b}$$

$$\theta_* = -\frac{\Phi_H}{\rho_a c_{pa} u_*} \tag{6.3.4c}$$

$$u\{z\} = \frac{u_*}{k_v}\left[\ln\left\{\frac{z}{z_0}\right\} - \psi_M\{z, L\} + \psi_M\{z_0, L\}\right] \tag{6.3.4d}$$

$$\theta\{z\} = \theta\{z_0\} + \frac{\theta_*}{k_v}\left[\ln\left\{\frac{z}{z_0}\right\} - \psi_H\{z, L\} + \psi_H\{z_0, L\}\right] \tag{6.3.4e}$$

$$\psi_{M,H}\{z, L\} = 2\ln\left\{\frac{1+\mu_{M,H}}{2}\right\} + \ln\left\{\frac{1+\mu_{M,H}^2}{1}\right\} - \arctan\left\{\mu_{M,H}\right\} + \frac{\pi}{2} \tag{6.3.4f}$$

$$\mu_M = \left(1 - \frac{16z}{L}\right)^{0.25} \tag{6.3.4g}$$

$$\mu_H = \left(1 - \frac{16z}{L}\right)^{0.5} \tag{6.3.4h}$$

- u $[\mathrm{m\,s^{-1}}]$ is the lateral mean wind speed within the mixing layer

- θ [K] is the lateral mean potential temperature within the mixing layer
- ζ [dimensionless] is the stability parameter, with $\zeta_0 = \frac{z_0}{L}$
- L [m] is the Obukhov length - a length scale depicting the height at which turbulence is generated more by buoyancy than by wind shear
- u_* [$\mathrm{m\,s^{-1}}$] is the shear velocity (formerly friction velocity) - a velocity scale used to describe shear-related motion in turbulent flow within the mixing layer
- θ_* [K] is the potential temperature scale - a temperature scale used to describe turbulent flow flow within the mixing layer
- Φ_H [$\mathrm{W\,s^{-1}}$] is the sensible surface heat flux, discussed in section 5.1
- k_v [dimensionless] is the von Kármán constant
- z_0 [m] is the roughness length - the height within the turbulent mixing layer at which the wind speed theoretically becomes zero
- g_0 is the standard acceleration due to gravity
- ψ_M [dimensionless] and ψ_H [dimensionless] are universal stability functions of the momentum and heat fluxes, respectively, within the mixing layer
- μ_M [dimensionless] and μ_H [dimensionless] are stability functions of the momentum and heat fluxes, respectively, within the CBL
- ρ_a is the standard air density
- c_{pa} is the specific heat capacity of dry air at constant pressure
- u_{ref} [$\mathrm{m\,s^{-1}}$] is the wind speed measured at the reference height for wind measurements ($z_{u_{ref}}$ [m])
- T_{ref} [K] is the air temperature measured at the reference height for temperature measurements ($z_{T_{ref}}$ [m])
- θ_1 [K] and θ_2 [K] are the potential temperature corresponding to the heights z_1 and z_2, respectively.

$$
\begin{aligned}
R_m &= (1-q)R_a + qR_v \\
c_{pm} &= (1-q)c_{pa} + qc_{pv} \\
a &= \frac{c_{pm}}{R_m} + \frac{c_{vl} - c_{pv}}{R_v} \\
b &= -\frac{E_{0v} - (c_{vv} - c_{vl})T_{trip}}{R_v T_{ref}} \\
c &= a/b \\
T_{LCL} &= c\left[W^{-1}\{(RH)^{\frac{1}{a}} c \exp\{c\}\}\right]^{-1} T_{ref} \\
h_{LCL} &= z_{T_{ref}} + \frac{c_{pm}}{g_0}(T_{ref} - T_{LCL}) \qquad \text{(5.8.5 revisited)}
\end{aligned}
$$

where

- W_{-1} is the -1 branch of the Lambert W function
- q [dimensionless] is the specific humidity
- T_{ref} [K], q [dimensionless] and RH [dimensionless] are the air temperature, specific humidity and fractional form of the relative humidity at the reference height for temperature measurements ($z_{T_{ref}}$ [m])
- c_{pa} is the specific heat capacity of air at constant pressure
- c_{va} is the specific heat capacity of dry air at constant volume
- c_{pv} is the specific heat capacity of water vapour at constant pressure
- c_{vv} is the specific heat capacity of water vapour at constant volume
- R_a is the specific gas constant of dry air
- R_v is the specific gas constant of water vapour
- g_0 is the standard acceleration due to gravity
- c_{vl} is the specific heat capacity of liquid water
- $T_{trip} = 273.16$ K

- $E_{0v} = 2.3740 \times 10^6 \ \mathrm{J\,k\,g^{-1}}$

$$Z_{LCL} = z_i + \frac{z_{i+1} - z_i}{P_{i+1} - P_i} \cdot (P_{LCL} - P_i), \quad P_i \geq P_{LCL} > P_{i+1} \tag{6.3.6}$$

where:

- Z_LCL [m] is the estimate of the mixing layer height
- P_{LCL} [h Pa] is the atmospheric pressure at the LCL
- P_i [h Pa] and P_{i+1} [h Pa] are values of atmospheric pressure at subsequent levels having heights z_i [m] and z_{i+1} [m] respectively.

Let φ be a random variable with a predictor denoted by $\varphi_{i,j,k}$. We measure the accuracy of the predictor $\varphi_{i,j,k}$ using a weighted MSE, given by the equation:

$$\mathrm{MSE}\{\varphi_{i,j,k}\} = \frac{1}{M} \sum_{m=1}^{M} \frac{1}{N} \sum_{n=1}^{N} \lambda_{n,m} \cdot ((\varphi)_{n,m} - (\varphi_{i,j,k})_{n,m})^2 \tag{6.3.7}$$

where:

- $(\varphi)_{n,m}$ is the measured value of the variable on m^{th} the day ($m \in (1, 2, ..., M)$) and at the n^{th} height level ($n \in (1, 2, ..., N)$).
- $(\varphi_{i,j,k})_{n,m}$ is the estimated value of the variable on m^{th} the day and at the n^{th} height level.
- $\lambda_{n,m} = \frac{|z_{n,m} - z_{ref}|}{\sum_{n=1}^{N} |z_{n,m} - z_{ref}|}$ is a weighting coefficient applied to each calculation on m^{th} the day and at the n^{th} height level, where $\sum_{n=1}^{N} \lambda_{n,m} = 1$.

Table 6.5: Weighted MSE of each $u_{i,j,k}$ estimator using both Z_LCL and h_{LCL} estimates of z_i

	Weighted MSE for each estimate of z_i	
Estimator	Z_LCL	h_{LCL}
$u_{1,1,1}$	0.0000106977	0.0000237916
$u_{1,1,2}$	0.0000128834	0.0000282429
$u_{1,1,3}$	0.0000135073	0.0000294045
$u_{1,2,1}$	0.0000079665	0.0000178041
$u_{1,2,2}$	0.0000092044	0.0000206538
$u_{1,2,3}$	0.0000096103	0.0000214971
$u_{2,1,1}$	0.0000136795	0.0000297381
$u_{2,1,2}$	0.0000160722	0.0000341957
$u_{2,1,3}$	0.0000166307	0.0000351476
$u_{2,2,1}$	0.0000100562	0.0000224154
$u_{2,2,2}$	0.0000117760	0.0000260313
$u_{2,2,3}$	0.0000117760	0.0000260313

Table 6.6: Weighted MSE of each $\theta_{i,j,k}$ estimator using both Z_LCL and h_{LCL} estimates of z_i

	Weighted MSE for each estimate of z_i	
Estimator	Z_LCL	h_{LCL}
θ_{AERMOD}	0.0000009762	0.0000019902
$\theta_{1,1,1}$	0.0000012860	0.0000018714
$\theta_{1,1,2}$	0.0000009398	0.0000013712
$\theta_{1,1,3}$	0.0000009274	0.0000014132
$\theta_{1,2,1}$	0.0000044859	0.0000095739
$\theta_{1,2,2}$	0.0000015925	0.0000029125
$\theta_{1,2,3}$	0.0000013958	0.0000024852
$\theta_{2,1,1}$	0.0000008610	0.0000012421
$\theta_{2,1,2}$	0.0000008707	0.0000014360
$\theta_{2,1,3}$	0.0000008775	0.0000014847
$\theta_{2,2,1}$	0.0000012047	0.0000019325
$\theta_{2,2,2}$	0.0000009308	0.0000013151
$\theta_{2,2,3}$	0.0000009308	0.0000013151

Appendix A

Sources of error using the Bowen ratio-energy balance (BREB) method

Table A.1

Error	Condition
A	$\Phi_N - \Phi_G > 0, \Delta e > 0$ and $B_0 < -1 + \lvert\epsilon\rvert$
B	$\Phi_N - \Phi_G > 0, \Delta e < 0$ and $B_0 > -1 + \lvert\epsilon\rvert$
C	$\Phi_N - \Phi_G < 0, \Delta e > 0$ and $B_0 > -1 + \lvert\epsilon\rvert$
D	$\Phi_N - \Phi_G < 0, \Delta e < 0$ and $B_0 < -1 + \lvert\epsilon\rvert$
E	Rapidly changing T and e

Summary of cases when the BREB method fails (Perez et al., 1999). $\Phi_N - \Phi_G$ is the available energy, Δe the vapor pressure difference between the lower and the upper measurement levels, B_0 the Bowen ratio, T and e the air temperature and vapor pressure, and ϵ the error interval defining the excluded interval of Bowen ratio values around -1.

Appendix B

An Integrated Approach to Estimating the Mixing Layer Height from Radiosonde Data

Radiosonde data can be used in integrated approach to estimating the mixing layer height z_i based on the potential temperature θ, relative humidity RH, specific humidity q and refractive index N (Wang and Wang, 2014). The mixing layer height estimated from each variable is based on widely accepted methods:

- θ- The mixing layer height derived from θ, referred to as $z_{i\theta}$, is the maximum gradient of the θ vertical profile.
- RH - The mixing layer height derived from RH, referred to as z_{iRH}, is the maximum gradient of the RH vertical profile.
- q - The mixing layer height derived from q, referred to as z_{iq}, is the maximum gradient of the q vertical profile.
- N- The mixing layer height derived from N, referred to as z_{iN}, is the maximum gradient of the N vertical profile.

The estimate for z_i is determined as follows:

1. Identify the height z_i that best meets the four individ- ual criteria:

a Smooth the gradient profiles of θ, RH, q and N by 1–2–1 smoother.

b Locate the altitudes of the 10 smallest gradients (or largest for θ) of the four variables. All 10 altitudes are considered to meet the criterion of the mixing layer top and are likely to be the h.

c Starting with the altitudes of the smallest gradients (or largest for θ), identify the first altitude where at least three of the four variables meet the criteria of h simultaneously. The altitude meeting these criteria is set as z_{i0}. The allowable error is 50 m. If all altitudes do not meet the criteria until the 10^{th} smallest gradient, then the mixing layer height for the specific record is missing.

2. Derive the location of the cloud:

a Transform the RH with respect to ice instead of liquid water for all of the levels with temperatures below 0^0C.

b Derive the boundary of the moist layer. The base of the moist layer is defined as the level where the RH exceeds the minimum RH corresponding to this level. Likewise, the top of the moist layer is determined as the level where the RH decreases to the minimum RH corresponding to the level or where the top of the profile is reached. Any moist layer with a base lower than 120 m was discarded. The minimum RH value is specified in Table 1.

c The moist layer is classified as a cloud layer if the maximum RH within this layer is greater than the corresponding maximum RH at the base of the moist layer. Two contiguous layers are considered a one- layer cloud if the distance between the two layers is less than 300 m or if the minimum RH over the distance is larger than the maximum inter-RH value within this distance. The maximum RH, inter-RH values are specified in Table 1.

3. Determine a consistent mixing layer height z_{icon}:

a If z_{i0} is lower than the base of the lowest cloud or identified in clear sky conditions, then the $z_{icon} = z_{i0}$.

b If z_{i0} is higher than the base of the lowest cloud, then scan from the lower three levels of the cloud base to the upper three levels of the cloud top to identify the first stable layer that is deeper than

100 m. Set the level of the sharpest inversion in the stable layer as z_{icon}. If a stable layer does not exist within the cloud, then the $z_{icon} = z_{i0}$.

Appendix C

Cloud Transmittances: Study 1

From a dataset of ten-year (1964–1973) continuous records at Hamburg, Germany, of hourly sums of solar and terrestrial, downward and upward radiation flux densities and simultaneous hourly cloud observations, Kasten and Czeplak (1980) evaluated the mean transmittance of each cloud type, given by:

Table C.1: Mean Transmittance of Cloud Types (Kasten and Czeplak, 1980)

Cloud Number	Cloud Type	Cloud Symbol	Mean Transmittance (k_{t_i})
0	Cirrus	Ci	0.61
1	Cirrocumulus	Cc	0.61
2	Cirrostratus	Cs	0.61
3	Altocumulus	Ac	0.27
4	Altostratus	As	0.27
5	Nimbostratus	Ns	0.16
6	Stratocumulus	Sc	0.25
7	Stratus	St	0.18
8	Cumulus	Cu	0.25
9	Cumulonimbus	Cb	0.25

Appendix D

Cloud Transmittances: Study 2

From datasets of clouds of different types and altitudes (Low, Middle and High) and solar radiation intensity incident on the horizontal surface, collected during the days of winter and spring months of 2004 – 2005, Waleed and Yussra (2006) evaluated the mean transmittance of each cloud type, given by:

Table D.1: Mean Transmittance of Cloud Types(Waleed and Yussra, 2006)

Cloud Number	Cloud Type	Cloud Symbol	Mean Transmittance (k_{t_i})
0	Cirrus	Ci	0.82
1	Cirrocumulus	Cc	N/A
2	Cirrostratus	Cs	0.84
3	Altocumulus	Ac	0.49
4	Altostratus	As	0.50
5	Nimbostratus	Ns	N/A
6	Stratocumulus	Sc	0.21
7	Stratus	St	N/A
8	Cumulus	Cu	0.19
9	Cumulonimbus	Cb	0.19 (assumed)

Appendix E

Albedo of Natural Surfaces in Barbados

Table E.1: Albedos of Natural Surfaces in Barbados (Chia, 1967)

Surface Cover Type	Percentage Area	Albedo
Sugar cane fields	47	0.17
Vegetable crops	8	0.155
Bare soil surfaces	5	0.11
Sour grass pastures, wasteland	15	0.20
Built-up areas, roads	25	0.15
Total land surface	100	
Average albedo		0.165

Appendix F

Seasonal Variations in Average Bowen Ratio used in AERMOD

Table A-2. Seasonal Values of Bowen Ratio for the NLCD92 21-Land Cover Classification System

Class Number	Class Name	Seasonal Bowen Ratio[1] – Average					Seasonal Bowen Ratio[1] - Wet					Seasonal Bowen Ratio[1] - Dry					Reference
		1	*2*	*3*	*4*[2]	*5*	*1*	*2*	*3*	*4*[2]	*5*	*1*	*2*	*3*	*4*[2]	*5*	
11	Open Water	0.1	0.1	0.1	0.1	0.1	0.1	0.1	0.1	0.1	0.1	0.1	0.1	0.1	0.1	0.1	AERMET&Oke[3]
12	Perennial Ice/Snow	0.5	0.5	0.5	0.5	0.5	0.5	0.5	0.5	0.5	0.5	0.5	0.5	0.5	0.5	0.5	AERMET&Oke[3]
21	Low Intensity Residential	0.8	1	1	0.5	0.8	0.6	0.6	0.6	0.5	0.6	2	2.5	2.5	0.5	2	Estimate[4]
22	High Intensity Residential	1.5	1.5	1.5	0.5	1.5	1	1	1	0.5	1	3	3	3	0.5	3	AERMET&Oke[3]
23	Commercial/Industrial/Transp (Site at Airport)	1.5	1.5	1.5	0.5	1.5	1	1	1	0.5	1	3	3	3	0.5	3	AERMET&Oke[3]
	Commercial/Industrial/Transp (Not at Airport)	1.5	1.5	1.5	0.5	1.5	1	1	1	0.5	1	3	3	3	0.5	3	AERMET&Oke[3]
31	Bare Rock/Sand/Clay (Arid Region)	4	6	6	NA	3	1.5	2	2	NA	1	6	10	10	NA	5	AERMET&Oke[3]
	Bare Rock/Sand/Clay (Non-arid Region)	1.5	1.5	1.5	0.5	1.5	1	1	1	0.5	1	3	3	3	0.5	3	AERMET&Oke[3]
32	Quarries/Strip Mines/Gravel	1.5	1.5	1.5	0.5	1.5	1	1	1	0.5	1	3	3	3	0.5	3	AERMET&Oke[3]
33	Transitional	1	1	1	0.5	1	0.7	0.7	0.7	0.5	0.7	2	2	2	0.5	2	Estimate[5]
41	Deciduous Forest	0.3	1	1	0.5	0.7	0.2	0.4	0.4	0.5	0.3	0.6	2	2	0.5	1.5	AERMET&Oke[3]
42	Evergreen Forest	0.3	0.8	0.8	0.5	0.7	0.2	0.3	0.3	0.5	0.3	0.6	1.5	1.5	0.5	1.5	AERMET&Oke[3]
43	Mixed Forest	0.3	0.9	0.9	0.5	0.7	0.2	0.35	0.35	0.5	0.3	0.6	1.75	1.75	0.5	1.5	(41+42)/2[6]
51	Shrubland (Arid Region)	4	6	6	NA	3	1.5	2	2	NA	1	6	10	10	NA	5	AERMET&Oke[3]
	Shrubland (Non-arid Region)	1	1.5	1.5	0.5	1	0.8	1	1	0.5	0.8	2.5	3	3	0.5	2.5	Estimate[7]
61	Orchards/Vineyards/Other	0.5	0.7	0.7	0.5	0.3	0.3	0.4	0.4	0.5	0.2	1.5	2	2	0.5	1	AERMET&Oke[3]
71	Grasslands/Herbaceous	0.8	1	1	0.5	0.4	0.4	0.5	0.5	0.5	0.3	2	2	2	0.5	1	AERMET&Oke[3]
81	Pasture/Hay	0.5	0.7	0.7	0.5	0.3	0.3	0.4	0.4	0.5	0.2	1.5	2	2	0.5	1	AERMET&Oke[3]
82	Row Crops	0.5	0.7	0.7	0.5	0.3	0.3	0.4	0.4	0.5	0.2	1.5	2	2	0.5	1	AERMET&Oke[3]
83	Small Grains	0.5	0.7	0.7	0.5	0.3	0.3	0.4	0.4	0.5	0.2	1.5	2	2	0.5	1	AERMET&Oke[3]

84	Fallow	0.5	0.7	0.7	0.5	0.3	0.3	0.4	0.4	0.5	0.2	1.5	2	2	0.5	1	AERMET&Oke[3]
85	Urban/Recreational Grasses	0.5	0.7	0.7	0.5	0.3	0.3	0.4	0.4	0.5	0.2	1.5	2	2	0.5	1	AERMET&Oke[3]
91	Woody Wetlands	0.2	0.2	0.3	0.5	0.2	0.1	0.1	0.1	0.5	0.1	0.2	0.2	0.2	0.5	0.2	Estimate[7]
92	Emergent Herbaceous Wetlands	0.1	0.1	0.1	0.5	0.1	0.1	0.1	0.1	0.5	0.1	0.2	0.2	0.2	0.5	0.2	AERMET&Oke[3]

[1] Values are listed for the following seasonal categories: *1 - Midsummer with lush vegetation; 2 - Autumn with unharvested cropland; 3 - Late autumn after frost and harvest; or winter with no snow; 4 - Winter with continuous snow on ground; 5 - Transitional spring with partial green coverage or short annuals.*

[2] Values for seasonal category 4 are based on the AERMET User's Guide (EPA, 2004a) and Oke (1978), Tables 4-2a-c, Bowen ratio values for winter with continuous snow cover, except for class 11 with the assumption the water does not freeze.

[3] Values for seasonal categories 1, 2, 3 & 5 are based on AERMET User's Guide (EPA, 2004a), Tables 4-2a-c and Oke (1978).

[4] Estimate based on composition being an equal mix of three classes: "High Intensity Residential", "Mixed Forest", and "Urban/Recreational Grasses."

[5] Estimate based on the Bowen ratio of "Transitional" being between the Bowen ratio of Classes 31 and 71.

[6] Assume "Mixed Forest" is composed of equal parts of "Deciduous Forest" and "Evergreen Forest."

[7] Estimate based on comparison to Bowen ratio for other classes.

Appendix G

USGC Land Cover Class Definitions

The following information, taken from the usgs documentation on the NLCD92, provides more detailed descriptions of the 21 land cover categories in NLCD92.

Water

Definition : All areas of open water or permanent ice/snow cover.

- Open Water - All areas of open water; typically 25 percent or greater cover of water (per pixel).
- Perennial Ice/Snow - All areas characterized by year-long cover of ice and/or snow.

Developed

Definition: Areas characterized by a high percentage (30 percent or greater) of constructed materials (e.g. asphalt, concrete, buildings, etc).

- Low Intensity Residential - Includes areas with a mixture of constructed materials and vegetation. Constructed materials account for 30-80 percent of the cover. Vegetation may account for 20 to 70 percent of the cover. These areas most commonly include single-family housing units. Population densities will be lower than in high intensity residential areas.

- High Intensity Residential - Includes highly developed areas where people reside in high numbers. Examples include apartment complexes and row houses. Vegetation accounts for less than 20 percent of the cover. Constructed materials account for 80 to100 percent of the cover.

- Commercial/Industrial/Transportation - Includes infrastructure (e.g. roads, railroads, etc.) and all highly developed areas not classified as High Intensity Residential.

Barren

Definition: Areas characterized by bare rock, gravel, sand, silt, clay, or other earthen material, with little or no "green" vegetation present regardless of its inherent ability to support life. Vegetation, if present, is more widely spaced and scrubby than that in the "green" vegetated categories; lichen cover may be extensive.

- Bare Rock/Sand/Clay - Perennially barren areas of bedrock, desert pavement, scarps, talus, slides, volcanic material, glacial debris, beaches, and other accumulations of earthen material.

- Quarries/Strip Mines/Gravel Pits - Areas of extractive mining activities with significant surface expression.

- Transitional - Areas of sparse vegetative cover (less than 25 percent of cover) that are dynamically changing from one land cover to another, often because of land use activities. Examples include forest clearcuts, a transition phase between forest and agricultural land, the temporary clearing of vegetation, and changes due to natural causes (e.g. fire, flood, etc.).

Forested Upland

Definition: Areas characterized by tree cover (natural or semi-natural woody vegetation, generally greater than 6 meters tall); tree canopy accounts for 25-100 percent of the cover.

- Deciduous Forest - Areas dominated by trees where 75 percent or more of the tree species shed foliage simultaneously in response to seasonal change.

- Evergreen Forest - Areas dominated by trees where 75 percent or more of the tree species maintain their leaves all year. Canopy is never without green foliage.

- Mixed Forest - Areas dominated by trees where neither deciduous nor evergreen species represent more than 75 percent of the cover present.

Shrubland

Definition: Areas characterized by natural or semi-natural woody vegetation with aerial stems, generally less than 6 meters tall, with individuals or clumps not touching to interlocking. Both evergreen and deciduous species of true shrubs, young trees, and trees or shrubs that are small or stunted because of environmental conditions are included.

- Shrubland - Areas dominated by shrubs; shrub canopy accounts for 25-100 percent of the cover. Shrub cover is generally greater than 25 percent when tree cover is less than 25 percent. Shrub cover may be less than 25 percent in cases when the cover of other life forms (e.g. herbaceous or tree) is less than 25 percent and shrubs cover exceeds the cover of the other life forms.

Non-natural Woody

Definition: Areas dominated by non-natural woody vegetation; non-natural woody vegetative canopy accounts for 25-100 percent of the cover. The non-natural woody classification is subject to the availability of sufficient ancillary data to differentiate non-natural woody vegetation from natural woody vegetation.

- Orchards/Vineyards/Other - Orchards, vineyards, and other areas planted or maintained for the production of fruits, nuts, berries, or ornamentals.

Herbaceous Upland Definition: Upland areas characterized by natural or semi-natural herbaceous vegetation; herbaceous vegetation accounts for 75- 100 percent of the cover.

- Grasslands/Herbaceous - Areas dominated by upland grasses and forbs. In rare cases, herbaceous cover is less than 25 percent, but exceeds

the combined cover of the woody species present. These areas are not subject to intensive management, but they are often utilized for grazing.

Planted/Cultivated

Definition: Areas characterized by herbaceous vegetation that has been planted or is intensively managed for the production of food, feed, or fiber; or is maintained in developed settings for specific purposes. Herbaceous vegetation accounts for 75-100 percent of the cover.

- Pasture/Hay - Areas of grasses, legumes, or grass-legume mixtures planted for livestock grazing or the production of seed or hay crops.
- Row Crops - Areas used for the production of crops, such as corn, soybeans, vegetables, tobacco, and cotton.
- Small Grains - Areas used for the production of graminoid crops such as wheat, barley, oats, and rice.
- Fallow - Areas used for the production of crops that are temporarily barren or with sparse vegetative cover as a result of being tilled in a management practice that incorporates prescribed alternation between cropping and tillage.
- Urban/Recreational Grasses - Vegetation (primarily grasses) planted in developed settings for recreation, erosion control, or aesthetic purposes. Examples include parks, lawns, golf courses, airport grasses, and industrial site grasses.

Wetlands

Definition: Areas where the soil or substrate is periodically saturated with or covered with water.

- Woody Wetlands - Areas where forest or shrubland vegetation accounts for 25-100 percent of the cover and the soil or substrate is periodically saturated with or covered with water.
- Emergent Herbaceous Wetlands - Areas where perennial herbaceous vegetation accounts for 75-100 percent of the cover and the soil or substrate is periodically saturated with or covered with water.

References

Ayres, J., K. Smallbone, S. Holgate, and G. Fuller (2011). Review of the uk air quality index.

Bærentsen, J. H. and R. Berkowicz (1984). Monte carlo simulation of plume dispersion in the convective boundary layer. *Atmospheric Environment (1967) 18*(4), 701–712.

Balsley, B., R. Frehlich, M. Jensen, and Y. Meillier (2006). High-resolution in situ profiling through the stable boundary layer: examination of the sbl top in terms of minimum shear, maximum stratification, and turbulence decrease. *Journal of the atmospheric sciences 63*(4), 1291–1307.

Barad, M. L. (1958). Project prairie grass, a field program in diffusion. volume 1. Technical report, AIR FORCE CAMBRIDGE RESEARCH LABS HANSCOM AFB MA.

Barbados Fire Service (2017). Fire statistics.

Beyrich, F. (1997). Mixing height estimation from sodar data?a critical discussion. *Atmospheric Environment 31*(23), 3941–3953.

Bianco, L. and J. M. Wilczak (2002). Convective boundary layer depth: Improved measurement by doppler radar wind profiler using fuzzy logic methods. *Journal of Atmospheric and Oceanic Technology 19*(11), 1745–1758.

Bolton, D. (1980). The computation of equivalent potential temperature. *Monthly weather review 108*(7), 1046–1053.

Bowen, I. S. (1926). The ratio of heat losses by conduction and by evaporation from any water surface. *Physical review 27*(6), 779.

Burridge, D. and A. Gadd (1977). *The Meteorological Office operational 10-level numerical weather prediction model (December 1975)*. HM Stationery Office.

Burton, R., J. Dudhia, A. Gadian, and S. Mobbs (2017). The use of a numerical weather prediction model to simulate the release of a dense gas with an application to the lake nyos disaster of 1986. *Meteorological Applications 24*(1), 43–51.

Carson, D. (1973). The development of a dry inversion-capped convectively unstable boundary layer. *Quarterly Journal of the Royal Meteorological Society 99*(421), 450–467.

Caughey, S., M. Kitchen, and J. Leighton (1983). Turbulence structure in convective boundary layers and implications for diffusion. *Boundary-Layer Meteorology 25*(4), 345–352.

Cenedese, A., G. Cosemans, H. Erbrink, R. Stubi, A. Lasserre-Bigorry, and H. Weber (1998). Vertical profiles of wind, temperature and turbulence. *Harmonisation of the pre-processing of meteorological data for atmospheric dispersion models. COST action 710.*

Chia, L.-S. (1967). Albedos of natural surfaces in barbados. *Quarterly Journal of the Royal Meteorological Society 93*(395), 116–120.

Cimorelli, A. J., S. G. Perry, A. , J. C. Weil, R. J. Paine, R. B. Wilson, R. F. Lee, W. D. Peters, and R. W. Brode (2004, 09). AERMOD: Description of Model Formulation. Technical report, United States Environmental Protection Agency.

Clarke, R. H., A. J. Dyer, R. R. Brook, D. G. Reid, and A. J. Troup (1971). Wangara experiment: boundary layer data.

Clothier, B., K. Clawson, P. Pinter Jr, M. Moran, R. J. Reginato, and R. Jackson (1986). Estimation of soil heat flux from net radiation during the growth of alfalfa. *Agricultural and forest meteorology 37*(4), 319–329.

Collier, L. and J. Lockwood (1975). The estimation of solar radiation under cloudless skies with atmospheric dust. *Quarterly Journal of the Royal Meteorological Society 101*(430), 1027–1029.

Davies, J. and T. Uboegbulam (1979). Parameterization of surface incoming radiation in tropical cloudy conditions. *Atmosphere-Ocean 17*(1), 14–23.

De Bruin, H. and A. Holtslag (1982). A simple parameterization of the surface fluxes of sensible and latent heat during daytime compared with the penman-monteith concept. *Journal of Applied Meteorology 21*(11), 1610–1621.

Deardorff, J. (1979). Prediction of convective mixed-layer entrainment for realistic capping inversion structure. *Journal of the Atmospheric Sciences 36*(3), 424–436.

Deardorff, J. (1980). Progress in understanding entrainment at the top of a mixed layer. WORKSHOP ON PLANETARY BOUNDARY LAYER (AMERICAN METEOROLOGICAL SOCIETY).

Deardorff, J. and G. Willis (1982). Ground-level concentrations due to fumigation into an entraining mixed layer. *Atmospheric Environment (1967) 16*(5), 1159–1170.

Deardorff, J. W. (1970). Convective velocity and temperature scales for the unstable planetary boundary layer and for rayleigh convection. *Journal of the atmospheric sciences 27*(8), 1211–1213.

Deardorff, J. W. (1974). Three-dimensional numerical study of turbulence in an entraining mixed layer. *Boundary-Layer Meteorology 7*(2), 199–226.

Department of the Environment and Heritage, Australia (2005). Sulphur dioxide (so2).

DiSano, J. (2002). Indicators of sustainable development: Guidelines and methodologies. *United Nations Department of Economic and Social Affairs, New York*.

Dupont, E., L. Menut, B. Carissimo, J. Pelon, and P. Flamant (1999). Comparison between the atmospheric boundary layer in paris and its rural suburbs during the eclap experiment. *Atmospheric Environment 33*(6), 979–994.

Dyer, A. (1974). A review of flux-profile relationships. *Boundary-Layer Meteorology 7*(3), 363–372.

Dyer, A. and B. Hicks (1970). Flux-gradient relationships in the constant flux layer. *Quarterly Journal of the Royal Meteorological Society 96*(410), 715–721.

EPA, U. (1995). User's guide for the industrial source complex (isc3) dispersion models. *Description of Model Algorithms, vol. IIU. S. Environmental Protection Agency. Office of Air Quality Planning and Standards. Emissions, Monitoring, and Analysis Division, Research Triangle Park, North Carolina*.

EPA, U. (2018). User's guide for the aermod meteorological preprocessor (aermet). *Research Triangle Park, NC, Office of Air Quality Planning and Standards*.

Ermak, D., S. Chan, D. Morgan, and L. Morris (1982). A comparison of dense gas dispersion model simulations with burro series lng spill test results. *Journal of Hazardous Materials 6*(1-2), 129–160.

Feng, X., B. Wu, and N. Yan (2015). A method for deriving the boundary layer mixing height from modis atmospheric profile data. *Atmosphere 6*(9), 1346–1361.

for Disease Control, C., Prevention, et al. (2005). 2005 behavioral risk factor surveillance system questionnaire.

Garratt, J. et al. (1992). The atmospheric boundary layer. cambridge atmospheric and space science series. *Cambridge University Press, Cambridge 416*, 444.

Global Initiative for Asthma (2016). Global strategy for asthma management and prevention: Online appendix 2016 update.

Goh, K.-T., D. Schwela, J. Goldammer, and O. Simpson (1999). *Health Guidelines for Vegetation Fire Events: Background Papers*. World Health Organization (WHO).

Hanna, S. R. and J. Chang (1991). Modification of the hybrid plume dispersion model (hpdm) for urban conditions and its evaluation using the indianapolis data set. *Vol. I. User's Guide for HPDM-Urban. Sigma Research Corporation, Concord, MA 1742*.

Hennemuth, B. and A. Lammert (2006). Determination of the atmospheric boundary layer height from radiosonde and lidar backscatter. *Boundary-Layer Meteorology 120*(1), 181–200.

Her Majesty?s Stationery Office (1875). Public health act, 1875.

Ho, P. N., D. N. Bach, and V. Van Manh (2009). Applying fixed box model to calculate the temporal variance of the concentration of pm10 in thanh xuan district, hanoi (vietnam). *tC 1*, 1–4.

Holtslag, A. (1984). Estimates of diabatic wind speed profiles from near-surface weather observations. *Boundary-Layer Meteorology 29*(3), 225–250.

Holtslag, A. and A. Van Ulden (1983). A simple scheme for daytime estimates of the surface fluxes from routine weather data. *Journal of climate and Applied Meteorology 22*(4), 517–529.

Hottel, H. C. (1976). A simple model for estimating the transmittance of direct solar radiation through clear atmospheres. *Solar Energy 18*(2), 129–134.

Hyun, Y.-K., K.-E. Kim, and K.-J. Ha (2005). A comparison of methods to estimate the height of stable boundary layer over a temperate grassland. *Agricultural and forest meteorology 132*(1), 132–142.

Institute for Health Metrics and Evaluation (2010). Gbd profile: Barbados.

Institute for Health Metrics and Evaluation (2016). Gbd profile: Barbados.

Jacob, D. (1999). *Introduction to atmospheric chemistry*. Princeton University Press.

Kanda, M., M. Kanega, T. Kawai, R. Moriwaki, and H. Sugawara (2007). Roughness lengths for momentum and heat derived from outdoor urban scale models. *Journal of Applied Meteorology and Climatology 46*(7), 1067–1079.

Kasten, F. and G. Czeplak (1980). Solar and terrestrial radiation dependent on the amount and type of cloud. *Solar energy 24*(2), 177–189.

Kelly, F. J., G. W. Fuller, H. A. Walton, and J. C. Fussell (2012). Monitoring air pollution: Use of early warning systems for public health. *Respirology 17*(1), 7–19.

Khan, M. M. and M. J. Ahmad (2012). Estimation of global solar radiation using clear sky radiation in yemen. *Journal of Engineering Science & Technology Review 5*(2).

Kunsch, J. and D. Webber (2000). Simple box model for dense-gas dispersion in a straight sloping channel. *Journal of hazardous materials 75*(1), 29–46.

Lee, B.-J., B. Kim, and K. Lee (2014). Air pollution exposure and cardiovascular disease. *Toxicological research 30*(2), 71.

Lin, K., J. Juang, Y.-W. Shiu, and L. Chang (2016). Estimating the bowen ratio for application in air quality models by integrating a simplified analytical expression with measurement data. *Journal of Applied Meteorology and Climatology 55*(4), 1041–1048.

Lumb, F. (1964). The influence of cloud on hourly amounts of total solar radiation at the sea surface. *Quarterly Journal of the Royal Meteorological Society 90*(383), 43–56.

Mansfield, C., F. R. Johnson, and G. Van Houtven (2006). The missing piece: Valuing averting behavior for children's ozone exposures. *Resource and Energy Economics 28*(3), 215–228.

Martucci, G., R. Matthey, V. Mitev, and H. Richner (2007). Comparison between backscatter lidar and radiosonde measurements of the diurnal and nocturnal stratification in the lower troposphere. *Journal of Atmospheric and Oceanic Technology 24*(7), 1231–1244.

McDermott, M., R. Srivastava, and S. Croskell (2006). Awareness of and compliance with air pollution advisories: a comparison of parents of asthmatics with other parents. *Journal of Asthma 43*(3), 235–239.

Monin, A. and A. Obukhov (1954). Basic laws of turbulent mixing in the surface layer of the atmosphere. *Contrib. Geophys. Inst. Acad. Sci. USSR 151*(163), e187.

Monteil, M. A., G. Joseph, C. Changkit, G. Wheeler, and R. M. Antoine (2005). Comparison of prevalence and severity of asthma among adolescents in the caribbean islands of trinidad and tobago: results of a nationwide cross-sectional survey. *BMC Public Health 5*(1), 96.

Neidell, M. and P. L. Kinney (2010). Estimates of the association between ozone and asthma hospitalizations that account for behavioral responses to air quality information. *environmental science & policy 13*(2), 97–103.

Nielinger, J., R. Röckle, H.-C. Höfl, and W.-J. Kost (2004). 5.29 lagrange versus eulerian dispersion modeling comparison for investigations concerning air pollution caused by traffic.

Nielsen-Gammon, J. W., C. L. Powell, M. J. Mahoney, W. M. Angevine, C. Senff, A. White, C. Berkowitz, C. Doran, and K. Knupp (2008). Multisensor estimation of mixing heights over a coastal city. *Journal of Applied Meteorology and Climatology 47*(1), 27–43.

Nieuwstadt, F. and R. Brost (1986). The decay of convective turbulence. *Journal of the atmospheric sciences 43*(6), 532–546.

Organization, W. M. (1982). Commission for Instruments and Methods of Observation (CIMO) - Abridged final report of the eighth session. Technical report, World Meteorology Organization.

Paine, R. and B. Egan (1987). User's guide to the rough-terrain diffusion model (rtdm)(rev. 3. 20). Technical report, Environmental Research and Technology, Inc., Concord, MA (USA).

Paine, R. J. and S. B. Kendall (1993). Comparison of observed profiles of winds, temperature, and turbulence with theoretical results. preprints. In *Joint Conf. of the American Meteorological Society and Air and Waste Management Association Specialty Conf.: The Role of Meteorology in Managing the Environment in the 90s*, pp. 395–413.

Pan American Health Organization (2012). Barbados.

Panofsky, H. A. and J. A. Dutton (1984). Atmospheric turbulence: models and methods for engineering applications. Technical report, Wiley.

Perez, P., F. Castellvi, M. Ibanez, and J. Rosell (1999). Assessment of reliability of bowen ratio method for partitioning fluxes. *Agricultural and Forest Meteorology 97*(3), 141–150.

Prospero, J. M. (2006). Saharan dust impacts and climate change. *Oceanography 19*(2), 60.

Romps, D. M. (2017). Exact expression for the lifting condensation level. *Journal of the Atmospheric Sciences 74*(12), 3891–3900.

Semenza, J. C., D. J. Wilson, J. Parra, B. D. Bontempo, M. Hart, D. J. Sailor, and L. A. George (2008). Public perception and behavior change in relationship to hot weather and air pollution. *Environmental research 107*(3), 401–411.

Sheppard, P. (1956). Airflow over mountains. *Quarterly journal of the Royal Meteorological society 82*(354), 528–529.

Shivalingaswamy, T. and B. Kagali (2012). Determination of the declination of the sun on a given day. *European Journal of Physics Education 3*(1).

Snyder, W. H., R. S. Thompson, R. E. Eskridge, R. E. Lawson, I. P. Castro, J. Lee, J. C. Hunt, and Y. Ogawa (1985). The structure of strongly stratified flow over hills: dividing-streamline concept. *Journal of Fluid Mechanics 152*, 249–288.

Stockie, J. M. (2011). The mathematics of atmospheric dispersion modeling. *Siam Review 53*(2), 349–372.

Stull, R. B. (1983). A heat-flux history length scale for the nocturnal boundary layer. *Tellus A: Dynamic Meteorology and Oceanography 35*(3), 219–230.

Sugiyama, G. and J. S. Nasstrom (1999). Methods for determining the height of the atmospheric boundary layer. *Lawrence Livermore National Laboratory Internal Report UCRL-ID-133200*.

Taconet, O. and A. Weill (1982). Vertical velocity field in the convective boundary layer as observed with an acoustic doppler sodar. *Boundary-Layer Meteorology 23*(2), 133–151.

Taylor, G. (1931). Effect of variation in density on the stability of superposed streams of fluid. *Proceedings of the Royal Society of London. Series A, Containing Papers of a Mathematical and Physical Character 132*(820), 499–523.

The Barbados Meteorological Services (2017). Synoptic weather observation data for the grantley adams international airport, barbados.

The Caribbean Institute for Meteorological and Hydrology (2017). Elevation across barbados at 100m resolution.

The International Union Against Tuberculosis and Lung Disease (2011). The global asthma report 2011.

The United Nations Environment Programme (2016). Air quality policies in barbados.

The US Environmental Protection Agency (2016). Patient exposure and the air quality index.

Timeanddate.com (2018). Sunrise and sunset time database for barbados.

US Environmental Protection Agency (2017). History of reducing air pollution from transportation in the united states (u.s.).

US National Park Services (2018). Where does air pollution come from?

Van Ulden, A. and A. Holtslag (1985). Estimation of atmospheric boundary layer parameters for diffusion applications. *Journal of Climate and Applied Meteorology 24*(11), 1196–1207.

Venkatram, A. (1980). Estimating the monin-obukhov length in the stable boundary layer for dispersion calculations. *Boundary-Layer Meteorology 19*(4), 481–485.

Venkatram, A. (1982). A semi-empirical method to compute concentrations associated with surface releases in the stable boundary layer. *Atmospheric Environment (1967) 16*(2), 245–248.

Venkatram, A., R. Brode, A. Cimorelli, R. Lee, R. Paine, S. Perry, W. Peters, J. Weil, and R. Wilson (2001). A complex terrain dispersion model for regulatory applications. *Atmospheric Environment 35*(24), 4211–4221.

Waleed, I. A.-R. and M. A. Yussra (2006). Effect of altitude and type of clouds on transmissivity of solar radiation intensity in mosul city. *Rafidain Journal of Science 17*(2), 20–30.

Wang, X. and K. Wang (2014). Estimation of atmospheric mixing layer height from radiosonde data. *Atmospheric Measurement Techniques 7*(6), 1701–1709.

Ward, D. (1989). Air toxics and fireline exposure. In *Proceedings of the 10th Conference on Fire and Forest Whitewood= Compte rendu du 10ieme Congress sur les incendies et la meterologie forestiere/editeurs DC Maiver, H. Auld, R. Whitewood*. Ottawa, Ont.? Forestry Canada 1989.

Weil, J. (1990). A diagnosis of the asymmetry in top-down and bottom-up diffusion using a lagrangian stochastic model. *Journal of the Atmospheric Sciences 47*(4), 501–515.

Weil, J. and R. Brower (1983). Estimating convective boundary layer parameters for diffusion application. *Draft Report Prepared by Environmental Center, Martin Marietta Corp. for Maryland Dept. of Natural Resources*.

Weil, J., L. Corio, and R. Brower (1997). A pdf dispersion model for buoyant plumes in the convective boundary layer. *Journal of Applied Meteorology 36*(8), 982–1003.

Wen, X.-J., L. Balluz, and A. Mokdad (2009). Association between media alerts of air quality index and change of outdoor activity among adult asthma in six states, brfss, 2005. *Journal of community health 34*(1), 40–46.

Wilczak, J. M. and M. S. Phillips (1986). An indirect estimation of convective boundary layer structure for use in pollution dispersion models. *Journal of climate and applied meteorology 25*(11), 1609–1624.

Willis, G. and J. Deardorff (1974). A laboratory model of the unstable planetary boundary layer. *Journal of the Atmospheric Sciences 31*(5), 1297–1307.

Willis, G. E. and J. Deardorff (1981). A laboratory study of dispersion from a source in the middle of the convectively mixed layer. *Atmospheric Environment (1967) 15*(2), 109–117.

World Health Organization (2013). Health effects of particulate matter: Policy implications for countries in eastern europe, caucasus and central asia.

World Health Organization (2014). Burden of disease from household air pollution for 2012.

World Health Organization (2016). Ambient air pollution: A global assessment of exposure and burden of disease.

World Health Organization (2017). Ambient air pollution: A global assessment of exposure and burden of disease.

Wyngaard, J. (1988). Structure of the pbl, lectures on air pollution modeling, a. *Venkatram and JC Wyngaard, Eds., Americ. Meteor. Soc., Boston*, 385.

Yamada, T. (2000). Lagrangian dispersion model for nonneutrally buoyant plumes. *Journal of Applied Meteorology 39*(3), 427–436.

Zannetti, P. (2013). *Air pollution modeling: theories, computational methods and available software*. Springer Science & Business Media.

Zeng, X., M. A. Brunke, M. Zhou, C. Fairall, N. A. Bond, and D. H. Lenschow (2004). Marine atmospheric boundary layer height over the eastern pacific: Data analysis and model evaluation. *Journal of Climate 17*(21), 4159–4170.

Zilitinkevich, S. (1972). On the determination of the height of the ekman boundary layer. *Boundary-Layer Meteorology 3*(2), 141–145.